Plant Communications
Research Article

CellPress
Partner Journal

A chromosome-level, haplotype-phased *Vanilla planifolia* genome highlights the challenge of partial endoreplication for accurate whole-genome assembly

Quentin Piet[1,17], Gaetan Droc[2,3,4,17,*], William Marande[5,17], Gautier Sarah[4,6,17], Stéphanie Bocs[2,3,4,17], Christophe Klopp[7,17], Mickael Bourge[8], Sonja Siljak-Yakovlev[9], Olivier Bouchez[10], Céline Lopez-Roques[10], Sandra Lepers-Andrzejewski[11], Laurent Bourgois[12], Joseph Zucca[13], Michel Dron[14], Pascale Besse[15], Michel Grisoni[16,*], Cyril Jourda[1,*] and Carine Charron[1,17]

[1]CIRAD, UMR PVBMT, 97410 Saint-Pierre, La Réunion, France

[2]CIRAD, UMR AGAP Institut, 34398 Montpellier, France

[3]UMR AGAP Institut, Univ Montpellier, CIRAD, INRAE, Institut Agro, 34398 Montpellier, France

[4]French Institute of Bioinformatics (IFB) - South Green Bioinformatics Platform, Bioversity, CIRAD, INRAE, IRD, 34398 Montpellier, France

[5]INRAE, CNRGV, Genotoul, 31326 Castanet-Tolosan, France

[6]AGAP, Univ. Montpellier, CIRAD, INRAE, Montpellier SupAgro, Montpellier, France

[7]Plateforme Bioinformatique, Genotoul, BioinfoMics, UR875 Biométrie et Intelligence Artificielle, INRAE, Castanet-Tolosan, France

[8]Cytometry Facility, Imagerie-Gif, Université Paris-Saclay, CEA, CNRS, Institute for Integrative Biology of the Cell (I2BC), 91198 Gif-sur-Yvette, France

[9]Université Paris-Saclay, CNRS, AgroParisTech, Ecologie Systématique Evolution (ESE), 91190 Gif-sur-Yvette, France

[10]INRAE, GeT-PlaGe, Genotoul, 31326 Castanet-Tolosan, France

[11]Etablissement Vanille de Tahiti, Uturoa, French Polynesia, France

[12]Eurovanille, Rue de Maresquel, 62870 Gouy Saint André, France

[13]Département Biotechnologie, V. Mane Fils, 06620 Le Bar Sur Loup, France

[14]Université Paris-Saclay, CNRS, INRAE, Univ. Evry, Institute of Plant Sciences Paris-Saclay (IPS2), 91405 Orsay, France

[15]Université de la Réunion, UMR PVBMT, Saint-Pierre, La Réunion, France

[16]CIRAD, UMR PVBMT, 501 Tamatave, Madagascar

[17]These authors contributed equally to this article.

***Correspondence: Gaetan Droc (gaetan.droc@cirad.fr), Michel Grisoni (michel.grisoni@cirad.fr), Cyril Jourda (cyril.jourda@cirad.fr)**

https://doi.org/10.1016/j.xplc.2022.100330

ABSTRACT

***Vanilla planifolia*, the species cultivated to produce one of the world's most popular flavors, is highly prone to partial genome endoreplication, which leads to highly unbalanced DNA content in cells. We report here the first molecular evidence of partial endoreplication at the chromosome scale by the assembly and annotation of an accurate haplotype-phased genome of *V. planifolia*. Cytogenetic data demonstrated that the diploid genome size is 4.09 Gb, with 16 chromosome pairs, although aneuploid cells are frequently observed. Using PacBio HiFi and optical mapping, we assembled and phased a diploid genome of 3.4 Gb with a scaffold N50 of 1.2 Mb and 59 128 predicted protein-coding genes. The atypical k-mer frequencies and the uneven sequencing depth observed agreed with our expectation of unbalanced genome representation. Sixty-seven percent of the genes were scattered over only 30% of the genome, putatively linking gene-rich regions and the endoreplication phenomenon. By contrast, low-coverage regions (non-endoreplicated) were rich in repeated elements but also contained 33% of the annotated genes. Furthermore, this**

Published by the Plant Communications Shanghai Editorial Office in association with Cell Press, an imprint of Elsevier Inc., on behalf of CSPB and CEMPS, CAS.

assembly showed distinct haplotype-specific sequencing depth variation patterns, suggesting complex molecular regulation of endoreplication along the chromosomes. This high-quality, anchored assembly represents 83% of the estimated *V. planifolia* genome. It provides a significant step toward the elucidation of this complex genome. To support post-genomics efforts, we developed the Vanilla Genome Hub, a user-friendly integrated web portal that enables centralized access to high-throughput genomic and other omics data and interoperable use of bioinformatics tools.

Keywords: vanilla, whole-genome sequencing, optical mapping, partial endoreplication, genome hub

Piet Q., Droc G., Marande W., Sarah G., Bocs S., Klopp C., Bourge M., Siljak-Yakovlev S., Bouchez O., Lopez-Roques C., Lepers-Andrzejewski S., Bourgois L., Zucca J., Dron M., Besse P., Grisoni M., Jourda C., and Charron C. (2022). A chromosome-level, haplotype-phased *Vanilla planifolia* genome highlights the challenge of partial endoreplication for accurate whole-genome assembly. Plant Comm. **3**, 100330.

INTRODUCTION

Endoreplication, characterized by a series of DNA replications in the nucleus without mitotic cell division, is found in a large number of both animal and plant species (Lee et al., 2009). During regular endoreplication, each step of this mechanism leads to a two-fold increase in nuclear DNA content in somatic cells (2C, 4C, 8C, 16C, etc.), where 1C corresponds to the DNA content of the non-replicated holoploid chromosome set. Endoreplication is very common in plants and is related to various biological processes, such as plant development and growth, and occurs in response to biotic and abiotic stresses (Bourdon et al., 2012; Lang and Schnittger, 2020). This phenomenon depends on the type of tissue and its stage of development, suggesting involvement in cell differentiation and maintenance of the final stage of differentiation (Bhosale et al., 2018). The molecular mechanisms involved in regular endoreplication have been particularly well studied in *Arabidopsis thaliana* over the past few years. A downregulation of mitotic activity caused by mitotic cyclin-dependent kinase (CDK)–cyclin complexes has been shown to be directly involved in the control of endoreplication (Lang and Schnittger, 2020).

In many orchid species, measurements of genomic content by flow cytometry (FCM) have not agreed with the commonly accepted model of complete endoreplication. In this case, nuclear DNA content in endoreplicated cells was present at less than twice the 2C cell content. Because this ratio was constant for a given *Vanilla* species, whatever the cell ploidy level, it was suggested that the nuclear DNA could be categorized into two parts: the P fraction, subject to endoreplication, and the F fraction, not endoreplicated (Brown et al., 2017). These fractions are constant in all cells undergoing partial endoreplication (PE), which suggests the fine regulation of genome rearrangements. The fact that the gametes are haploid also suggests the presence of molecular mechanisms that enable the isolation of the holoploid genome. This type of endoreplication, which appears to be specific to the Orchidaceae lineage in plants, has been successively termed "progressively PE" (Bory et al., 2008; Trávníček et al., 2015; Hřibová et al., 2016), strict PE (Brown et al., 2017), and more recently, PE (Chumová et al., 2021; Trávníček et al., 2019). To be in line with the latest works and to harmonize the terminology for this phenomenon, the term PE will be used in this work. To date, PE has been observed in all species studied within the genus *Vanilla* (Bory et al., 2008; Brown et al., 2017; Lepers-Andrzejewski et al., 2011; Trávníček et al., 2015).

Vanilla planifolia G. Jackson is an emblematic orchid cultivated for its fruit (pod) fragrance. Pods contain many aromatic compounds, particularly vanillin in high proportion (Perez-Silva et al., 2006). In this species, diploid nuclei (2C) are found mainly in nodal tissues (with PE up to 32E), whereas the nuclei of mature leaf cells contain a low 2C fraction and show PE up to 64E (Brown et al., 2017). The F fraction was estimated to be 71.6% of the genome, whereas the P fraction (28.4%) could be duplicated up to 64E. In addition, the proportion of the non-endoreplicated (F) genome varies greatly from species to species. It is very high in *Vanilla pompona* (F = 81%) but rather low in *Vanilla mexicana* (F = 17%) (Brown et al., 2017). Several studies on orchids have also shown that species prone to PE have a larger genome than those prone to conventional endoreplication (Trávníček et al., 2015, 2019; Chumová et al., 2021). Nevertheless, the molecular mechanisms involved in PE are not yet elucidated.

A chromosome-scaled, phased *V. planifolia* genome (Daphna cultivar) was recently reported, highlighting haplotype differences and one ancestral whole-genome duplication shared by all sequenced orchids (Hasing et al., 2020). However, the 1.5 Gb size of the assembled genome was far from the *V. planifolia* genome size, estimated to be about 4 Gb using FCM measurement (Bory et al., 2008; Lepers-Andrzejewski et al., 2011), suggesting that the Daphna genome assembly may be highly incomplete. As mentioned by Hasing et al. (2020), the reason for the genome size discrepancy between FCM and assembly results remains to be elucidated. With about 65% of the *V. planifolia* genome missing in the Daphna assembly, we hypothesize that the missing part of the genome corresponds mainly to the F (non-endoreplicated) fraction (71.6%) (Brown et al., 2017), whose lower representation results in a lower sequencing depth.

Here, we address this issue by developing an approach that combines FCM, cytogenetics, and whole-genome sequencing using the most recently developed technologies (Supplemental Figure 1) with a tissue that is enriched in the 2C fraction (nodes), resulting in a reduced P/F ratio and therefore a greater proportion of the F fraction. We demonstrate that the genome size discrepancy was due to the occurrence of PE, for which

further knowledge at the chromosome scale was gained from this study. We present the most complete version to date of a high-quality, chromosome-level phased genome of *V. planifolia* using a traditional vanilla cultivar from the Indian Ocean region (CR0040). Our results are shared through a web portal that facilitates data access, use, and analyses by a wide community.

RESULTS

Genome size, ploidy level, and chromosome content

The 2C genome size of *V. planifolia* CR0040, a traditional vanilla cultivar from La Reunion island (Supplemental Note 1), was estimated in nodal tissues to be 4.18 ± 0.08 pg by FCM (Supplemental Note 1), corresponding to 4.09 Gb (Doležel et al., 2003). To estimate PE levels, the fluorescence ratio of DNA content between consecutive peaks of endoreplication levels was estimated (Supplemental Note 1; Supplemental Figure 2; Supplemental Table 1). Results showed no significant differences (calculated t-values of 1.116, 1.900, 0.935, and 0.365 compared with Student table t-value [$\alpha = 0.05$] of 2.131) between the PE pattern of CR0040 and those of other *V. planifolia* cultivars, such as CR1110 (2C = 4.16 ± 0.04 pg), studied by Brown et al. (2017). The replicated fraction P was also calculated (P = 30.5% ± 3.2%). The equivalent amount 2p was then P × 2C = 1.275 pg, which meant that the absolute quantity p was 0.637 pg, and the absolute quantity f of fixed amount was 1.453 pg (Figure 1A and 1B; Supplemental Note 1). The karyotype of *V. planifolia* obtained by cytogenetics approaches (Supplemental Note 1) appeared to be of bimodal type, composed of 16 both large and small chromosome pairs (Figures 2A–2C), although aneuploid cells were frequently observed, such as those with only 28 chromosomes (Figure 2D and 2E). *V. planifolia* chromosomes possess important portions of telomeric and pericentromeric heterochromatin, which made the determination of their morphology difficult. In the interphase nuclei, this heterochromatin was present in the form of numerous chromocenters that were clearly visible after staining with both orcein (Figure 2F) and DAPI (Figure 2G). This type of heterochromatin is unspecific, whereas heterochromatin linked to rRNA genes is rich in G-C bases. Only one locus (two spots) of rDNA (18S-5.8S-26S) was present in the genome of *V. planifolia* (Figure 2H, arrows), evidenced after chromomycin (CMA3) staining. After Hoechst 33258 staining, our results also revealed that AT-rich DNA regions were more common than GC-rich regions in the *V. planifolia* chromosomes and that some chromosomes were entirely or almost entirely heterochromatinized (Figure 2I).

Whole-genome assembly and k-mer analysis

CR0040 genome sequencing produced 69 Gb of Pacific Biosciences (PacBio) HiFi long reads, 147 Gb of Oxford Nanopore Technology (ONT) long reads, and 200 Gb of Illumina 10X Genomics short reads (Supplemental Note 1; Supplemental Table 2). These DNA sequencing (DNA-seq) reads were assembled using different bioinformatics pipelines. The best result was obtained using only high-quality HiFi long reads (Supplemental Note 2; Supplemental Tables 3 and 4). Contigs from the HiFi read assembly were scaffolded with optical maps to obtain a final phased assembly of 3.4 Gb (1.5 Gb for haplotype A and 1.9 Gb for haplotype B), representing around 83% of the expected genome size. One third of the assembly could be anchored onto 14 chromosomes using published Daphna chromosomes as references (Hasing et al., 2020). Unfortunately, no data could help to organize the remaining contigs into the two missing chromosomes. Therefore, the remaining two-thirds correspond to unanchored additional sequences that were compiled into two unknown random pseudomolecules, A0 and B0. The final assembly comprised 24 534 contigs with a contig N50 length of 924 kb. The lengths of the 14 chromosomes ranged from 73.5 Mb (Chr01) to 20 Mb (Chr14). Main genome assembly statistics are synthesized in Table 1.

In order to understand how PE affects the assembly, a k-mer analysis was produced. The results should reflect the sequencing coverage of the different genome fractions present in our raw data and assembly. In brief, the reads were split into overlapping k-mers (47-mers in our case). K-mers were then sorted and occurrences counted. These counts were then used to produce a histogram. A spectra-cn plot was used to compare the k-mers found in the reads versus the k-mers found in the assembly (Supplemental Figure 3). The x axis gives the number of times a given k-mer was found in all the reads, reflecting the coverage of the k-mer. The y axis gives a value representing the number of k-mers that were found a specified number of times (x axis value). Interestingly, two k-mer distributions were centered at 42× and 84×, representing a classical diploid distribution with heterozygous and homozygous k-mer content. We assumed that these peaks represented the k-mers of the endoreplicated fraction with a high sequencing depth due to higher representation. Remarkably, the graph also showed an additional k-mer distribution centered around 10× (Supplemental Figure 3, red arrow). This distribution could easily be mistaken for an erroneous k-mer distribution, but we assumed that it represented non-endoreplicated k-mers of the *V. planifolia* genome, with low-sequencing depth due to lower representation.

To validate the assembly and compare it with the already published reference, we produced four k-mer spectra-cn plots showing k-mer distributions of Daphna Illumina reads and CR0040 HiFi reads colored both with the Daphna and CR0040 assemblies (Figure 3). A spectra-cn plot enables comparison of the k-mers found in the reads versus the k-mers found in the assembly. The k-mer histogram from the reads is colored based on the number of times each k-mer is found in the assembly. For a heterozygous diploid assembly, we expected to find two distributions: on the left, the heterozygous distribution, which should be colored in red because each k-mer is only found once in the assembly, and on the right, the homozygous distribution, which is purple because the corresponding k-mers are found twice in the assembly. The black area at the far left of the diagram corresponds to k-mers that include sequencing errors; these are found a limited number of times in the reads and never in the assembly. Daphna Illumina sequencing, being deeper, resulted in better separation between the homozygous (80× sequencing depth) and heterozygous (160× depth) k-mer fractions in the spectra-cn graph compared with CR0040 (Figure 3A and 3B against 3C and 3D). The same pattern occurred for CR0040 HiFi data around 45× and 90× (Figure 3C). The differences between Figure 3A and 3C come from the sequencing depth and the type of tissue used: mature leaves with a higher proportion of

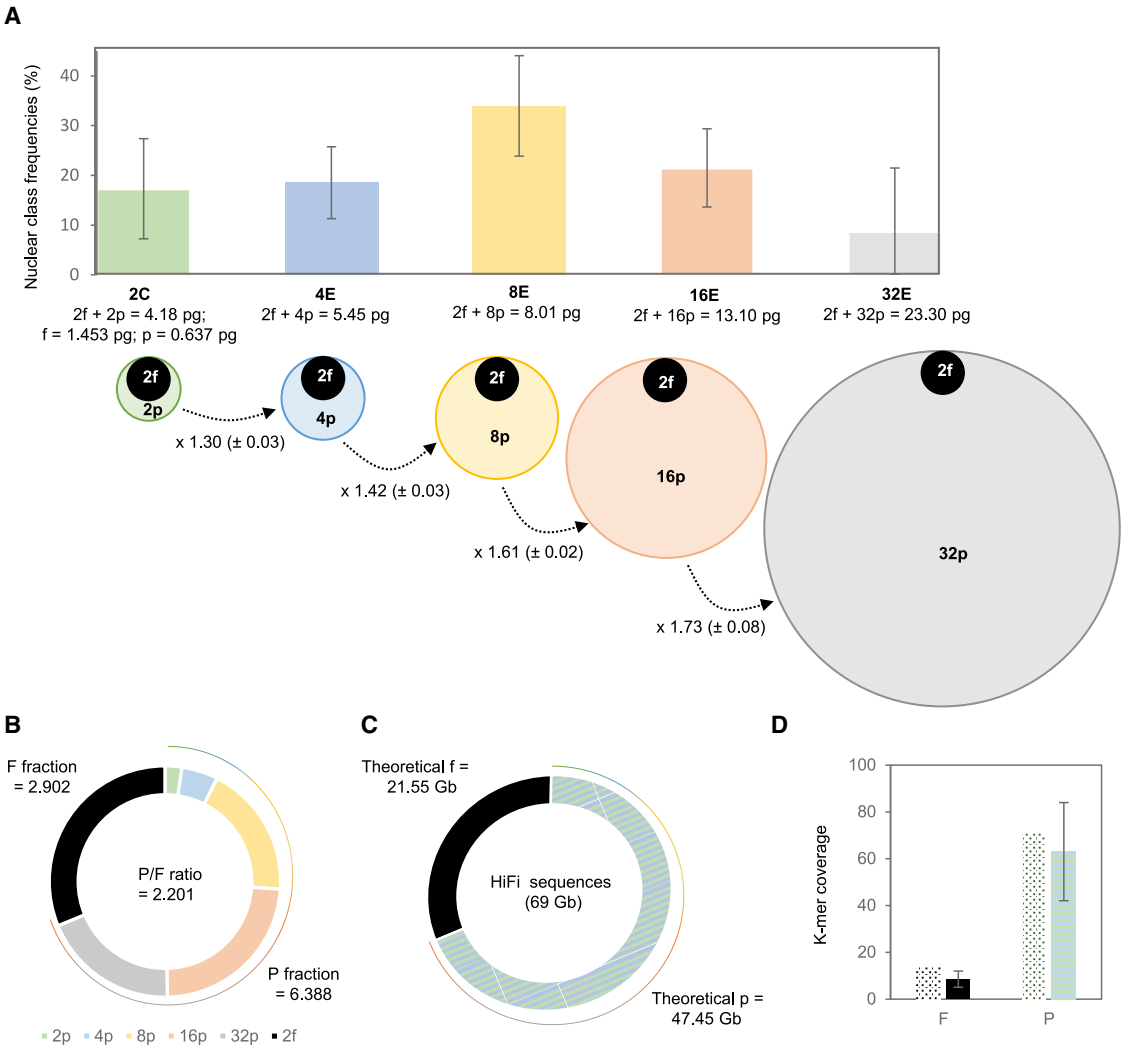

Figure 1. Endoreplicated and non-endoreplicated fractions in the CR0040 *Vanilla planifolia* genome.

(A) The histogram represents the distribution of nuclei in *V. planifolia* nodal tissues according to the partial endoreplication state of cells, from 2C (green) to 4E (blue), 8E (yellow), 16E (orange), and 32E (gray). The disks below represent the endoreplicated (colored) and non-endoreplicated (black) DNA content for each class of nuclei, proportionally to their mass (pg). The lowercase f and p denote the respective DNA quantities of the F fraction (fixed proportion of the haploid genome that cannot endoreplicate) and the P fraction (part that participates in endoreplication). The mean and the standard deviation (SD) of the interpeak ratio have been indicated below the dotted arrows.

(B) F and P fractions and P/F ratio values obtained by flow cytometry and detailed for the P fraction for each nuclear class (2C, green; 4E, blue; 8E, yellow; 16E, orange; and 32E, gray).

(C) Theoretical F and P fractions expected from HiFi sequencing and from flow-cytometry data.

(D) Theoretical (dotted) and experimental k-mer coverages for F (black) and P (hatched) fractions.

the P fraction for Daphna and nodal tissues with a lower P/F ratio for CR0040. The k-mer distribution of the non-endoreplicated fraction (low coverage) was not found in the Daphna assembly (black area left of Figure 3B and 3D) but is mostly present in the CR0040 assembly. Regarding the completeness of the Daphna reference assembly, the spectra-cn plots (Figure 3B and 3D) showed that part of the heterozygous fraction was missing (orange arrows), and some k-mers were in overrepresented copies (>2×) in both heterozygous and homozygous fractions (Figure 3B, black arrows). The spectra-cn diagram also showed heterozygous content present two or more times instead of once in this assembly (Figure 3, black arrows), which could indicate spurious duplications. As a whole, our CR0040 genome assembly is close in size to the FCM estimate and has the expected k-mer diploid profile, with a well-represented non-endoreplicated fraction (Figure 1C and 1D).

Gene and transposable element annotation

The assembled genome supplemented with transcriptomic data from nine distinct tissues made it possible to identify 59 128 protein-coding genes (26 392 for haplotype A and 32 736 for haplotype B), 90.31% of which could be associated with a function (Supplemental Note 3; Supplemental Tables 5–10). Sixty-seven percent of the predicted genes were anchored onto the 14 chromosome pairs and the remaining 33% onto the two random mosaic

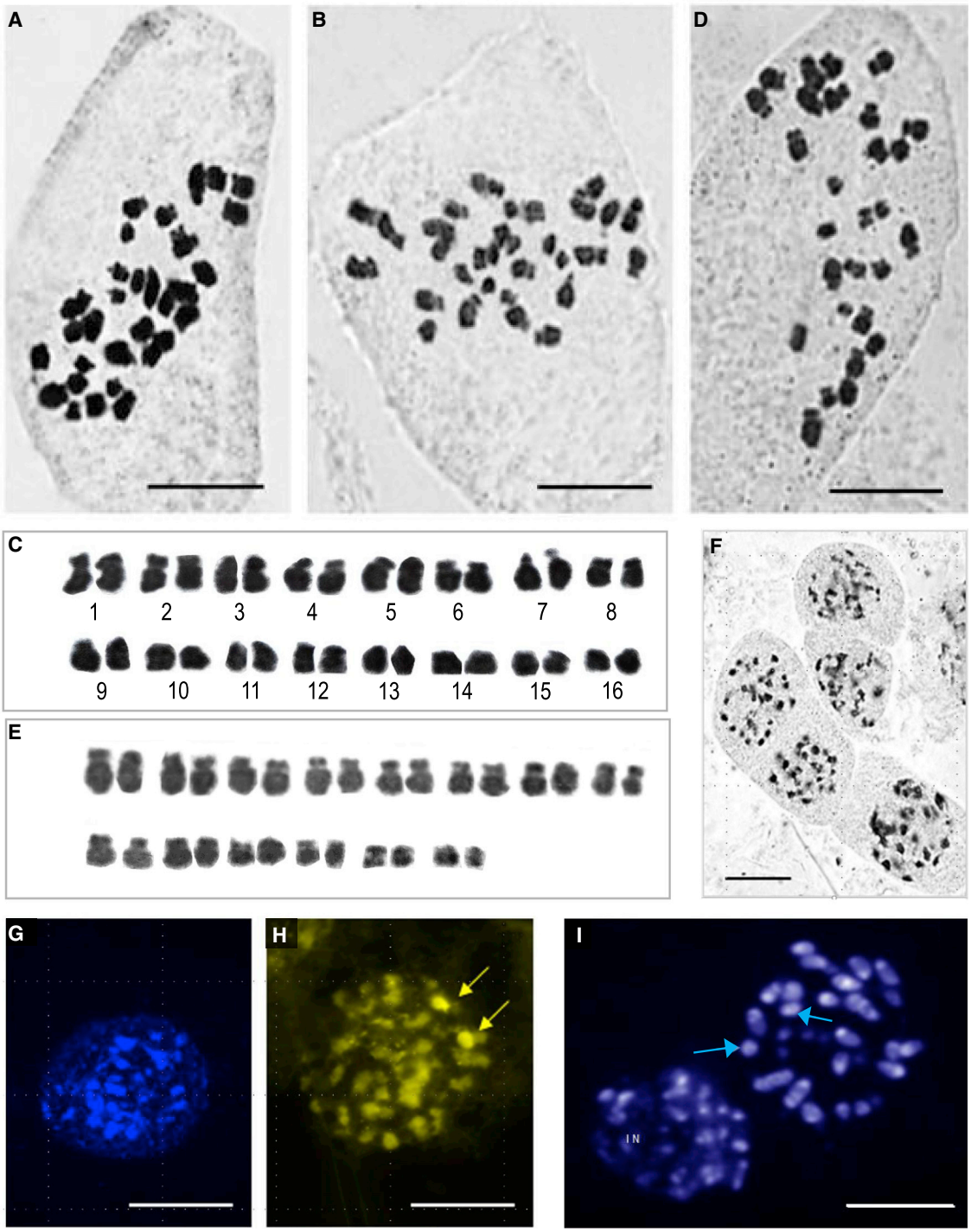

Figure 2. Cytogenetic analysis of *Vanilla planifolia* CR0040.
(A–D) Orcein staining: **(A** and **B)** mitotic metaphases with 2n = 32 chromosomes; **(C)** karyotype corresponding to **(B)**; **(D)** hypoaneuploid mitotic metaphase with 2n = 28 chromosomes; **(E)** karyotype corresponding to **(D)**; **(F)** interphase nuclei showing heterochromatic chromocenters; **(G)** DAPI-stained interphase nucleus showing unspecific heterochromatin; **(H)** chromomycin fluorochrome staining with two CMA^+ regions (arrows) corresponding to rDNA sites; **(I)** Hoechst-stained AT-rich DNA in metaphase and interphase nucleus (IN), with two fully heterochromatinized chromosomes (arrows). Scale bars represent 10 μm.

chromosomes that were constructed from the unanchored scaffolds and contigs (Figure 4A, blue distributions). We estimated the annotation completeness at 93.2% with the Benchmarking Universal Single-Copy Orthologs approach using the Viridiplantae database. In total, 72% of the assembly consisted of repeats, including single-sequence repeats (15.4%), and 9.7% of other low-complexity regions (Supplemental Note 3; Supplemental Table 11). A high content of retrotransposons was found (41.5%),

Total assembly size (Gb)	3.4
Total contig number	24 534
Contig N50 length (Mb)	0.924
Maximum contig length (Mb)	31
GC content (%)	31.6
Number of protein-coding genes	59 128
Benchmarking Universal Single-Copy Orthologs completeness (%)	93.2
Total of interspersed repeats (%)	47.0

Table 1. HiFi assembly and annotation statistics of the diploid CR0040 genome

whereas the content of DNA transposons was low (1.4%). The long terminal repeat retrotransposon content was richer in Gypsy (9.7%; Figure 4A, purple distributions) than in Copia (6.1%; Figure 4A, orange distribution), although a number of annotated retrotransposons (12.5%) were not more precisely classified. The two random mosaic chromosomes were enriched in repeats and showed low gene density and low sequencing depth (Figure 4A, green distributions, and Supplemental Table 12). Indeed, compared with the 14 chromosome sequences, the unanchored regions showed higher proportions of long interspersed nuclear element sequences (8% and 14.05%), and this was true for both haplotypes. By contrast, DNA transposons (3.14% and 0.93%), short interspersed nuclear elements (0.12% and 0.05%), and long terminal repeats (21.67% and 15.57%) represented a larger part of the 14 chromosome sequences than of the unanchored regions. The biggest difference in unanchored regions was observed for unclassified retrotransposons, which represented 16.76% of the unanchored sequences versus 3.28% of the 14 chromosome sequences. Main genome annotation statistics are synthesized in Table 1.

V. planifolia pangenomics and whole-genome duplication

The comparison of the four mosaic haplotypes from the two *V. planifolia* cultivars, CR0040 and Daphna (Supplemental Tables 12 and 13), showed that the 14 pseudomolecules of CR0040 were shorter and contained fewer genes than those of Daphna and that a large number of regions in the CR0040 pseudomolecules (haplotype A or B) were not located in the Daphna pseudomolecules (Supplemental Figure 4). Pangenomic analysis of the orthogroups from proteomes derived from the 14 chromosomes only (Supplemental Figure 5; Supplemental Table 14; Supplemental Note 4) indicated that the core genome was composed of 14 210 families and 77 692 genes (35 972 CR0040 and 41 720 Daphna). The dispensable genome of CR0040 contains 1266 families and 3613 genes specific to CR0040. The dispensable genome of Daphna contains 3997 Daphna-specific families and 13 645 genes. Finally, we looked at the expansion or reduction of gene families in relation to six proteomes (CR0040, Daphna, *Phalaenopsis equestris*, *Phalaenopsis aphrodite*, *A. thaliana*, and *Oryza sativa*; Supplemental Figure 6). From an orchid perspective, the expansion number for the orchid node is rather low (+36), whereas the Daphna-specific number is rather high (A +1841 and B +1943) compared with CR0040 (A +418 and B +826).

To identify whole-genome duplications (WGDs), pairwise genome synteny analyses between CR0040, Daphna, and *P. aphrodite* and within themselves were carried out (Supplemental Figures 7 and 8; Supplemental Notes 4 and 6). The CR0040 haplotype A dot plot validated at least one pan-orchid WGD (α°, the origin of the paleo-allotetraploid) previously found by Hasing et al. (2020). An additional dot plot diagonal and dS peak suggested a second WGD, possibly the tau of Monocots (τ^{m}).

Detection of non-endoreplicated regions

PE induces highly unbalanced DNA representation with a P/F DNA ratio ranging from 3 to 10, depending on the tissue. This was reflected in our assembly by highly variable sequencing depth (Figure 4A, green lane). The two random mosaic chromosomes that showed a low sequencing depth at most loci may therefore contain a large part of the non-endoreplicated F fraction of the genome. It is likely that a large number of unanchored sequences originate from the two fully heterochromatinized chromosomes observed in the interphase nuclei (Figure 2I), possibly chromosome pairs 15 or 16. The remaining unanchored sequences should correspond to missing fractions in the anchored chromosomes. Interestingly, the sequencing reads that mapped to the CR0040 and Daphna assemblies also showed intra-chromosomal sequencing depth variations (Figure 4B). These patterns were consistent, regardless of the technology used. To observe this phenomenon globally on all chromosomes and genomes with all technologies (HiFi, ONT, and Illumina), sequencing depth analysis tools were used and manual validation performed (Supplemental Note 5; Supplemental Tables 15 and 16). Two patterns of sequencing depth variation were identified along all chromosomes. The first one (indicated with a dotted box labeled "1" in Figure 4B and Supplemental Figure 9) corresponded to a sharp decrease in sequencing depth for both cultivars, with all sequencing technologies, which dropped down from 45×–120× to less than 20×. Surprisingly, this pattern occurred independently on the two haplotypes. A total of 37 very low-coverage regions with this pattern (from 0.4 to 6 Mb in length) were identified along the chromosomes (24 in haplotype A and 13 in haplotype B) for a cumulative size of 60.1 Mb. In a large portion of these regions, we found low gene density and high repeat density. This pattern could correspond to non-endoreplicated regions present in both the Daphna and CR0040 genomes. The fact that these patterns are systematically located at junctions between super-scaffolds is consistent with the decrease in sequencing depth caused by non-endoreplication, which impaired the assembly of the endoreplicated regions located on either side. The second pattern (indicated with a dotted box labeled "2" in Figure 4B and Supplemental Figure 9) corresponded to 36 regions (from 1.2 Mb to 20 Mb in length; cumulative size of 207.2 Mb) with segmental sequencing depth variation present in CR0040 (with HiFi, ONT, and Illumina) but not in Daphna (with ONT and Illumina). Furthermore, these variations were syntenic along the two haplotypes, but the direction of variation was inverted between the two phases. Their respective levels of sequencing depth differ by a factor of about three in CR0040. The cause of these apparently coordinated sequencing depth inversions between CR0040 haplotypes remains unclear. After analyzing the locations of these k-mers in the CR0040 assembly, it appeared that these low depth k-mers (between 5× and 15×) were mostly present in the unanchored part of the genome

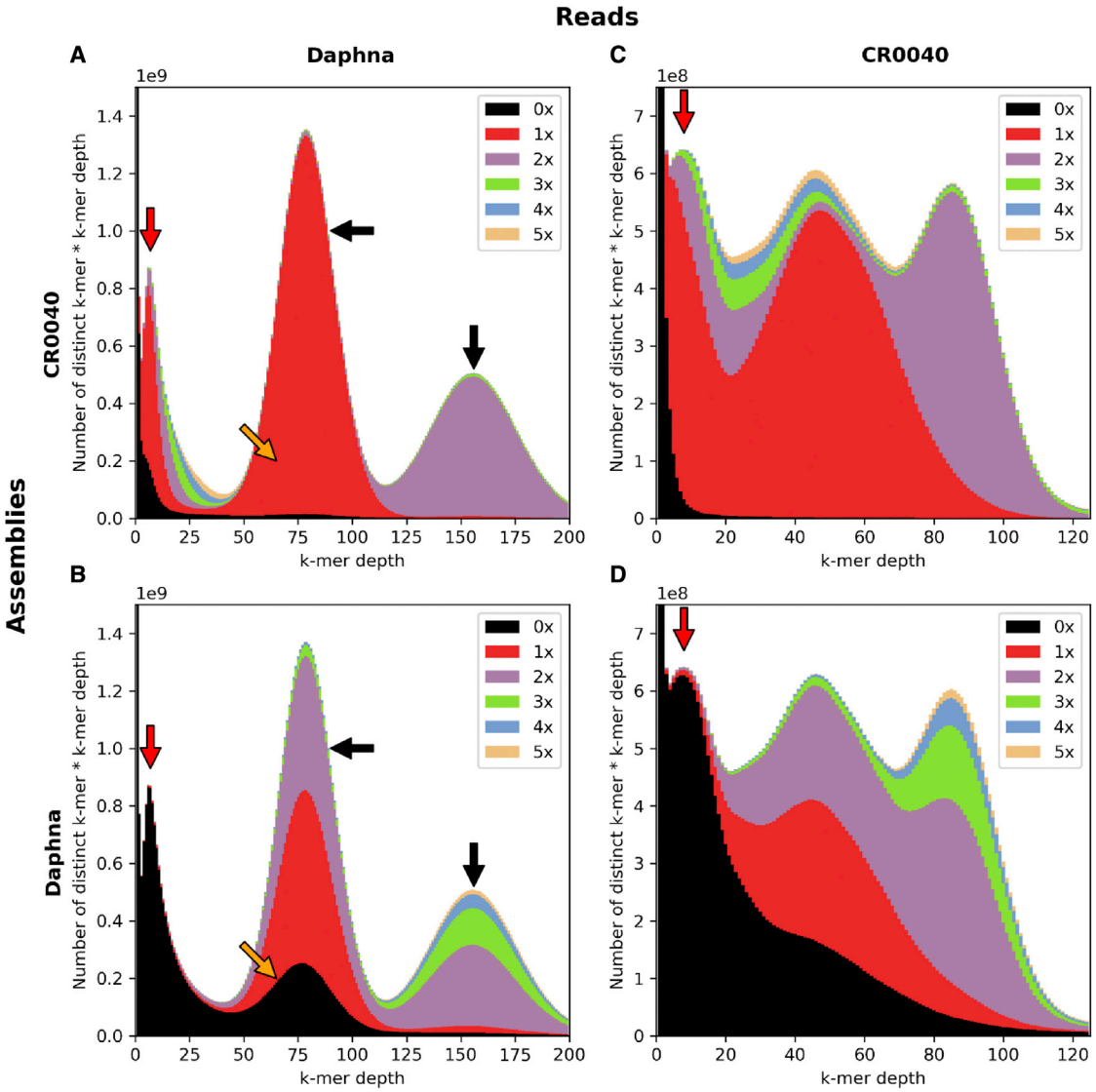

Figure 3. Assembly k-mer content comparison between CR0040 PacBio HiFi long reads and Daphna Illumina short reads using spectra-cn graph.

(A–D) The x axis represents k-mer multiplicity (counts), and the y axis indicates the number of distinct k-mers multiplied by their counts. Because of different sequencing depths between read sets, the y axis upper values are 10^9 for **(A)** and **(B)** and 10^8 for **(C)** and **(D)**. The area colors indicate the number of k-mer copies found in the assembly (black: 0× or missing k-mers, red: 1×, purple: 2×, green: 3×, blue: 4×, and orange: 5×). Four spectra-cn plots are presented: **(A)** Daphna reads versus CR0040 assembly, **(B)** Daphna reads versus Daphna assembly, **(C)** CR0040 reads versus CR0040 assembly, and **(D)** CR0040 reads versus Daphna assembly. The red arrows point toward a low-coverage k-mer distribution not expected in a diploid genome assembly spectra-cn graph. The black arrows point toward the heterozygous (on the left) and homozygous (on the right) k-mer distributions expected in a diploid genome assembly. The orange arrows point toward missing k-mers in the heterozygous k-mer distribution. The lower the black distribution at this location, the fewer k-mers are missing in the assembly.

compared to the chromosome sequences (Figure 5), with median ratio values equal to 0.27 and 0.036, respectively, showing a significant difference (Wilcoxon-Mann-Whitney test; p = 4e−13). However, chromosomes 7A and 6B were outliers, showing also a high proportion of low-depth k-mers. In addition, the distribution of these k-mers along the genome was globally consistent with the areas identified, except for some discrepancies (Supplemental Figure 10). Chromosomes 6B and 7A showed strong signals in terms of low-depth k-mer proportions, as already pointed out in Figure 5. Indeed, on chromosome 6B, k-mers of this type were positioned on nearly all the assembled sequence, whereas they were localized on approximately half of the assembled chromosome 7A sequence.

Orthologs of cell cycle regulator genes involved in *A. thaliana* endoreplication

A search for orthologs of the CDK and cyclin (Cyc) families of *A. thaliana*, involved in the regular endoreplication mechanism, showed that representatives of these two families were indeed found in the proteomes of CR0040 and *P. aphrodite* (Supplemental Table 17). However, the number of genes

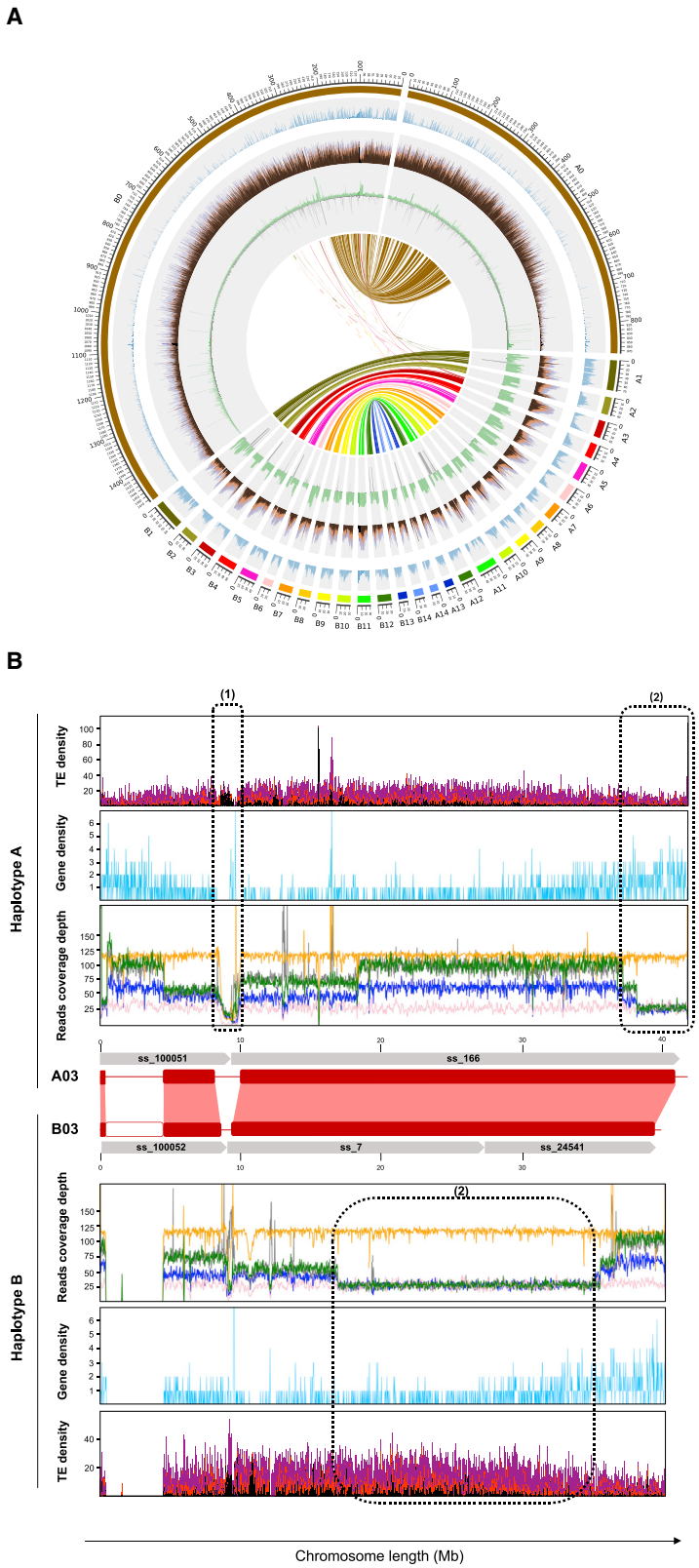

Figure 4. Overview of the assembled vanilla genome.

(A) Circos plot of the genomic content along *V. planifolia* haplotypes A and B and the relationship between them. All tracks are divided into 500 kb genomic windows. From the outside to the inside of the circular representation, ideograms of 28 chromosomes and two random mosaic chromosomes that contain the unanchored scaffolds are shown. Gene density (blue) and interspersed repeat RepeatMasker hit density (black: retroelements; orange: long terminal repeat/Copia; purple: long terminal repeat/Gypsy) are shown. Sequencing depth was obtained by mapping CR0040 PacBio HiFi reads on the assembly (green) and N density (gray). Syntenic blocks across haplotypes are connected by lines in the innermost part of the figure.

(B) Sequencing depth along the CR0040 A03 and B03 chromosomes (red rectangles) obtained by mapping Daphna Illumina (yellow) and ONT (pink) reads and CR0040 PacBio HiFi (blue), Nanopore (green), and Illumina (gray) reads onto the CR0040 assembly. Synteny between homologous chromosomes is represented by red boxes. Gaps (N stretches) that explain sudden drops in sequencing depth are shown with white blocks. (1) Low level of sequencing depth for all data is shown. (2) Inverted level of sequencing depth for CR0040 between haplotypes A and B and constant level of sequencing depth for both Daphna haplotypes are shown. Gene and retrotransposon distributions along the chromosomes are represented by a blue line chart and a stacked histogram (Copia: red; Gypsy: purple; other retrotransposons: black), respectively.

encoding CDKs and Cycs found via the orthogroups approach was lower for these two species. For example, the gene encoding CycD3-1 in *A. thaliana* (At4g34160) was part of a species-specific orthogroup that contained some other D-type Cyc genes. Regarding genes encoding regulatory proteins of the CDK–Cyc complexes, all of them had orthologs in both orchids. However, it appeared that these multigenic families were slightly under-represented in the CR0040 gene annotation compared with those of *A. thaliana* and *P. aphrodite*. Finally, an imbalance between the A and B haplotypes was observed for Fizzy-related proteins and CDK inhibitor (Krp) orthologs.

Vanilla Genome Hub

The Vanilla Genome Hub (VGH) (https://vanilla-genome-hub.cirad.fr) has been developed to support post-genomics efforts. It centralizes vanilla genomic information with a set of user-friendly interconnected modules and interfaces for the analysis and visualization of genomic data. From the main menu of the VGH (Supplemental Note 6; Figure 6A), the search for genes of interest to biologists is simplified using the interoperable system by the identification of paralogous genes using keywords and sequence homology (Figure 6B and 6C) and the production of an information report with gene name, gene localization, and polypeptide function (Figure 6D). The genome browser was built to offer tracks of supplemental information, such as GC content, gene structure, gene expression, DNA-seq depth, and repeat composition to support the identification of new genes of interest (Figure 6E and Supplemental Figure 11). A metabolic pathway reconstruction and visualization tool enables the identification of annotated genes involved in pathways (Figure 6F). A Gene Ontology enrichment tool enables testing and visualization of enrichment according to a Gene Ontology category of a gene group (Figure 6G). Finally, comparative analysis at the genome scale is supported by an interactive multiscale synteny visualization (Figure 6H).

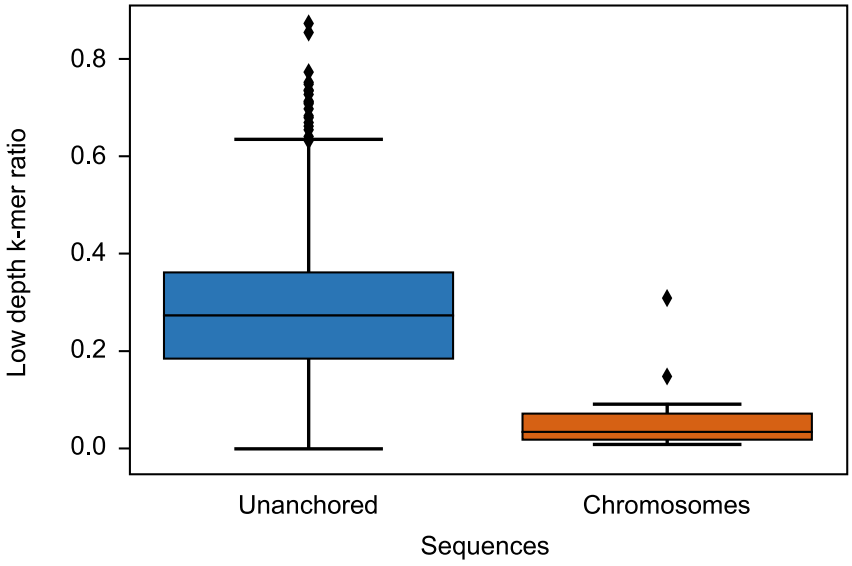

Figure 5. Ratio of k-mers within unanchored and anchored CR0040 genome.
This boxplot shows the ratio of k-mers with a depth less than 15 in our HiFi reads within unanchored sequences (blue) and within chromosomes (orange).

DISCUSSION

Flow cytometry and cytogenetic data validate genome size and chromosome content

Genome size, ploidy level, and chromosome content of the *V. planifolia* CR0040 cultivar were validated by FCM and cytogenetic analyses. The estimated size of 4.09 Gb indicated a ploidy level similar to those of other traditional diploid *V. planifolia* cultivars (Bory et al., 2008; Lepers-Andrzejewski et al., 2011). Estimation of endoreplication levels confirmed PE, as previously described in *V. planifolia* (Brown et al., 2017). This species was shown to exhibit diploidized meiotic chromosome pairing with 16 bivalents (Bory, 2007). This result demonstrates the complete diploidization of this supposed segmental paleo-allotetraploid (Ravindran, 1979; Nair and Ravindran, 1994). The same meiotic observation was also performed for *Vanilla* × *tahitensis* by Lepers-Andrzejewski et al. (2011). Aneuploid chromosome numbers were frequently observed in mitotic metaphases of *V. planifolia* (Nair and Ravindran, 1994; Bory et al., 2008), possibly owing to the observed mitotic associations that could lead to unequal anaphase separation. This may lead to errors in the evaluation of basic chromosome number, as was the case in a recent paper in which the authors considered that the basic number was $x = 14$ (Hasing et al., 2020). The phenomenon of aneuploidy apparently occurs only in somatic cells, whereas meiosis appears to be regular, with a stable number of chromosomes (Bory, 2007). Although the CR0040 assembly is more complete than that of Daphna, only 14 pseudomolecules were obtained because CR0040 scaffolds were anchored on the 14 Daphna pseudomolecules. Chromosomes 15 and 16 are probably non-endoreplicated and present in the unanchored part (CR0040_A0 and CR0040_B0).

PE hinders whole-genome assembly

Given the CR0040 diploid genome size estimate of 4.09 Gb by FCM, our genome assembly represented around 83% of the expected genome size and was twice the size of the Daphna genome published previously (Hasing et al., 2020). This difference could be explained by the fact that the CR0040 genome was assembled from HiFi reads that enabled the assembly of repetitive regions in different contigs despite their low sequencing depth. We were thus able to assemble a greater number of repeated sequences that may correspond to a large fraction of the non-endoreplicated genome and were missing from the Daphna genome assembly. The biological reality of this hypothesis is reinforced by the consistency of the k-mer depth profiles and sequencing depth patterns that resulted from the mapping of reads from different sequencing technologies (HiFi, 10X, and ONT) tested in this study for CR0040 (Supplemental Figure 9). A k-mer spectra-cn diagram is an efficient tool for visually comparing the k-mer compositions of reads and assemblies. Such diagrams are used to validate diploid or haploid assembly quality (Yen et al., 2020). The k-mer spectra-cn diagram clearly shows a general diploid pattern, with a heterozygous distribution containing only k-mers present once in the assembly and a homozygous distribution containing, as expected, only k-mers present twice in the assembly. Unexpectedly for a diploid genome, this figure includes a third distribution that is located in the low-coverage area of the diagram. The color pattern shows clearly that these k-mers present in low frequencies (5–15 times) are also present in our assembly. These k-mers represent the non-repeated fraction of low-coverage sections of the assembly, which are mainly located in the unanchored sequences but are also present in low-coverage sections of other chromosomes. Even if the unanchored sequences are mainly built of repeats, they also harbor genes and other non-repeated blocks, and these portions are large enough in terms of k-mers to generate this unexpected k-mer distribution in the spectra-cn plot. These k-mers are not present in the public *V. planifolia* Daphna assembly, and therefore, the corresponding distribution is black in Figure 3B.

Molecular signatures of partial endoreplication

The abundance of interspersed repeats detected in CR0040 was consistent with already mentioned data in other orchids, such as *P. equestris* (Cai et al., 2015) and *P. aphrodite* (Chao et al., 2018), and in other lineages, like the *Oryza* genus (Stein et al., 2018). The high content of retrotransposons and low content of DNA transposons were in the range of what has been found for different orchids (Cai et al., 2015; Chao et al., 2018). High repeat content was found in candidate non-endoreplicated regions, which is in agreement with previous descriptions in other orchids (Chumová et al., 2021). Furthermore, some types of repeats may be preferentially found in non-endoreplicated regions, as shown by differences in repeat proportions, particularly

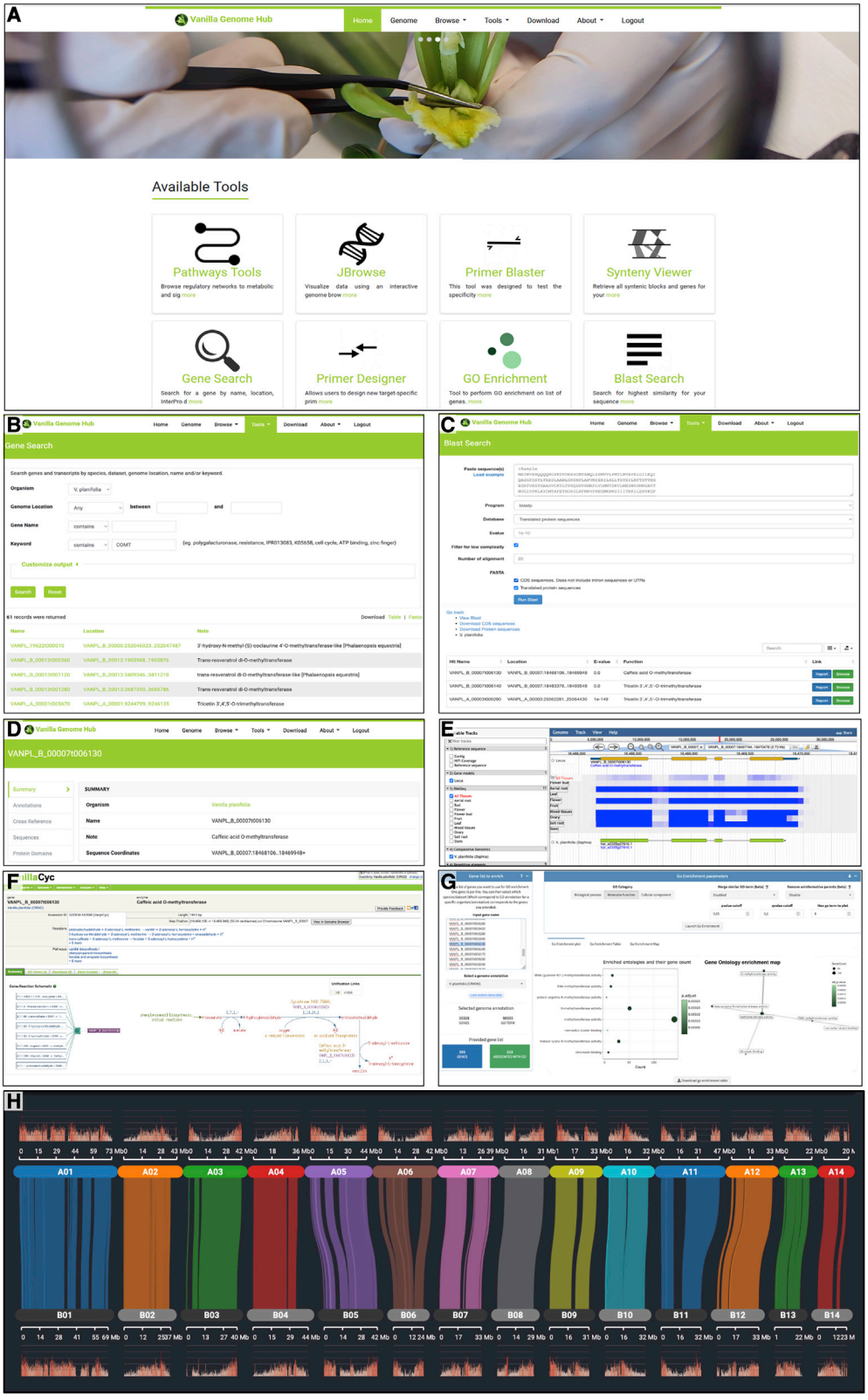

Figure 6. Overview (screen shots) of some interoperable vanilla genome analysis tools integrated into the Vanilla Genome Hub.
(A) Main menu.
(B) Gene search (Tripal MegaSearch).
(C) Sequence homology search (Blast).

(legend continued on next page)

retrotransposon proportions, between assembled chromosomes and unanchored sequences. Thus, long interspersed nuclear elements, for example, occupy a larger portion of the unanchored regions than of the 14 chromosomes, even though these regions are overrepresented in the present assembly. However, the lack of a more detailed annotation of the retrotransposon class hampers the search for a potential preferential distribution of repeat families between endoreplicated and non-endoreplicated regions. It is therefore crucial to better annotate these repeats in order to determine exactly which kinds are found preferentially in the two fractions of the genome. On the other hand, the distribution of genes in the genome shows the opposite trend, with approximately two-thirds of the protein-coding sequences localized in the anchored region.

The distinct sequencing depth profiles observed between CR0040 and Daphna probably reflected a tissue-specific endoreplication pattern. Indeed, the nodes used to sequence the CR0040 genome are growing and differentiating tissues, whereas the leaves used to sequence the Daphna genome are composed of fully differentiated cells. The irregular haplotype-specific endoreplication pattern (segmental or not) observed in CR0040 could thus result from a peculiar physiological activity. Whatever the reason, this intriguing pattern suggests a complex and fine regulation of PE at the chromosome level, which deserves further study. Although no previous study has demonstrated the mechanisms underlying PE in orchids, many works have focused on the regulation of regular endoreplication found in a large number of plant species and well analyzed in tomato and *Arabidopsis* (Lang and Schnittger, 2020). The common mechanism that triggers endoreplication is a downregulation of mitotic CDK activity to suppress mitosis and a fine regulation of this activity throughout the induced endocycle, with an alternation between high and low activity levels at specific checkpoints in order to maintain the replication process (De Veylder et al., 2011; Shimotohno et al., 2021). CDK controls cell-cycle progression and mitosis entry via its phosphorylation activity, which is activated by association with CYC proteins. Recently, Inada et al. (2021) demonstrated the involvement of actin and actin-binding protein in the regulation of *A. thaliana* endoreplication. The present whole-genome analysis made it possible to identify orthologous CDK, Cycs, CDK-activators and repressors, and actin depolymerizing factors in *V. planifolia* CR0040. A first step in understanding orchid PE would therefore be to further analyze these molecular regulators. Indeed, the recognition of orthologs and paralogs in large gene families, such as the CDK–Cyc complex, is challenging and requires deeper investigation by high-quality manual annotation of the genes of interest (Vaattovaara et al., 2019).

Although PE seems specific to orchids in plants (Trávníček et al., 2015), this phenomenon of under-represented genomic regions is well known in metazoans. Ciliates, such as *Paramecium tetraurelia* and *Tetrahymena thermophile*, show programmed DNA elimination following endoreplication in their macronucleus (MAC), involving chromosome fragmentation and elimination of specific sequences called internal eliminated sequences (IESs) (Bracht et al., 2013; Sellis et al., 2021). However, FCM approaches in *Ludisia discolor*, an orchid subject to PE, have ruled out the possibility of such DNA elimination and favor the hypothesis of under-replication (Hřibová et al., 2016). Under-replication has also been studied in several organisms, such as *Drosophila*, in which it has been proposed that a reduction in the expression of genes involved in DNA replication may lead to a slower mitosis S phase and an incomplete replication of genomic regions during late S phase (Lilly and Spradling, 1996). Molecular mechanisms described in Drosophila highlighted an inhibition of replication fork progression involving Rif1 protein, which interacts with the SUUR protein (Munden et al., 2018; Armstrong et al., 2019).

Finally, cytogenetic studies using *in situ* hybridization techniques (fluorescence *in situ* hybridization [FISH] and genomic *in situ* hybridization) could also be used to increase our knowledge of the molecular signatures of PE (Younis et al., 2015). A recent advance in FISH is the development of probes based on synthetic oligonucleotides specific to repetitive sequences or to particular chromosome regions (Jiang, 2019). This new generation of FISH probes in plants has been applied to species with sequenced genomes, such as *Zea* and *Cucumis* species (Han et al., 2015; Martins et al., 2019; Braz et al., 2020; Zhang et al., 2021a). Endoreplicated versus non-endoreplicated genomic regions could be used to synthesize oligo-based FISH probes specific to each fraction in order to precisely locate these PE signatures on chromosomes. The genomic *in situ hybridization* technique uses the total genomic DNA of a species, in contrast to FISH. We hypothesize that hybridizing the total DNA of highly endoreplicated nuclei (16E and 32E) to CR0040 chromosomes would induce a more intense hybridization signal in endoreplicated regions, thus enabling us to identify non-endoreplicated areas that showed little hybridization.

Impact of technologies on whole-genome evolution analysis

The strategy of combining optical mapping with HiFi long-read sequencing for the CR0040 genome assembly resulted in a haplotype A with 14 pseudomolecules of better quality and with fewer scaffolding errors than the Daphna haplotype A, which was built with Hi-C and ONT technologies (Hasing et al., 2020). Indeed, comparisons between the Daphna and CR0040 A haplotypes revealed a dual-haplotype conservation problem in the Daphna phased assembly, which is reflected in the Daphna Hi-C scaffolding. The use of HiFi long reads and optical maps enabled more accurate haplotype separation, as shown in previous works (Matthews et al., 2018; Du et al., 2020). In the case of CR0040, not only did HiFi enable better assembly of non-endoreplicated regions but also Hifiasm allowed better separation of haplotypes. These improvements were therefore necessary to better solve the sequencing of the complex vanilla genome, with a high rate of heterozygosity (Ho *V. planifolia*

(D) Gene report (Tripal).
(E) Genome Browser (JBrowse).
(F) Metabolic pathway visualization (Pathway Tools).
(G) Gene Ontology enrichment (DIANE).
(H) Comparison of genomic sequences (SynVisio).

cultivars = 0.362; Favre et al., 2022) and subjected to PE (Brown et al., 2017). However, this dual-haplotype conservation problem observed in Daphna, and not in CR0040, impacted comparative pan-genomics analyses and distorted the results obtained. Thus, the differences observed between the two *V. planifolia* genomes (number of paralogs, numbers of gene families with expansions and contractions, and complete and duplicated Benchmarking Universal Single-Copy Orthologs scores) could be explained by these mosaic assembly problems and therefore by an incorrect separation between haplotypes A and B.

Monocot genome evolution analyses were carried out using the high-quality haplotype A sequence of CR0040. Dot plot results were in agreement with the fact that *V. planifolia* is a diploidized paleo-polyploid species with a primary basic chromosome number $x = 8$ and a secondary basic number $x = 16$, as described for the whole *Vanilla* genus (Felix and Guerra, 2005). Moreover, only one locus (two spots) of rDNA (18S-5.8S-26S) was identified in the genome of *V. planifolia* by cytogenetic approaches, which provides additional evidence of an ancient diploidization of this supposed segmental paleo-allotetraploid. Finally, two WGDs, possibly corresponding to α° and τ^{m}, were highlighted, as also described for the *Dendrobium chrysotoxum* chromosome-scale genome assembly (Zhang et al., 2021b).

Efficiency of an integrative approach combining cytogenetics with high-quality whole-genome sequencing

In this study, we confirmed the size and structure of the *V. planifolia* genome using both cytogenetics and nuclear DNA-seq methods. The particular phenomenon of PE at play in many orchids has been explored at the chromosome level for the first time in plants, to our knowledge. Our data showed that the non-endoreplicated sequences are very predominantly made up of repeated sequences. This confirmed, at the genomic level, previous findings in orchids by Chumová et al. (2021) based on a phylogenetics generalized least squares model and by Brown et al. (2017), who used nuclei imaging to demonstrate that in *Vanilla*, on the other hand, the endoreplicated part was transcribed. We nevertheless revealed that 33% of the 59 128 annotated protein-coding genes were present in the two random mosaic chromosomes, corresponding mainly to the non-endoreplicated part, as shown by low sequencing depth. In addition, a thorough examination of sequencing depths along anchored chromosomes with three different technologies revealed 73 regions whose different endoreplication levels vary with haploid phase, half of which may be linked to tissue type (leaves versus nodes). This last conclusion remains to be confirmed with DNA-seq from different tissues of the same cultivar. This work constitutes considerable progress in our understanding of *V. planifolia* genomics and sheds light on the most relevant methodologies for further deciphering this complex genome and the PE phenomenon. The VGH was built to help the community to address major unresolved questions about vanilla, such as PE, biosynthesis of aromatic compounds, and resistance to pathogens. We are working on a new version of the vanilla nuclear genome sequence that will be improved in terms of haplotype separation, chromosome reconstruction, and gene and repeat element annotation in order to further investigate the molecular mechanisms of PE with appropriate plant material, biotechnologies, and bioinformatics tools.

METHODS

Cytometry, cytogenetics, and DNA sequencing

A traditional vanilla cultivar (CR0040) from Reunion Island was used in this study (Supplemental Note 1). FCM and cytogenetics studies were performed using protocols described in Supplemental Note 1. High-molecular-weight DNA and ultra-high-molecular-weight DNA were extracted from node tissues and sequenced using PacBio HiFi, ONT, and Illumina technologies (Supplemental Note 1). Optical genome maps were produced using the Bionano Genomics protocol and the Saphyr G1 System (Supplemental Note 1).

Genome assembly and analysis

HiFi reads were assembled into contigs using Hifiasm 0.13 with default parameters (Cheng et al., 2021). The hybrid scaffolding between DNA contigs and optical genome maps was performed using the hybrid Scaffold pipeline of Bionano Genomics with default parameters. These scaffolds were phased into two haplotypes using in-house scripts, and the unscaffolded contigs were phased using purge dups (https://github.com/dfguan/purge_dups). Then, pseudomolecules were reconstructed using alignments of the phased assembly on Daphna chromosomes (Hasing et al., 2020; Supplemental Note 2). The assembly quality was estimated with QUAST 5.1.0 (Gurevich et al., 2013) and using the approach of Benchmarking Universal Single-Copy Orthologs (version 5.0.0) (Simao et al., 2015; Supplemental Note 2). The k-mer analysis was performed with kat 2.4.2 using the comp tool (Mapleson et al., 2017). The plot script was slightly modified to project on the y axis the number of distinct k-mers multiplied by the k-mer multiplicity instead of just the number of distinct k-mers. In parallel, k-mers of size 47 with a depth between 5 and 15 were extracted within PacBio sequences using Jellyfish 2.3.0 (Marcais and Kingsford, 2011). These k-mers were repositioned on our reference using the tool "query_per_sequence" (https://github.com/gmarcais/Jellyfish/tree/master/examples/query_per_sequence), and the ratio of these k-mers was computed among each sequence of our genome. These sequences were split between chromosomes and unanchored sequences, and the repartition of the k-mer ratio was drawn using the python seaborn library (https://seaborn.pydata.org/).

Structural and functional genome annotation

Automatic gene prediction was performed on CR0040 contigs with the EuGene Eukaryotic Pipeline (EGNEP version 1.5) (Sallet et al., 2019; Supplemental Note 3). Transcriptomic data from CR0040 were produced using RNA sequencing of nine organs with Illumina technology (Supplemental Note 3). In addition, gene expression profiles and putative novel isoforms were identified with StringTie v.2.0.3 (Kim et al., 2019; Supplemental Note 3). Transcriptomic data from *V. planifolia* cultivars (CR0040, Daphna [NCBI BioProjects: PRJNA668740 and PRJNA633886], and an unspecified cultivar [NCBI GEO: GSE134155]); proteomic data from *V. planifolia* Daphna (Hasing et al., 2020), *P. equestris* (NCBI BioProject: PRJNA382149), and the *Liliopsida* class (Swissprot: 2020_06); and a custom orchid-specific statistical model for splice-site detection were used for this analysis (Supplemental Note 3). Functions were assigned through InterProScan domain searches as well as similarity searches against the UniProt/Swissprot and UniProt/TrEMBL databases (BlastP). Gene Ontology terms were assigned through InterProScan (Jones et al., 2014) results, and enzyme classification numbers were predicted by combining the tools PRIAM (Claudel-Renard et al., 2003) and BlastKOALA (Kanehisa et al., 2016).

Repeats were first identified using RepeatModeler v.2.0.1 (Flynn et al., 2020), RepeatScout v.1.0.5, and transposable element genes predicted from EGNEP annotation and then classified with REPET v.3.0 (Flutre

et al., 2011) and PASTEC v.2.0 (Hoede et al., 2014) according to Wicker's transposable element classification (Wicker et al., 2007). After cleaning steps (see details in Supplemental Note 3), repeats were clustered using CD-HIT v.4.8.1 (Fu et al., 2012) to produce two banks of repeats. The CR0040 genome was then annotated for repeats using previous banks, RepeatMasker v.4.1.1 (Tarailo-Graovac and Chen, 2009), and bedtools intersect v.2.29.2 (Quinlan and Hall, 2010).

Genomic comparisons and reconstruction of gene families

To compare the 14 haplotype A chromosomes of both vanilla cultivars, check the completeness of the *Vanilla* genome, and study the pan-orchid α° WGD, a series of analyses were performed with the CoGe SynMap pipeline as described in Supplemental Note 4. Gene family reconstruction was performed using OrthoFinder2 (v.2.4.0) (Emms and Kelly, 2019). Genes known to be involved in cell cycle control in *A. thaliana*, such as Cycs, CDKs, and known regulators of these genes, were searched in the CR0040 and *P. aphrodite* proteomes with a combination of BlastP searches and orthogroups. This analysis was applied to CDK-A and B types as well as Cyc-A, B, and D types. Regulators of these genes included CDK inhibitor (KRP), transcriptional repressor ILP1, WEE1, actin depolymerizing factor, and Fizzy-related proteins.

Detection of non-endoreplicated genomic regions

Reads from each sequencing technology used in this study (HiFi, ONT, and Illumina reads from CR0040), as well as ONT and Illumina reads from Daphna, were mapped onto the CR0040 assembly. Illumina short reads and long reads (HiFi and ONT) were mapped onto the CR0040 assembly using BWA-MEM2 (Vasimuddin et al., 2019) and Minimap2 (Li, 2018), respectively. Sequencing depths were averaged for genomic windows of 20 kb. To detect sequencing depth bias and limit the risk of detecting false positives, the mean sequencing depth for every 20 successive 20-kb windows was computed using Illumina reads for Daphna and using long reads (HiFi and ONT) for CR0040. Identified regions were manually validated and refined by visualization of sequencing depth drops for each CR0040 chromosome and for all available sequencing datasets (see details in Supplemental Note 5).

VGH

The VGH was constructed using the Tripal system, a specific toolkit for the construction of online community genomic databases, by integrating the GMOD Chado database schema and the Drupal open-source platform (https://www.drupal.org/). The VGH implements a set of interconnected modules and user-friendly interfaces (details in Supplemental Note 6).

Data availability

The chromosome assembly and accompanying data received the following identifiers in NCBI: BioProject (with SRA database) ID: PRJNA753216 (haplotype A) and PRJNA754028 (haplotype B) BioSample (node) SAMN20691751.

RNA sequencing data are readily accessible on the NCBI portal: BioSamples SAMN20691786 (fruit), SAMN20691787 (leaf), SAMN20691788 (flower), SAMN20691789 (stem), SAMN20691790 (soil root), SAMN20691791 (aerial root), SAMN20691792 (bud), SAMN20691793 (flower bud), SAMN20691794 (ovary), SAMN20691795 (mixed tissues) and SRA: SRR15411867 (mixed tissues), SRR15411868 (ovary), SRR15411869 (flower bud), SRR15411870 (bud), SRR15411871 (aerial root), SRR15411872 (soil root), SRR15411873 (stem), SRR15411874 (flower), SRR15411875 (leaf), and SRR15411876 (fruit)

In addition, these data and various exploration tools are accessible at VGH (https://vanilla-genome-hub.cirad.fr/).

SUPPLEMENTAL INFORMATION

Supplemental information can be found online at *Plant Communications Online*.

FUNDING

This work was supported by grants from Eurovanille and V. Mane Fils companies. The research was co-funded by the Centre de Coopération Internationale en Recherche Agronomique pour le Développement (CIRAD), the Université de La Réunion (UR), the Institut National de Recherche pour l'Agriculture l'Alimentation et l'Environnement (INRAE), the Centre National de la Recherche Scientifique (CNRS), and the Etablissement Vanille de Tahiti (EVT). This work was also supported by grants from the European Regional Development Fund (ERDF), the Conseil Régional de la Réunion, and the Conseil Départemental de la Réunion. This work was supported by France Génomique National infrastructure, funded as part of "Investissement d'avenir" program managed by Agence Nationale pour la Recherche (contrat ANR-10-INBS-09) and has also benefited from Imagerie-Gif core facility supported by l'Agence Nationale de la Recherche (ANR-11-EQPX-0029/Morphoscope, ANR-10-INBS-04/FranceBioImaging; ANR-11-IDEX-0003-02/Saclay Plant Sciences).

AUTHOR CONTRIBUTIONS

C.J., M.D., M.G., and P.B. contributed to conceptualization of the study. C.C., C.J., G.S., M.B., M.D., O.B., S.B., and W.M. designed the experiments. M.B. and S.S.-Y. performed flow cytometry and cytogenetic experiments and analyses. L.B. and J.Z. contributed to the funding of the research, monitored the progress of the work, and supported the researchers throughout the project. C.C., C.L.-R., O.B., and W.M. performed nucleic acid preparation and sequencing. C.C., C.J., C.K., G.D., G.S., Q.P., S.B., and W.M. performed sequence analyses and assemblies. C.C., G.D., Q.P., S.B., and S.L.-A. performed genome annotation and built the genome hub. C.C., C.J., C.K., M.G., Q.P., and W.M. outlined the manuscript and wrote first drafts. C.C., C.J., C.K., C.L.-R., G.D., G.S., M.B., M.D., M.G., P.B., Q.P., S.B., S.S.-Y., and W.M. provided input and revisions to the manuscript.

ACKNOWLEDGMENTS

We are grateful to Jean Bernard Dijoux and Katia Jade for preparing the plant material and to the Plant Protection Platform (3P, IBISA) for lab facilities and access to plant resources (BRC Vatel). We acknowledge the SouthGreen Bioinformatics Platform (http://www.southgreen.fr/) for access to computational resources and the GeT-PlaGe platform (INRAE, Toulouse, France) for the use of sequencing facilities. Finally, the authors would like to thank the reviewers for their suggestions, which helped to improve the manuscript. No conflict of interest is declared.

Received: October 30, 2021
Revised: April 10, 2022
Accepted: April 27, 2022
Published: May 5, 2022

REFERENCES

Armstrong, R.L., Penke, T., Chao, S.K., Gentile, G.M., Strahl, B.D., Matera, A.G., McKay, D.J., and Duronio, R.J. (2019). H3K9 promotes under-replication of pericentromeric heterochromatin in Drosophila salivary gland polytene chromosomes. Genes **10**:93. https://doi.org/10.3390/genes10020093.

Bhosale, R., Boudolf, V., Cuevas, F., Lu, R., Eekhout, T., Hu, Z.B., Van Isterdael, G., Lambert, G.M., Xu, F., Nowack, M.K., et al. (2018). A spatiotemporal DNA endoploidy map of the Arabidopsis root reveals roles for the endocycle in root development and stress adaptation. Plant Cell **30**:2330–2351. https://doi.org/10.1105/tpc.17.00983.

Bory, S. (2007). Diversity of *Vanilla planifolia* in the Indian Ocean and its Related Species : Genetics, Cytogenetics and Epigenetics Aspect (France: Université de La Réunion).

Bory, S., Catrice, O., Brown, S., Leitch, I.J., Gigant, R., Chiroleu, F., Grisoni, M., Duval, M.F., and Besse, P. (2008). Natural polyploidy in *Vanilla planifolia* (Orchidaceae). Genome **51**:816–826. https://doi.org/10.1139/G08-068.

Bourdon, M., Pirrello, J., Cheniclet, C., Coriton, O., Bourge, M., Brown, S., Moise, A., Peypelut, M., Rouyere, V., Renaudin, J.P., et al. (2012). Evidence for karyoplasmic homeostasis during endoreduplication and a ploidy-dependent increase in gene transcription during tomato fruit growth. Development **139**:3817–3826. https://doi.org/10.1242/dev.084053.

Bracht, J.R., Fang, W., Goldman, A.D., Dolzhenko, E., Stein, E.M., and Landweber, L.F. (2013). Genomes on the edge: programmed genome instability in ciliates. Cell **152**:406–416. https://doi.org/10.1016/j.cell.2013.01.005.

Braz, G.T., do Vale Martins, L., Zhang, T., Albert, P.S., Birchler, J.A., and Jiang, J.M. (2020). A universal chromosome identification system for maize and wild Zea species. Chromosome Res. **28**:183–194. https://doi.org/10.1007/s10577-020-09630-5.

Brown, S.C., Bourge, M., Maunoury, N., Wong, M., Wolfe Bianchi, M., Lepers-Andrzejewski, S., Besse, P., Siljak-Yakovlev, S., Dron, M., and Satiat-Jeunemaître, B. (2017). DNA remodeling by strict partial endoreplication in orchids, an original process in the plant kingdom. Genome Biol. Evol. **9**:1051–1071. https://doi.org/10.1093/gbe/evx063.

Cai, J., Liu, X., Vanneste, K., Proost, S., Tsai, W.C., Liu, K.W., Chen, L.J., He, Y., Xu, Q., Bian, C., et al. (2015). The genome sequence of the orchid *Phalaenopsis equestris*. Nat. Genet. **47**:65–72. https://doi.org/10.1038/ng.3149.

Chao, Y.T., Chen, W.C., Chen, C.Y., Ho, H.Y., Yeh, C.H., Kuo, Y.T., Su, C.L., Yen, S.H., Hsueh, H.Y., Yeh, J.H., et al. (2018). Chromosome-level assembly, genetic and physical mapping of *Phalaenopsis aphrodite* genome provides new insights into species adaptation and resources for orchid breeding. Plant Biotechnol. J. **16**:2027–2041. https://doi.org/10.1111/pbi.12936.

Cheng, H., Concepcion, G.T., Feng, X., Zhang, H., and Li, H. (2021). Haplotype-resolved de novo assembly using phased assembly graphs with hifiasm. Nat. Methods **18**:170–175. https://doi.org/10.1038/s41592-020-01056-5.

Chumová, Z., Záveská, E., Hloušková, P., Ponert, J., Schmidt, P.A., Čertner, M., Mandáková, T., and Trávníček, P. (2021). Repeat proliferation and partial endoreplication jointly shape the patterns of genome size evolution in orchids. Plant J. Cel. Mol. Biol. **107**:511–524. https://doi.org/10.1111/tpj.15306.

Claudel-Renard, C., Chevalet, C., Faraut, T., and Kahn, D. (2003). Enzyme-specific profiles for genome annotation: PRIAM. Nucleic Acids Res. **31**:6633–6639. https://doi.org/10.1093/nar/gkg847.

De Veylder, L., Larkin, J.C., and Schnittger, A. (2011). Molecular control and function of endoreplication in development and physiology. Trends Plant Sci. **16**:624–634. https://doi.org/10.1016/j.tplants.2011.07.001.

Doležel, J., Bartoš, J., Voglmayr, H., and Greilhuber, J. (2003). Letter to the editor. Cytom. Part A **51A**:127–128.. https://doi.org/10.1002/cyto.a.10013.

Du, K., Stock, M., Kneitz, S., Klopp, C., Woltering, J.M., Adolfi, M.C., Feron, R., Prokopov, D., Makunin, A., Kichigin, I., et al. (2020). The sterlet sturgeon genome sequence and the mechanisms of segmental rediploidization. Nat. Ecol. Evol. **4**:841–852. https://doi.org/10.1038/s41559-020-1166-x.

Emms, D.M., and Kelly, S. (2019). OrthoFinder: phylogenetic orthology inference for comparative genomics. Genome Biol. **20**, 20Artn. https://doi.org/10.1186/S13059-019-1832-Y.

Favre, F., Jourda, C., Grisoni, M., Piet, Q., Rivallan, R., Dijoux, J.B., Hascoat, J., Lepers-Andrzejewski, S., Besse, P., and Charron, C. (2022). A genome-wide assessment of the genetic diversity, evolution and relationships with allied species of the clonally propagated crop *Vanilla planifolia* Jacks. Ex Andrews. Genet. Resour. Crop Ev. https://doi.org/10.1007/s10722-022-01362-1.

Felix, L.P., and Guerra, M. (2005). Basic chromosome numbers of terrestrial orchids. Plant Syst. Evol. **254**:131–148. https://doi.org/10.1007/s00606-004-0200-9.

Flutre, T., Duprat, E., Feuillet, C., and Quesneville, H. (2011). Considering transposable element diversification in de novo annotation approaches. Plos One **6**:e16526, **6**ARTN. https://doi.org/10.1371/journal.pone.0016526.

Flynn, J.M., Hubley, R., Goubert, C., Rosen, J., Clark, A.G., Feschotte, C., and Smit, A.F. (2020). RepeatModeler2 for automated genomic discovery of transposable element families. Proc. Natl. Acad. Sci. U S A **117**:9451–9457.. https://doi.org/10.1073/pnas.1921046117.

Fu, L.M., Niu, B.F., Zhu, Z.W., Wu, S.T., and Li, W.Z. (2012). CD-HIT: accelerated for clustering the next-generation sequencing data. Bioinformatics **28**:3150–3152. https://doi.org/10.1093/bioinformatics/bts565.

Gurevich, A., Saveliev, V., Vyahhi, N., and Tesler, G. (2013). QUAST: quality assessment tool for genome assemblies. Bioinformatics **29**:1072–1075. https://doi.org/10.1093/bioinformatics/btt086.

Han, Y.H., Zhang, T., Thammapichai, P., Weng, Y.Q., and Jiang, J.M. (2015). Chromosome-specific painting in Cucumis species using bulked oligonucleotides. Genetics **200**:771–779. https://doi.org/10.1534/genetics.115.177642.

Hasing, T., Tang, H.B., Brym, M., Khazi, F., Huang, T.F., and Chambers, A.H. (2020). A phased *Vanilla planifolia* genome enables genetic improvement of flavour and production. Nat. Food **1**:811–819. https://doi.org/10.1038/s43016-020-00197-2.

Hoede, C., Arnoux, S., Moisset, M., Chaumier, T., Inizan, O., Jamilloux, V., and Quesneville, H. (2014). PASTEC: an automatic transposable element classification tool. PLoS One **9**:e91929, **9**ARTN e91929. https://doi.org/10.1371/journal.pone.0091929.

Hřibová, E., Holušová, K., Trávníček, P., Petrovská, B., Ponert, J., Šimková, H., Kubátová, B., Jersáková, J., Čurn, V., Suda, J., et al. (2016). The enigma of progressively partial endoreplication: new insights provided by flow cytometry and next-generation sequencing. Genome Biol. Evol. **8**:1996–2005. https://doi.org/10.1093/gbe/evw141.

Inada, N., Takahashi, N., and Umeda, M. (2021). Arabidopsis thaliana subclass I ACTIN DEPOLYMERIZING FACTORs and vegetative ACTIN2/8 are novel regulators of endoreplication. J. Plant Res. **134**:1291–1300. https://doi.org/10.1007/s10265-021-01333-0.

Jiang, J.M. (2019). Fluorescence *in situ* hybridization in plants: recent developments and future applications. Chromosome Res. **27**:153–165. https://doi.org/10.1007/s10577-019-09607-z.

Jones, P., Binns, D., Chang, H.Y., Fraser, M., Li, W., McAnulla, C., McWilliam, H., Maslen, J., Mitchell, A., Nuka, G., et al. (2014). InterProScan 5: genome-scale protein function classification. Bioinformatics (Oxford, England) **30**:1236–1240. https://doi.org/10.1093/bioinformatics/btu031.

Kanehisa, M., Sato, Y., and Morishima, K. (2016). BlastKOALA and GhostKOALA: KEGG tools for functional characterization of genome and metagenome sequences. J. Mol. Biol. **428**:726–731. https://doi.org/10.1016/j.jmb.2015.11.006.

Kim, D., Paggi, J.M., Park, C., Bennett, C., and Salzberg, S.L. (2019). Graph-based genome alignment and genotyping with HISAT2 and HISAT-genotype. Nat. Biotechnol. **37**:907–915. https://doi.org/10.1038/s41587-019-0201-4.

Lang, L., and Schnittger, A. (2020). Endoreplication - a means to an end in cell growth and stress response. Curr. Opin. Plant Biol. **54**:85–92. https://doi.org/10.1016/j.pbi.2020.02.006.

Lee, H.O., Davidson, J.M., and Duronio, R.J. (2009). Endoreplication: polyploidy with purpose. Genes Dev. **23**:2461–2477. https://doi.org/10.1101/gad.1829209.

Lepers-Andrzejewski, S., Siljak-Yakovlev, S., Brown, S.C., Wong, M., and Dron, M. (2011). Diversity and dynamics of plant genome size: an example of polysomaty from a cytogenetic study of Tahitian vanilla (Vanilla ×tahitensis, Orchidaceae). Am. J. Bot. **98**:986–997. https://doi.org/10.3732/ajb.1000415.

Li, H. (2018). Minimap2: pairwise alignment for nucleotide sequences. Bioinformatics **34**:3094–3100. https://doi.org/10.1093/bioinformatics/bty191.

Lilly, M.A., and Spradling, A.C. (1996). The Drosophila endocycle is controlled by Cyclin E and lacks a checkpoint ensuring S-phase completion. Genes Dev. **10**:2514–2526. https://doi.org/10.1101/gad.10.19.2514.

Mapleson, D., Garcia Accinelli, G., Kettleborough, G., Wright, J., and Clavijo, B.J. (2017). KAT: a K-mer analysis toolkit to quality control NGS datasets and genome assemblies. Bioinformatics **33**, btw663–576. https://doi.org/10.1093/bioinformatics/btw663.

Marcais, G., and Kingsford, C. (2011). A fast, lock-free approach for efficient parallel counting of occurrences of k-mers. Bioinformatics **27**:764–770. https://doi.org/10.1093/bioinformatics/btr011.

do Vale Martins, L., Yu, F., Zhao, H.N., Dennison, T., Lauter, N., Wang, H.Y., Deng, Z.H., Thompson, A., Semrau, K., Rouillard, J.M., et al. (2019). Meiotic crossovers characterized by haplotype-specific chromosome painting in maize. Nat. Commun. **10**, **10**Artn. https://doi.org/10.1038/s41467-019-12646-z.

Matthews, B.J., Dudchenko, O., Kingan, S.B., Koren, S., Antoshechkin, I., Crawford, J.E., Glassford, W.J., Herre, M., Redmond, S.N., Rose, N.H., et al. (2018). Improved reference genome of *Aedes aegypti* informs arbovirus vector control. Nature **563**:501–507. https://doi.org/10.1038/s41586-018-0692-z.

Munden, A., Rong, Z., Sun, A., Gangula, R., Mallal, S., and Nordman, J.T. (2018). Rif1 inhibits replication fork progression and controls DNA copy number in Drosophila. eLife **7**:e39140.. https://doi.org/10.7554/eLife.39140.

Nair, R.R., and Ravindran, P.N. (1994). Somatic association of chromosomes and other mitotic abnormalities in *Vanilla planifolia* (andrews). Caryologia **47**:65–73. https://doi.org/10.1080/00087114.1994.10797284.

Perez-Silva, A., Odoux, E., Brat, P., Ribeyre, F., Rodriguez-Jimenes, G., Robles-Olvera, V., Garcia-Alvarado, M.A., and Gunata, Z. (2006). GC-MS and GC-olfactometry analysis of aroma compounds in a representative organic aroma extract from cured vanilla (*Vanilla planifoli*a G. Jackson) beans. Food Chem. **99**:728–735. https://doi.org/10.1016/j.foodchem.2005.08.050.

Quinlan, A.R., and Hall, I.M. (2010). BEDTools: a flexible suite of utilities for comparing genomic features. Bioinformatics **26**:841–842.. https://doi.org/10.1093/bioinformatics/btq033.

Ravindran, P.N. (1979). Nuclear behavior in the sterile pollen of *Vanilla planifolia* (andrews). Cytologia **44**:391–396. https://doi.org/10.1508/cytologia.44.391.

Sallet, E., Gouzy, J., and Schiex, T. (2019). EuGene: an automated integrative gene finder for eukaryotes and prokaryotes. Gene Prediction: Methods Protoc. **1962**:97–120. https://doi.org/10.1007/978-1-4939-9173-0_6.

Sellis, D., Guérin, F., Arnaiz, O., Pett, W., Lerat, E., Boggetto, N., Krenek, S., Berendonk, T., Couloux, A., Aury, J.M., et al. (2021). Massive colonization of protein-coding exons by selfish genetic elements in Paramecium germline genomes. PLoS Biol. **19**:e3001309. https://doi.org/10.1371/journal.pbio.3001309.

Shimotohno, A., Aki, S.S., Takahashi, N., and Umeda, M. (2021). Regulation of the plant cell cycle in response to hormones and the environment. Annu. Rev. Plant Biol. **72**:273–296. https://doi.org/10.1146/annurev-arplant-080720-103739.

Simao, F.A., Waterhouse, R.M., Ioannidis, P., Kriventseva, E.V., and Zdobnov, E.M. (2015). BUSCO: assessing genome assembly and annotation completeness with single-copy orthologs. Bioinformatics **31**:3210–3212.. https://doi.org/10.1093/bioinformatics/btv351.

Stein, J.C., Yu, Y., Copetti, D., Zwickl, D.J., Zhang, L., Zhang, C., Chougule, K., Gao, D., Iwata, A., Goicoechea, J.L., et al. (2018). Genomes of 13 domesticated and wild rice relatives highlight genetic conservation, turnover and innovation across the genus *Oryza*. Nat. Genet. **50**:285–296. https://doi.org/10.1038/s41588-018-0040-0.

Tarailo-Graovac, M., and Chen, N. (2009). Using RepeatMasker to identify repetitive elements in genomic sequences. In Current Protocols in Bioinformatics, A.D. Baxevanis, ed.

Trávníček, P., Čertner, M., Ponert, J., Chumová, Z., Jersáková, J., and Suda, J. (2019). Diversity in genome size and GC content shows adaptive potential in orchids and is closely linked to partial endoreplication, plant life-history traits and climatic conditions. New Phytol. **224**:1642–1656. https://doi.org/10.1111/nph.15996.

Trávníček, P., Ponert, J., Urfus, T., Jersáková, J., Vrána, J., Hřibová, E., Doležel, J., and Suda, J. (2015). Challenges of flow-cytometric estimation of nuclear genome size in orchids, a plant group with both whole-genome and progressively partial endoreplication. Cytometry Part A. Journal Int. Soc. Anal. Cytol. **87**:958–966. https://doi.org/10.1002/cyto.a.22681.

Vaattovaara, A., Leppälä, J., Salojärvi, J., and Wrzaczek, M. (2019). High-throughput sequencing data and the impact of plant gene annotation quality. J. Exp. Bot. **70**:1069–1076. https://doi.org/10.1093/jxb/ery434.

Vasimuddin, M., Misra, S., Li, H., and Aluru, S. (2019). Efficient architecture-aware acceleration of BWA-MEM for multicore systems. Int. Parall Distrib P, 314–324. https://doi.org/10.1109/Ipdps.2019.00041.

Wicker, T., Sabot, F., Hua-Van, A., Bennetzen, J.L., Capy, P., Chalhoub, B., Flavell, A., Leroy, P., Morgante, M., Panaud, O., et al. (2007). A unified classification system for eukaryotic transposable elements. Nat. Rev. Genet. **8**:973–982, nrg2165 [pii]. https://doi.org/10.1038/nrg2165.

Yen, E.C., McCarthy, S.A., Galarza, J.A., Generalovic, T.N., Pelan, S., Nguyen, P., Meier, J.I., Warren, I.A., Mappes, J., Durbin, R., et al. (2020). A haplotype-resolved, de novo genome assembly for the wood tiger moth (*Arctia plantaginis*) through trio binning. GigaScience **9**:giaa088, ARTN. https://doi.org/10.1093/gigascience/giaa088.

Younis, A., Ramzan, F., Hwang, Y.J., and Lim, K.B. (2015). FISH and GISH: molecular cytogenetic tools and their applications in ornamental plants. Plant Cell Rep. **34**:1477–1488. https://doi.org/10.1007/s00299-015-1828-3.

Zhang, T., Liu, G.Q., Zhao, H.N., Braz, G.T., and Jiang, J.M. (2021a). Chorus2: design of genome-scale oligonucleotide-based probes for fluorescence *in situ* hybridization. Plant Biotechnol. J. **19**:1967–1978. https://doi.org/10.1111/pbi.13610.

Zhang, Y.X., Zhang, G.Q., Zhang, D.Y., Liu, X.D., Xu, X.Y., Sun, W.H., Yu, X., Zhu, X.E., Wang, Z.W., Zhao, X., et al. (2021b). Chromosome-scale assembly of the *Dendrobium chrysotoxum* genome enhances the understanding of orchid evolution. Hortic. Res-england **8**, **8** artn. https://doi.org/10.1038/s41438-021-00621-z.

Plant Communications, Volume *3*

Supplemental information

A chromosome-level, haplotype-phased *Vanilla planifolia* genome highlights the challenge of partial endoreplication for accurate whole-genome assembly

Quentin Piet, Gaetan Droc, William Marande, Gautier Sarah, Stéphanie Bocs, Christophe Klopp, Mickael Bourge, Sonja Siljak-Yakovlev, Olivier Bouchez, Céline Lopez-Roques, Sandra Lepers-Andrzejewski, Laurent Bourgois, Joseph Zucca, Michel Dron, Pascale Besse, Michel Grisoni, Cyril Jourda, and Carine Charron

SUPPLEMENTAL INFORMATION

Supplemental Note 1

Global strategy for the sequencing and assembly of *V. planifolia* CR0040 genome

The assembly of the CR0040 genome and the study of the partial endoreplication (PE) phenomenon required interdisciplinary work and a multitude of sequencing technologies, which has proven to be crucial for the detection to detect PE along the assembled chromosomes (Supplemental Figure 1).

Plant material

A traditional *Vanilla planifolia* cultivar from La Reunion was used for this study. It is conserved by CIRAD under the accession number CR-VA-00040 ("CR0040") in the Biological Resources Center Vatel (Saint Pierre, La Réunion) where it is maintained by cuttings under shade-house and by *in vitro* culture established from axillary buds. The vitroplants were propagated by micro-cuttings in basal Murashige and Skoog media (Duchefa Biochemie, The Netherlands) without any phytohormone. They were grown at 24-26°C, 12H light/day. Morphological data and genetic analyses confirm its taxonomic position within the *V. planifolia* species (Bory et al., 2008; Bouétard et al., 2010; Favre et al., 2022), and its membership of the group of vanilla cultivars usually grown in the Indian Ocean region. The profile of aromatic precursors identified in its fruits is typical of vanillas used for Bourbon vanilla production (Perez-Silva et al., 2006).

Flow cytometry

The total nuclear DNA amount was assessed by flow cytometry (FCM) as described in Bourge et al. (2018). Internal reference used for cytometry was *Petunia hybrida* Vilm. "PxPc6" (2C=2.85 pg). Leaves of the internal standard and nodal tissues from three to five month-old *in vitro V. planifolia* CR0040 were chopped using a razor blade in a plastic Petri dish with 1 ml of Gif nuclei-isolation buffer (45 mM $MgCl_2$, 30 mM sodium citrate, 60 mM MOPS, 1% (w/v) polyvinylpyrrolidone 10,000, pH 7.2) containing 0.2% (w/v) Triton X–100, supplemented with 5 mM sodium metabisulphite and RNAse (2.5 U/mL). The suspension was filtered through 50-µm nylon mesh. The nuclei were stained with 70-100 µg/ml propidium iodide, a specific DNA fluorochrome intercalating dye, and kept 5 min at 4°C. DNA content of 5,000–10,000 stained nuclei were determined for each sample using a cytometer (CytoFLEX S, Beckman Coulter, Excitation 561 nm; emission through a 610/20 nm band-pass filter). Nuclei were identified by a gate on Side-Scatter and propidium iodide (PI)-Area and the cytogram of PI-Area versus PI-Height signals served to

select singlets, to eliminate doublets and to detect any degradation. Different cell ploidy levels were identified by their fluorescence intensity in PI, compared to the standard. The DNA histogram of nodal tissues from *Vanilla planifolia* CR0040 and nuclear classes in FCM samples are illustrated in the Supplemental Figure 2 and Supplemental Table 1, respectively. Note that there was a large variability between each endoploidy proportions for the 13 individuals.

The component F represents the Fixed part of the haploid genome which does not endoreplicate. The component P represents the part potentially participating in endoreplication. P and F are proportions (and not amounts) of the genome (%), whereas p and f are amounts (typically pg). Note that, as proportions, F and P have the same value whether referring to the haploid or to the diploid genome. As described in Brown et al. 2017, the replicate fraction P is assessed from the relative fluorescence intensity (I, arbitrary units) of peak#2 (4E, the first endocycle population) to peak#1 (2C nuclei): $P = [(Ipeak2 / Ipeak1) – 1] \times 100$

In quantitative terms, the haploid nucleus is (1f+1p) pg, and diploid nucleus is (2f+2p) pg. So 4E nuclei have four copies of the part of the genome which replicates, and two copies of the rest of the genome which does not replicate, in total 2f+4p (pg). The 8E nuclei have 2f+8p (pg), etc.

Cytogenetics

Root tips were obtained from *Vanilla planifolia* CR0040 plantlets cultivated in vitro in the VATEL biological resource center based in La Réunion. They were pretreated with 0.05% colchicine aqueous solution at room temperature during 1h and then fixed in absolute ethanol and glacial acetic acid (3:1) for at least two days at 4 °C. Root tips were hydrolyzed in 1 M HCl for 12 min at 60 °C, washed in distilled water at room temperature, and stained in 1% orcein in 45% acetic acid for about 30 min. Root tip meristems were squashed in a droplet of acetic carmine and observed under Zeiss Axiophot microscopes. Chromosome number was determined on five to seven well-spread metaphase plates from each of seven of those in vitro cultivated plantlets. The best metaphase plates were photographed using a CCD camera (RETIGA 2000R; Princeton Instruments, Evry, France).

For fluorochrome banding (Chromomycin A_3, Hoechst 33258 and DAPI- 4′,6-diamidino-2-phenylindole), the meristems were hydrolyzed for about 1 h at 37° C in an enzymatic mixture composed of 4% cellulase RS (Onozuka Yakult Honsha Co.), 1% pectolyase Y23 (Seishin Pharmaceutical Co, Tokyo, Japan), and 4% hemicellulase (Sigma Chemical Co) in 0.01M citrate buffer at pH 4.6. Thus, digested meristems were squashed into a drop of freshly prepared 50% acetic acid and the preparations were observed using an epifluorescence Zeiss Axiophot microscope with different combinations of excitation and emission filter sets (01, 07, 15, and triple 25). The best slides were frozen at -80ºC at least during 12 h. The coverslips were removed and the slides

were rinsed with absolute ethanol and air-dried. To detect GC- and AT-rich DNA regions, meristematic tissue was stained respectively with chromomycin A_3 (CMA) (Serva, France) according to Schweizer (1976), and with Hoechst 33258 (Ho; Sigma) according to Martin and Hesemann (1988) with minor modifications of Siljak-Yakovlev et al. (2002). The slides were mounted in citifluor AF2 (Agar Scientific Oxford Instruments, Stanstead, UK). The DAPI was used to observe an unspecific heterochromatin. The acquisition and treatment of images were performed using a highly sensitive CCD camera (RETIGA 2000R, Princeton Instruments, Evry, France) and an image analyzer (MetaVue, Evry, France).

High molecular weight DNA extraction and sequencing

High molecular weight (HMW) DNA was extracted from 1g of nodal tissues from *in vitro* cultured *Vanilla planifolia* CR0040 in order to minimize the endoreplicated phenomenon using QIAGEN genomic tip kit. DNA libraries and sequencing were performed at GeT-PlaGe core facility, INRAe Toulouse.

The Sequel2 HiFi library preparation and sequencing were performed according to the manufacturer's instructions "Procedure and Checklist Preparing HiFi SMRTbell Libraries using SMRTbell Express Template Prep Kit 2.0". At each step, DNA was quantified using the Qubit dsDNA HS Assay Kit (Life Technologies). DNA purity was tested using the nanodrop (Thermofisher) and size distribution and degradation assessed using the Femto pulse Genomic DNA 165 kb Kit (Agilent). Purification steps were performed using AMPure PB beads (PacBio) and 15µg of DNA was purified then sheared at 15kb using the Megaruptor3 system (Diagenode). A single strand overhang removal and a DNA and END damage repair step were performed on 10µg of sample using SMRTbell Express Template prep kit 2.0. Then blunt hairpin adapters were ligated to the library. The library was treated with an exonuclease cocktail to digest unligated DNA fragments. A size selection step using a 12kb cutoff was performed on the BluePippin Size Selection system (Sage Science) with "0.75% DF Marker S1 3-10 kb Improved Recovery" protocol. Using Sequel® II Binding kit 2.0 and sequencing kit 2.0, the primer V2 annealed and polymerase 2.0 bounded library was sequenced by diffusion loading onto 3 SMRTcells on Sequel2 instrument at 55pM with a 2 hours pre-extension and a 30 hours movie. HiFi reads are produced by calling consensus from subreads generated by multiple passes of the enzyme around a circularized template from a single zero mode waveguide. HiFi reads were generated with the "Circular Consensus Sequencing (CCS)" pipeline in SMRT Link v8.0 (ccs, version 4.0.0) with default parameters (minimum predicted accuracy of 0.99, minimum number of passes = 3)".

The Chromium libraries were prepared according to 10X Genomics' protocols using the Genome Reagent Kits v2. The sample quantity and quality controls were validated on Qubit, Nanodrop and

Femto. Optimal performance has been characterized on input gDNA with a mean length greater than 50 kb. The libraries were prepared from 3 µg of HMW gDNA (cut off at 50Kb using the BluePippin system). Briefly, in the microfluidic Genome Chip, a library of Genome Gel Beads is combined with HMW template gDNA in Master Mix and partitioning oil to create Gel Bead-In-EMulsions (GEMs) in the Chromium. Each Gel Bead is functionalized with millions of copies of a 10x™ Barcoded primer. Upon dissolution of the Genome Gel Bead in the GEM, primers containing (i) an Illumina R1 sequence (Read 1 sequencing primer), (ii) a 16 bp 10x Barcode, and (iii) a 6 bp random primer sequence are released. Read 1 sequence and the 10x™ Barcode are added to the molecules during the GEM incubation. P5 and P7 primers, read 2, and sample index are added during library construction. 10 cycles of PCR were applied to amplify libraries. Library quality was assessed using a Fragment Analyser and libraries were quantified by QPCR using the Kapa Library Quantification Kit. The libraries have been performed on an Illumina HiSeq3000 using a paired-end read length of 2x150 pb with the Illumina HiSeq3000 sequencing kits.

Oxford Nanopore Technologies (ONT) library preparation and sequencing were performed according to the manufacturer's instructions "1D gDNA selecting for long reads (SQK-LSK109)". At each step, DNA was quantified using the Qubit dsDNA HS Assay Kit (Life Technologies). DNA purity was tested using the nanodrop (Thermofisher) and size distribution and degradation assessed using the Fragment analyzer (AATI) High Sensitivity DNA Fragment Analysis Kit. Purification steps were performed using AMPure XP beads (Beckman Coulter). 8 libraries were prepared, for each library, 5µg of DNA was purified then sheared at 20kb to 40kb using the megaruptor 1 system (diagenode). A one step DNA damage repair + END-repair + dA tail of double stranded DNA fragments was performed on 2µg of sample. Then adapters were ligated to the library. Libraries were loaded onto 3 R9.4.1 revD GridION flowcells and sequenced on GridION instrument at 30fmol within 48H and onto 5 R9.4.1 revD PromethION flowcells and sequenced on PromethION instrument at 25 fmol within 72H.

DNA-seq data production per technology and instrument are indicated in the Supplemental Table 2.

Ultra-HMW DNA extraction and Optical mapping

Ultra-HMW DNA were purified from one gram of nodal tissues at the base of the young leaves according to the Bionano Prep Plant tissue DNA Isolation Liquid Nitrogen Grinding Protocol (30177 - Bionano Genomics) with the following specifications and modifications. Briefly, the tissues were broken in liquid nitrogen and then ground with rotor stator in the homogenization buffer. Nuclei were washed and then embedded in agarose plugs. After overnight proteinase K digestion in the presence of Lysis Buffer (Bionano Genomics) and one-hour treatment with RNAse A (Qiagen), plugs were washed four times in 1x Wash Buffer (Bionano Genomics) and five times

in 1x TE Buffer (ThermoFisher Scientific). Then, plugs were melted two minutes at 70°C and solubilized with 2 µL of 0.5 U/µL AGARase enzyme (ThermoFisher Scientific) for 45 minutes at 43°C. A dialysis step was performed in 1x TE Buffer (ThermoFisher Scientific) for 45 minutes to purify DNA from any residues. The DNA samples were quantified by using the Qubit dsDNA BR Assay (Invitrogen). The presence of mega base size DNA was visualized by pulsed field gel electrophoresis. Labeling and staining of the uHMW DNA were performed according to the Bionano Prep Direct Label and Stain (DLS) protocol (30206 - Bionano Genomics). Briefly, labeling was performed by incubating 750 ng genomic DNA with 1× DLE-1 Enzyme (Bionano Genomics) for 2 hours in the presence of 1× DL-Green (Bionano Genomics) and 1× DLE-1 Buffer (Bionano Genomics). Following proteinase K digestion and DL-Green cleanup, the DNA backbone was stained by mixing the labeled DNA with DNA Stain solution (Bionano Genomics) in presence of 1× Flow Buffer (Bionano Genomics) and 1× DTT (Bionano Genomics), and incubating overnight at room temperature. The DLS DNA concentration was measured with the Qubit dsDNA HS Assay (Invitrogen). Labelled and stained DNA was loaded on the Saphyr chip. Loading of the chip and running of the Bionano Genomics Saphyr System were all performed according to the Saphyr System User Guide (30247 - Bionano Genomics). Data processing was performed using the Bionano Genomics Access software (https://bionanogenomics.com/support-page/bionano-access-software/). A total of 590 Gb data with molecules larger than 150kb was produced and then *de novo* assembled according to the Access software. It produced 950 genome maps with a N50 of 4.6 Mbp for a total genome map length of 2,115 Gbp.

Supplemental Note 2

Genome assembly and pseudomolecules construction

Illumina 10X, ONT and PacBio HiFi reads were assembled using respectively Supernova (v.2.1.1, Weisenfeld et al., 2017), Flye (v.2.4.2-release, https://github.com/fenderglass/Flye, Kolmogorov et al., 2019) followed by three iterative polishing with Illumina data using Pilon (v.1.22, https://github.com/broadinstitute/pilon, Walker et al., 2014) and Hifiasm v.0.13 (Cheng et al., 2021), with default parameters. A meta-assembly of corrected ONT reads from Canu and PacBio HiFi reads was tentatively generated using Hifiasm. The assembly metrics were computed with QUAST 5.1.0 (Gurevich et al., 2013) and summarized in Supplemental Table 3.

Hybrid scaffolding was performed between the best assembly (PacBio HiFi assembly) and optical genome maps with hybridScaffold pipeline and default parameters (https://bionanogenomics.com/wp-content/uploads/2018/04/30073-Bionano-Solve-Theory-of-

Operation-Hybrid-Scaffold.pdf). We obtained 874 hybrid scaffolds with the maximum size of 32 Mb, reaching 1.9 Gb and N50 of 6.2Mb. The not anchored contigs represent 1,529 Mb and 23,037 contigs from the PacBio assembly. This hybrid scaffold file is composed of the 2 allelic versions of the genome. In order to separate the alleles, we used an in-house script. Briefly, the fasta file is transformed into an optical maps file (.cmap). This cmap file is aligned against itself using Bionano tools to create a xmap file that has the information of all the scaffold id that align against each scaffold id. With this information, a parsing algorithm, coded in java, produces 2 files with 1 allele in each file. Contigs not belonging to scaffolds were split among haplotype using purge dups (https://github.com/dfguan/purge_dups). We then only kept contigs that were unassigned to scaffolds and added those from the "hap" file to haplotype A and those from the "purged" file to haplotype B. To organize the scaffolds into pseudomolecules, haplotype A fasta file was aligned against Daphna haplotype A chromosomes using the same Bionano tools. In that way, 36 scaffolds were organized in 14 chromosomes for haplotype A and 49 scaffolds for haplotype B.

Evaluation of assembly quality

The metrics for the best assembly were: assembly for haplotype A has 1.5 Gb, N50 = 3 Mb and 3,874 scaffolds or contigs and assembly for haplotype B has 1.9 Gb, N50 =0.4Mb and 17,655 scaffolds or contigs (Supplemental Table 4). We then looked for universal single copy orthologs genes with BUSCO 5.0.0. This analysis was done for the whole assembly and for both haplotypes apart on three levels of taxonomy using the following databases: viridiplantae_odb10, embryophyta_odb10 and liliopsida_odb10 (Supplemental Table 5).

Supplemental Note 3

RNA extraction and sequencing

Total RNA was extracted from nine organs (fruit, leaf, flower, stem, soil root, aerial root, axillary stem bud, flower bud and ovary) using the RNeasy Plant Mini kit, according to the manufacturer's protocol (Qiagen, Hilden, Germany). RNA purity, quantification, and integrity were evaluated using a NanoDrop 2000 spectrophotometer (Thermo Scientific, USA) and Agilent 4200 bioanalyzer (Agilent Technologies, Santa Clara, CA, USA). Only samples with an RNA Integrity Number (RIN) ≥ 8 were subjected to subsequent analysis and indicated in Supplemental Table 6.

RNA-seq libraries were prepared according to Illumina's protocols using the Illumina TruSeq Stranded mRNA sample prep kit to analyze mRNA at the GeT-PlaGe core facility, INRAe Toulouse. Briefly, mRNAs were selected using poly-T beads and then fragmented to generate

double stranded cDNA. Adaptors were ligated to cDNA and 11 cycles of PCR were applied to amplify libraries. Library quality was assessed using a Fragment Analyzer and then quantified by qPCR using the Kapa Library Quantification Kit. RNA-seq experiments were performed on an Illumina NovaSeq using a paired-end read length of 2x150 pb with the Illumina NovaSeq sequencing kits.

RNA-seq assembly and gene expression

RNA-seq reads of ten samples (the nine sequenced organs and a mix of them) were mapped onto the *Vanilla planifolia* CR0040 contig assembly using hisat2 (v.2.1.0) with default parameters (Kim et al., 2019), which resulted in one alignment file per sample. Each of these files were then coordinate-sorted and converted to BAM format in order for them to be compatible with the StringTie (v.2.0.3, Pertea et al., 2015), the RNA-seq alignment assembler used with default parameters. The resulting output files (gtf format) were used for a last StringTie run with the "--merge" option, thus producing a non-redundant set of transcripts as a single output file, corresponding to the final set of assembled transcripts. Main statistics of the RNA-seq experiment are detailed in Supplemental Table 7.

To estimate gene expression in the nine different tissues and to identify putative novel isoforms, we followed the StringTie's recommended protocol by realigning the corresponding RNA-Seq reads to the reference with hisat2 (v.2.2.1) using perl scripts provided by hisat2 (*extract_exon.py* and *extract_splice_sites.py*) to extract exon and splice site information from the annotation of the CR0040 final assembly. Alignment files were sorted by coordinates and converted to BAM format with the samtools utility (v.1.10). Then, RNA-seq reads were assembled using StringTie (v.2.0.3) with a GTF file containing transcripts coordinates from the annotation of the CR0040 assembly (-G option to specify the file), that is used to guide the assembly. The output files were then merged to remove redundancy between samples (StringTie v.2.0.3 with --merge and -G options) and to generate a single gtf file containing their coordinates. Finally, a final StringTie run was performed in order to re-estimate transcript abundance and generate read coverage tables (-B and -e options were used) for each sample, in regards to the merged set (-G option). These tables were then used by the prepDe.py script to compute genes and transcripts count matrices (see RNA-seq tracks in https://vanilla-genome-hub.cirad.fr/content/v-planifolia-cr0040).

A BUSCO analysis was performed using the Viridiplantae database to estimate the genic completeness for each transcriptome and for merged transcriptomes (Supplemental Table 8).

Structural and functional genome annotation

Automatic gene prediction was performed using EuGene Eukaryotic Pipeline (EGNEP v.1.5 with EuGene v.4.2a), an integrative gene finder software that is able to combine several sources of information in order to predict genes (Sallet et al., 2019). This pipeline can infer a structural gene annotation considering homology with known sequences, structural information in the form of GFF3 files and statistical information.

EuGene's internal prediction model can be built and trained using proteomic and transcriptomic data. Thus, a set of annotated *V. planifolia Daphna* proteins (NCBI Genomes: haplotype A, BioProject Accession: PRJNA633886, GenBank assembly accession: GCA_016413895.1 and haplotype B, BioProject Accession: PRJNA668740, GenBank assembly accession: GCA_016413885.1) as well as a combination of the non-redundant set of transcripts of *V. planifolia* CR0040 assembled with Stringtie and the *V. planifolia* Daphna annotated transcripts (*.rna_from_genomic.fna.gz) were submitted to the pipeline for this task. The rest of the proteomic data used as evidence are a combination of *Phalaenopsis equestris* proteins retrieved from RefSeq (NCBI RefSeq Genome: BioProject Accession: PRJNA382149, Annotation Release 100 accession: GCF_001263595.1) and the Uniprot/Swissprot *Liliopsida* database (2020_06 version). One Trinity assembly of a *Vanilla planifolia Jacks* (Solano-De la Cruz et al., 2019) retrieved from the NCBI database (NCBI Transcriptome: BioProject Accession: PRJNA554104, GEO Series: GSE134155) was also used as transcriptomic evidence. The pipeline comes with repeat detection software such as Red (Girgis et al., 2015) and LTRharvest (Ellinghaus et al., 2008), and similarity searches against RepBase (REPET, version 20.05) are also performed to clean the proteomic datasets at the start of the annotation process.

As EuGene also uses statistical models for splice sites detection, we built an orchids specific model from the genomic and transcriptomic data of *V. planifolia Daphna*, *Dendrobium catenatum* (NCBI RefSeq Genome: BioProject Accession: PRJNA453230, Annotation Release 101 acc: GCF_001605985.2), *Phalaenopsis equestris* (NCBI RefSeq), and our *V. planifolia* CR0040 clone using the egn_build_wam.pl companion script.

In order to assign functions to the predicted protein coding genes. InterProScan domain searches as well as similarity searches (BlastP) against Uniprot/Swissprot and Uniprot/TrEMBL databases were performed. Putative gene models were sorted into six confidence classes (from ISS_1 to ISS_6) based on their functional annotation. In order to filter protein coding genes, ISS_6 genes (96,224 sequences), ISS_5 genes with protein sequence shorter than 150 amino acids (aa) and with untranslated region (UTR) shorter than 35 base pairs (bp), and ISS_4 genes with protein sequences shorter than 80 amino acids and without UTR sequence were removed (98,718 sequences). Among remaining putative genes, ISS_5 genes, ISS_4 genes and ISS_3 fragments genes coding for protein sequences with matches in RepBase were also removed (3,527 sequences). In addition, putative

gene models with protein sequences predicted to have MULE transposase interpro domains (IPR018289) without match on FAR protein (FAR-RED impaired response 1, transcription activator that derived from ancient transposases) domain (IPR031052), or reverse transcriptase domain (IPR000477) without NMAT (nuclear intron maturase 1 mitochondrial, IPR024937) domain and TERT family domains (telomerase reverse transcriptase, IPR003545) were removed (589 sequences). Putative genes encoding for gagpol polyprotein and not associated to Benchmarking Universal Single-Copy Orthologs (BUSCO) and putative genes located on organellar contigs were removed (23,237 sequences). After filtering steps, 59,128 high-confidence protein coding genes were kept. The number of these genes per chromosome and per haplotype as well as main statistics of these genes are indicated in the Supplemental Tables 9 and 12.

Functions were assigned through InterProScan domain searches as well as similarity searches against Uniprot/Swissprot and Uniprot/TrEMBL databases (BlastP). Gene Ontology (GO) terms were assigned through InterProScan (Jones et al., 2014) results while Enzyme Classification (EC) numbers were predicted combining both tools PRIAM (Claudel-Renard et al., 2003) and BlastKOALA (Kanehisa et al., 2016).

Enzymes and metabolic pathways were predicted from the protein-coding genes using Pathway Tools (Karp et al., 2002). A file in the PathoLogic format was created, which included gene functional descriptions, GO terms and enzyme commission numbers. This file will be used to set up Pathways tools (see Supplemental Note 6). In order to assess the completeness of the resulting set of protein coding gene models, a BUSCO (Benchmarking Universal Single-Copy Orthologs) analysis (v4.0.5) was carried out using three different databases, namely Viridiplantae, Embryophyta and Liliopsida (Supplemental Table 10).

From repeats detected by EGNEP, 1,472 interspersed repeats were selected based on the consensi found by RepeatModeler (v2.0.1) (Flynn et al., 2020), enriched with consensi of RepeatScout (v1.0.5) (Price et al, 2005) and transposable element genes (TEG) predicted from EGNEP (REGN TEG), according to the following procedure of classification, filtering and clustering.

Consensi families were generated by RepeatScout (RS) and RepeatModeler (RM) from the CR0040 genome assembly (21,529 sequences): 1,247 TEG, 1,958 RS consensi and 1,236 RM consensi were then classified with REPET (v3.0) and PASTEC (v2.0) (Hoede et al., 2014) according to the Wicker's TE classification (Wicker et al., 2007) and using RepBase (REPET, version 23.12), cleaned by removing SSR and rDNA sequences, requalified with REPET postProcessClassif.py, then potential host genes were removed and finally clustered with CD-HIT (v4.8.1) (Fu et al., 2012). A first clustering (cd-hit -c 1 -sc 1) was made between the three filtered sets (1,072 RM, 1,748 RS and 284 TEG) to remove identical sequences. 46 repetitive sequences were removed by manual curation of the 42 clusters with more than 2 sequences (out of the 3,057 CD-HIT clusters

including 3,015 singletons) leading to 3,058 sequences. A second clustering (cd-hit -c 0.85 -sc 1 -aS 0.75) was made on the 3,058 sequences to help us to select 767 transposable elements TE, as follow: 338 RM TEs, 103 RS TE CD-HIT cluster representatives, 35 REGN TEG cluster representatives, 7 RS SINEs (RSX) that were not cluster representatives, 259 RS TE singletons not classified as unknown retrotransposon (RXX) and 25 REGN TEG singletons classified as DNA transposon (DTX). A third clustering (cd-hit -c 0.85 -sc 1 -aS 0.75) was made on the 693 RM unknown interspersed repeats (neither classified by RM nor by PASTEC) leading to a reduction of the set to 639 sequences. This sequence set was concatenated with the 66 RS TE singletons of the previous clustering and classified as unknown retrotransposon (RXX) and considered as doubtful TE, leading to 705 unknown interspersed repeats. Then, the genome assembly was annotated with RepeatMasker (v4.1.1, Tarailo-Graovac et al, 2009) using the two CR0040 interspersed repeat banks separately (sequences of 767 transposable elements and 705 unknown interspersed repeats available at https://vanilla-genome-hub.cirad.fr/filebrowser/download/188). Bedtools intersect (v2.29.2, Quinlan et al., 2010) allowed the TE annotation to be given priority over the unknown interspersed repeat annotation. Summary report of the repeat annotation is detailed in the Supplemental Table 11.

Supplemental Note 4

Gene families clustering

Polypeptide sequences of five plant species and CR0040 (14 chromosomes and CR0040_A0 and CR0040_B0 random mosaic chromosomes of unanchored scaffolds) were retrieved in order to carry out comparative genomic analyses between them: *Arabidopsis thaliana (*TAIR10, Phytozome) (Lamesch et al., 2012), *Oryza sativa* (IRGSP-1.0, RAP-DB), *Phalaenopsis equestris* (NCBI RefSeq), *Vanilla planifolia* Daphna (NCBI Genomes) and *Phalaenopsis aphrodite* (Orchidstra 2.0, Chao et al., 2017). For genes with alternative splicing variants, only the polypeptide corresponding to the longest transcript was kept and the two haplotypes of each *V. planifolia* cultivar were separated for the analyses. A total of 237,645 proteins were clustered with Orthofinder2 (v.2.4.0) using default parameters (Emms et al., 2019). A total of 212,852 proteins (89.5%) were clustered to 27,815 orthogroups (https://vanilla-genome-hub.cirad.fr/filebrowser/download/187) with 10.5% of the whole set were part of species-specific orthogroups, 8,317 were conserved in all the species/haplotypes and 1,426 corresponded to single-copy orthogroups. With this Orthofinder analysis, made from proteomes derived from the 14 chromosomes and unanchored scaffolds, we began to glimpse into the vanilla pangenome. The vanilla core genome is composed of 14,403

families and 86,688 genes, common to both CR40 and Daphna genomes. The dispensable genome of CR0040 contains 3,637 families and 17,258 genes specific to CR0040. The dispensable genome of Daphna contains 3,804 Daphna specific families and 13,529 genes.

The inferred orthogroups were visualized with the UpsetR (Conway et al., 2017) R package to generate the UpSet plot (Supplemental Figure 5). Among the compared datasets, 596 orthogroups were only shared by orchids and 1,029 were only shared by the 4 haplotypes of *V. planifolia* (Daphna and CR0040). Number of conserved and specific gene groups are detailed in the Supplemental Table 14.

Expansion and reduction of gene families with CAFE

Forty-seven protein coding genes involved in cell cycle regulation in *A. thaliana* were focused on (Supplemental Table 17), and orthogroups containing them were analyzed in terms of family evolution using CAFE (v5, Mendes et al., 2020). Orthogroups showing expansions and/or contractions in copy numbers, among the six compared plant lineages, were identified using a P value threshold of 0.001. For this, orthogroups (made from proteomes derived from the 14 chromosomes only) and the species tree produced by orthofinder were used as input. Prior to this analysis, orthogroups that contained genes in only one species or with more than 100 gene copies for at least one species were removed. The species tree was made into an ultrametric one with the make_ultrametric_tree.py script bundled with the orthofinder package using an original divergence of 152 Mya for the analyzed species, as referenced in the TreeTime database (Kumar et al., 2017). These filtered orthogroups, and the ultrametric species tree were utilized to estimate the expansion/contraction of orthogroups using one lambda (λ) model, where λ is a random birth-death parameter.

Construction of syntenic blocks

The SynMap workflow (Haug-Baltzell et al., 2017) of the CoGe comparative genomics platform (Lyons and Freeling, 2008) was used to generate syntenic dotplots between two organism genomes (haplotypes A of CR0040 and Daphna, as well as *P. aphrodite*). SynMap relies on pairwise comparison of Coding Sequences (CDS) between the two genomes and allows to compute the synonymous mutation rate of syntenic CDS pairs.

SynMap requires the genome sequence and a gene annotation file of each compared organism. Prior to the analyses, annotated genes in each species were filtered to keep only the longest isoform of each gene. For each genome in the comparison, the chromosome fasta file and the gene annotation gff3 file were loaded using the iCommands to the CyVerse's cloud-based Data Store. Be careful that all CDS of the same mRNA (*e.g.* ID=VANPL_A_00001g000010.mRNA1) should have the

same identifier (e.g. ID=VANPL_A_00001c000010; Parent=VANPL_A_00001g000010.mRNA1) otherwise SynMap will overestimate the number of CDSs and this will cause problems during the tandem gene filtering step. First, tandem duplications are filtered out with the blast_to_raw program (SynMap Analysis Log file of CR0040_A, https://genomevolution.org/coge/data/diags/62209/62209/1j9ym.log, source code https://github.com/LyonsLab/coge). Syntenic pairs of CDSs are then identified by finding collinear series of putative homologous sequences using DAGChainer (Haas et al., 2004). A global alignment is performed on these syntenic CDS pairs using the Needleman-Wunsch algorithm implemented in nwalign (https://pypi.org/project/nwalign/) using the BLOSUM62 scoring matrix, after which a back translation of this alignment into a codon alignment is processed. Then, codeml-coge, a modified implementation of CodeML from the PAML package (Yang et al., 2007) is used to compute the rate of synonymous substitutions per synonymous site for each pair of CDSs (dS called Ks on the SynMap interface). In the particular case where a genome was aligned against itself, the identical CDS pairs were removed from the analysis and therefore do not appear in either the SynMap dotplot (no dots on the central diagonal) or the Ks distribution. However, the dotplot is symmetrical around the central diagonal so only half the dotplot can be considered.

Visual quality control of the assemblies and whole genome duplication exploration using pairwise orchid genome synteny

In order to check the quality of the 14 chromosomes of the CR0040 A haplotype (CR0040_A) *V. planifolia* genome, to compare the 14 chromosomes of haplotype A of both *Vanilla* cultivars and to study the pan-orchid alpha Whole Genome Duplication (α^o WGD), a series of analyses were performed with the CoGe Synmap pipeline, as described above. Synmap pairwise genome synteny analyses between CR0040_A and Daphna A haplotype (D_A) and between themselves were illustrated in the Supplemental Figure 7. The dotplot of the CDS pairs of the 14 chromosomes of CR0040_A (Supplemental Figure 7E) and the histogram of the CDS pair Ks values (Supplemental Figure 7F) gives a genomic representation suggesting that the 14 chromosomes of CR0040_A and the gene annotation is complete and of high quality. The comparison of the CR0040_A dotplot with the D_A dotplot (Supplemental Figure 7A) shows that CR0040 A looks cleaner, with more continuous paralog diagonals. Also, the dotplot of D_A CDS against itself displays an unexpected dotted central diagonal indicating physically close duplicated genes. The cyan color of the diagonal indicates that the similar CDS pairs belong to the peak with a very low number of synonymous substitutions per synonymous site ($\log10(Ks) \approx -1.5$, light blue bars in the Supplemental Figure 7B). This artificial peak would correspond to allelic forms due to the heterozygosity and not to WGD paralogs. This peak could come from a problem of dual haplotype conservation during contig

phasing (difficulties to separate the two haplotypes when too close). The D_A karyotype illustrating the α° WGD (Hasing et al., 2020) was aligned onto the 14 chromosomes of the D_A to identify by projection the doplot diagonals corresponding to these 13 blocks of ohnologs (α° WGD paralogs). The ancestral karyotype of CR0040_A was drawn, using an in-house Perl script, from the D_A gene pair blocks (Table S10 in Hasing et al., 2020), transferred to CR0040_A genes via reciprocal best hits computed in Supplemental Note 6. On the CR0040_A dotplot, the diagonals corresponding to the 13 ohnologous blocks were also found, but with slight differences. For example, the difference found for block number 13, between chromosome 10 and 11, could be due to the fact that CR0040_A chromosome 11 (47 Mb with Ns; Supplemental Table 12) is longer than the D_A chromosome 11 (38 Mb; Supplemental Table 13). Similarly, on the dotplot of D_A versus CR0040_A (Supplemental Figure 7D), the karyotypes were aligned along the 14 chromosomes, allowing to find the diagonals corresponding to the 13 ohnolog blocks present on D_A and CR0040_A. The histogram of Ks values of CDS pairs between D_A and CR0040_A (Supplemental Figure 7C) shows two distinct peaks. The first one corresponds to allelic gene pairs between D_A and CR0040_A and the second one to onholog pairs. These analyses validate the already known pan-orchid WGD. Additional short diagonals on the CR0040_A dotplot and the second peak on the CR0040_A Ks histogram suggest an older WGD, probably the tau (τ^m) of Monocots (Hasing et al., 2020). The blue-green diagonals would correspond to the α° WGD (*e.g.* log10(Ks) < 0.2) while the shorter green-red ones would correspond to the monocot τ^m WGD (*e.g.* log10(Ks) > 0.2). The paralogous diagonals between chromosomes 3-5-6-14 could be taken as an example on the CR0040_A dotplot (Supplemental Figure 7E). Knowing that the α° WGD is relatively old (90 Mya; Hasing et al., 2020) and the sequence of the 14 pseudomolecules of CR0040_A is of high fidelity, it is possible that τ^m traces are seen. The biology of the species is also a consideration. Vanilla is perennial with predominant vegetative multiplication that could decrease the mutation rate (Sandler et al., 2020). The classical formula T = Ks / (2r) was applied, on a rough example from Supplemental Figure 7F, with a mutation rate 'r' of 6.5E-9 synonymous substitutions per synonymous site per generation (Tang et al., 2010). For instance, with a log10(Ks) peak median of 0.09, then the α° WGD would be dated at ≈ 95 Mya and with a median at 0.35, the τ^m WGD would be dated at ≈ 172 Mya, in agreement with Jiao et al., 2014.

Missing pairs of chromosomes 15 and 16 in the *V. planifolia* genome were tentatively searched by comparison with the *P. aphrodite* genome. Due to problems with *P. aphrodite* CDS positions at the chromosome level, gene sequences of *P. aphrodite* contigs were aligned to the *P. aphrodite* chromosomes using Liftoff (Shumate and Salzberg, 2021) as described in Supplemental Note 6 and these results were used for comparative genomics with CR0040 haplotype A sequence. Synmap pairwise genome synteny analyses of the 14 pseudomolecules of CR0040_A *V. planifolia*, the

pseudomolecules and longest scaffolds of *P. aphrodite* and between themselves were illustrated in the Supplemental Figure 8.

A first correspondence between the chromosomes of the two species was obtained using the SynMap Syntenic path assembly (SPA) option (Supplemental Figure 8D, see correspondences at https://genomevolution.org/coge/data/diags/62209/62346/html/master_62209_62346.CDS-CDS.last.tdd10.cs0.filtered.dag.all.go_D20_g10_A5.aligncoords.gcoords_ct0.w1000.spa-1.mcs1000000.ks.sr.cs1.csoN.log.nsd.spa_info.txt). This initial analysis does not show any *P. aphrodite*'s chromosomes that would not have a match in CR0040. Given the information available: genome size, chromosome size, complete BUSCO score for the annotated protein coding genes, and comparative genomics results, there is no strong evidence that essential protein-coding genes are missing from the current CR0040 genome assembly (chromosomes 15 and 16 would be in the unplaced scaffolds).

Comparison between CR0040 and *P. aphrodite* for the analysis of the pan-orchid WGD is difficult, in part because the 19 chromosomes of the latter are not well enough assembled. However, the chromosome 1 of CR0040 contains internal duplications as if the same two ancestral chromosomes (pre-α° WGD) had been merged (Supplemental Figure 8C). This is not observed in *P. aphrodite* that seems to have four chromosomes (1, 2, 10b, 17) corresponding to the Vanilla chromosome 1. The comparison of the two Ks histograms of a genome against itself (Supplemental Figure 8B and 7F) indicated the same kind of peak profile but narrower for *P. aphrodite*. Comparison of the vanilla genome with the genome of other orchids to search for the missing vanilla chromosomes 15 and 16 does not seem to be an appropriate approach because these chromosomes are probably small, specific and contain few genes. Their absence would therefore not be an obstacle to the study of the evolution of monocot genomes.

Supplemental Note 5

Detection of non-endoreplicated genomic regions

Reads from each sequencing technology used in this study (HiFi long reads, ONT long reads and Illumina short reads from CR0040), as well as ONT long reads and Illumina short reads from Daphna were mapped onto the CR0040 assembly. Minimap2 (Li, 2018) was used for long reads mapping with the following parameters: -a -x asm20 -t8, and Illumina short reads were mapped using bwa-mem2 (https://github.com/bwa-mem2/bwa-mem2) with default parameters. Sequencing depths were extracted with the samtools depth script for each position. These values were averaged for genomic windows of 20Kb which were used to compute global statistics on chromosomes and to plot depth distributions along the 28 chromosomes and the two random mosaic chromosomes

(chr0). Mean sequencing depth of the genome was 19.57, 29.82 and 52.50 for CR0040 cultivar with HiFi, ONT and Illumina reads, and 27.29 and 46.03 for Daphna cultivar with ONT and Illumina reads. The chromosome 11A is less covered by sequencing due to the presence of large gaps in its assembly. The sequencing depth of CR0040 genome per technology is summarized in the Supplemental Table 15.

The sequencing depth of CR0040 genome using Daphna data sequences (Hasing et al., 2020) is summarized in the Supplemental Table 16. The mean sequencing depth of the two random mosaic chromosomes (chr0) was lower than the one of the 14 pseudochromosomes for long reads sequencing technologies (Supplemental Tables 15 and 16). To detect sequencing depth bias and to limit the risk to detect false positives, the mean of sequencing depth for every 20 successive windows of 20Kb was computed using Illumina reads for Daphna and using long reads (HiFi + ONT) for CR0040. All regions with a sequencing depth inferior to 20% of mean sequencing depth of chromosomes were selected for both Daphna and CR0040. Regions with a decrease in sequencing depth for both cultivars were identified using the 'bedtools intersect' (version 2.29.2) and correspond to the endoreplication pattern 1. Low coverage regions identified from the HiFi CR0040 reads mapping that did not overlap with those identified from the Daphna Illumina reads mapping corresponded to the endoreplication pattern 2. All automatically identified regions were manually validated and refined by visualization of sequencing depth drops for each CR0040 chromosome and for all available sequencing datasets (Supplemental Figure 9).

Supplemental Figure 10 shows low depth k-mers information in addition to the coverage depth information presented in Supplemental Figure 9. The ratios of k-mers of depth between 5x and 15x were computed for genomic windows of 20Kb and plotted along each pair of chromosomes.

Supplemental Note 6

Database implementation for Vanilla Genome Hub (VGH)

The VGH was constructed using the Tripal v3 framework, a specific toolkit for the construction of online community genomic databases, by integrating the GMOD Chado database schema and the Drupal open source platform (https://www.drupal.org/). The genome sequences, predicted gene models, mRNA and protein sequences were loaded into the database using the 'Data Loaders' function of Tripal. The Drupal theme of the website is derived from the hardwood genomics website (https://github.com/statonlab/hardwood).

Gene Search

Gene search can be done in two ways, (i) by querying genes using the Tripal MegaSearch module (Jung, et al, 2021) and various filters such as name, chromosome position and functional annotation (putative function, InterPro domain and gene ontology, Figure 6B), (ii) by similarity using BLAST. The BLAST search interface provides access to datasets from the current genome release, allowing users to conduct sequence searches against the coding sequences, transcripts, proteins and the whole-genome assembly (Figure 6C).

For both, results are displayed as a dynamic table that summarizes the relevant information on the corresponding search with a link to the gene report and onto the genome browser.

Gene report page provides the user with a view of the metadata associated with the gene models. These include protein domain composition identified by InterProScan, Gene Ontology (GO) annotations and KEGG BlastKOALA (Figure 6D).

Genome Browser

Genome visualization was implemented using the Tripal JBrowse module (https://github.com/tripal/tripal_jbrowse) (Figure 6E). The module embeds JBrowse (Buels et al., 2016), an interactive, client-side genome browser, into a Drupal webpage. JBrowse allows users to visualize features of the reference genome. Each chromosome can be selected from a drop-down menu, and the browser displays information about the sequence and corresponding gene models. The gene expression profiles are also displayed in JBrowse. To display RNA-Seq expression profiles in JBrowse, the read alignment file in BAM format for each accession was converted to coverage tracks in bigwig format using DeepTools2, and these coverage tracks were then loaded onto JBrowse.

Metabolic pathway

The Pathologic file previously produced was processed by Pathway Tools, which predicted a total of 678 metabolic pathways in vanilla. A pathway database, VanillaCyc (https://vanilla-genome-hub.cirad.fr/content/pathways-tools), was built based on these predicted pathways using the web server of Pathway Tools (Figure 6F). Users can search and browse the predicted pathways, as well as perform comparative and omics data analysis through the VanillaCyc database.

If we take the example of the methyltransferase gene family (Enzyme Commission Number 2.1.1.-), 415 methyltransferases were predicted on both haplotypes CR0040_A and CR0040_B. The O-methyltransferase are involved, among other things, in four phenylpropanoid biosynthetic pathways predicted by Pathway Tools:

The phenylpropanoid biosynthesis (PWY-361)

The free phenylpropanoid acid biosynthesis (PWY-2181)

The vanillin biosynthesis I (PWY-5665)

The phenylpropanoids methylation (ice plant; PWY-7498)

If we focus on the example of two CR0040 methyltransferases:

VANPL_B_00007t006130 (OG0000841), the only Caffeic acid O-methyltransferase predicted in the vanillin biosynthesis I pathway and also putatively involved in the phenylpropanoid biosynthesis and

VANPL_B_00011t00710 (OG0000449), OMT4 (Vpl_s126Bg26946.1) homolog possibly involved in the phenylpropanoid biosynthesis and the phenylpropanoids methylation (ice plant).

Phylogenetic trees of the orthogroups of these polypeptides showed clusters of genes encoding for Caffeic acid O-methyltransferase (COMT, OG0000841; Supplemental Figure 11A, B) and for O-methyltransferase (OMT, OG0000449; Supplemental Figure 11C, D). The two OrthoFinder gene families, OG0000449.fa and OG0000841.fa, are available in the VGH (see download section below). They were reanalyzed with https://ngphylogeny.fr/ using the PhyML/OneClick workflow and advanced setting. Default parameters were used except for PhyML. Tree topology search and branch support option were set to “best of nearest neighbor interchange (NNI) and subtree pruning and regrafting (SPR)” and approximate likelihood-ratio test, respectively. Gene names are indicated in blue, green, red, black, magenta and orange for CR0040 *V. planifolia*, Daphna *V. planifolia*, *Arabidopsis thaliana*, *Oryza sativa* subsp. *japonica* and *Phalaenopsis equestris*, respectively.

Regarding these two OrthoFinder orthogroups, we observed that there is a higher number of genes predicted in the Daphna genome than in the CR0040 one and for CR0040, methyltransferases are preferentially found on haplotype B (Supplemental Figure 11). This could suggest phenomena that may be concomitant such as variations of the dispensable genome, assembly problems in the two *Vanilla planifolia* genomes or annotations. Indeed, in both gene families, the Daphna haplotype A appears to contain tandem methyltransferase clusters (green boxes on DA07 and DA11 genomic regions in JBrowse; Supplemental Figure 11B, D). However, it can be seen in the genomic region containing a tandem methyltransferase cluster on Daphna_A chromosome 7, that the cluster is interrupted by genes that are repeated in 5' (grey boxes in the Supplemental Figure 11B): Protein disulfide-isomerase LQY1, Type I inositol-1,4,5-trisphosphate 5-phosphatase, Pentatricopeptide repeat-containing protein, Activating signal cointegrator 1. This may reflect the assembly of two allelic long reads instead of them being separated in each of the two Daphna haplotypes. This is consistent with other remarks already made along these lines in this article (e.g. optical mapping, syntenic dotplot). As illustrated with theses isozyme examples, it is therefore possible that this is the same reason why the chromosome scaffolded part is larger in Daphna than in CR0040 and why the

number of paralogs is overestimated in Daphna compared to CR0040. On the contrary, the CR0040_A chromosomes would possibly underestimate tandem gene clusters.

GO enrichment analysis

From a list of genes of interest, it can be interesting to look for enriched biological processes, molecular functions, or cellular components. This functionality is brought by DIANE (Dashboard for the Inference and Analysis of Networks from Expression data), as described in Cassan, et al (2021). Results can be obtained as a data table, a dotplot of enriched GO terms with associated gene counts and p-values, or an enrichment map linking co-occurring GO terms (Figure 6G).

Synteny analysis and visualization

Syntenic blocks and homologous gene pairs within syntenic blocks were identified in the two vanilla genome sequences, including comparisons both within each genome and between any two genomes (haplotypes). The protein sequences were first aligned against themselves (within each genome) as well as between each other (pairwise comparisons) using a reciprocal best hit approach. Based on the BLASTP results and gene positions, syntenic blocks were determined using MCScanX with default parameters (Wang et al., 2012). To further facilitate comparative analyses of genomes, the Synvisio extension module (https://www.drupal.org/project/synvisio) was implemented. The module embeds Synvisio (Bandi, 2020), an interactive multiscale synteny visualization tool for MCScanX, into a Drupal webpage and provides a simple interface for managing and creating Synvisio instances (Figure 6H). Liftoff (Shumate and Salzberg, 2021) was used to align the gene sequences of Daphna to the CR0040 genome. For each gene, Liftoff finds the alignments of the exons that maximize sequence identity while preserving the transcript and gene structure. This track can be loaded onto JBrowse to visualize the collinearity between the 2 sets of annotations.

Download section

A download section grants users direct access to the data used by the different tools that compose the hub. Assembly of pseudomolecules as well as their structural and functional annotations are available in FASTA and in GFF3 formats respectively at https://vanilla-genome-hub.cirad.fr/content/download. This section was created using the Filebrowser module (https://www.drupal.org/project/filebrowser).

Supplemental References

Bandi, V. K. (2020). SynVisio: a multiscale tool to explore genomic conservation, Master of Science (M.Sc.) dissertation, University of Saskatchewan. 82p.

Bory, S., Da Silva, D., Risterucci, A.M., Grisoni, M., Besse, P., and Duval, M.F. (2008). Development of microsatellite markers in cultivated vanilla: Polymorphism and transferability to other vanilla species. *Scientia Horticulturae***,** 115, 420-425. 10.1016/j.scienta.2007.10.020.

Bouétard, A., Lefeuvre, P., Gigant, R., Bory, S., Pignal, M., Besse, P., and Grisoni, M. (2010). Evidence of transoceanic dispersion of the genus *Vanilla* based on plastid DNA phylogenetic analysis. *Molecular Phylogenetics and Evolution*, 55(2), 621-630.

Bourge, M., Brown, S. C., and Siljak-Yakovlev, S. (2018). Flow cytometry as tool in plant sciences, with emphasis on genome size and ploidy level assessment. *Genetics and Applications*, 2(2), 1-12.

Brown, S.C., Bourge, M., Maunoury, N., Wong, M., Bianchi, M.W., Lepers-Andrzejewski, S., Besse, P., Siljak-Yakovlev, S., Dron, M., and Satiat-Jeunematre, B. (2017). DNA remodeling by strict partial endoreplication in Orchids, an original process in the plant kingdom. *Genome Biology and Evolution*, 9, 1051-1071. 10.1093/gbe/evx063.

Buels, R., Yao, E., Diesh, C. M., Hayes, R. D., Munoz-Torres, M., Helt, G., Goodstein, D. M., Elsik, C. G., Lewis, S. E., Stein, L., and Holmes, I. H. (2016). JBrowse: a dynamic web platform for genome visualization and analysis. *Genome biology*, 17, 66. https://doi.org/10.1186/s13059-016-0924-1.

Cassan, O., Lèbre, S. and Martin, A. (2021). Inferring and analyzing gene regulatory networks from multi-factorial expression data: a complete and interactive suite. *BMC Genomics* 22, 387. https://doi.org/10.1186/s12864-021-07659-2.

Chao, Y. T., Yen, S. H., Yeh, J. H., Chen, W. C., and Shih, M. C. (2017). Orchidstra 2.0-A Transcriptomics Rresource for the orchid family. *Plant and cell physiology*, 58(1), e9. https://doi.org/10.1093/pcp/pcw220.

Cheng, H., Concepcion, G. T., Feng, X., Zhang, H., and Li, H. (2021). Haplotype-resolved de novo assembly using phased assembly graphs with hifiasm. *Nature methods*, 18(2), 170–175. https://doi.org/10.1038/s41592-020-01056-5.

Claudel-Renard, C., Chevalet, C., Faraut, T., and Kahn, D. (2003). Enzyme-specific profiles for genome annotation: PRIAM. *Nucleic acids research*, 31(22), 6633–6639. https://doi.org/10.1093/nar/gkg847.

Conway, J. R., Lex, A., and Gehlenborg, N. (2017). UpSetR: an R package for the visualization of intersecting sets and their properties. *Bioinformatics*, 33(18), 2938–2940. https://doi.org/10.1093/bioinformatics/btx364.

Emms, D. M., and Kelly, S. (2019). OrthoFinder: phylogenetic orthology inference for comparative genomics. *Genome biology*, 20(1), 238. https://doi.org/10.1186/s13059-019-1832-y

Ellinghaus, D., Kurtz, S., and Willhoeft, U. (2008). LTRharvest, an efficient and flexible software for de novo detection of LTR retrotransposons. *BMC bioinformatics*, 9, 18. https://doi.org/10.1186/1471-2105-9-18.

Favre, F., Jourda, C., Grisoni, M., Rivallan, R., Dijoux, J. B., Hascoat, J., Lepers, S., Besse, P., and Charron, C. (2022) A genome-wide assessment of the genetic diversity, evolution and relationships with allied species of the clonally propagated crop *Vanilla planifolia*. *Genetic Resources and Crop Evolution*, in press. https://doi.org/10.1007/s10722-022-01362-1.

Flynn JM, Hubley R, Goubert C, Rosen, J., Clark, A. G., Feschotte, C., and Smit, A. F. (2020) RepeatModeler2 for automated genomic discovery of transposable element families. *Proceedings of the National Academy of Sciences of the United States of America*, 117(17):9451-9457. doi:10.1073/pnas.1921046117.

Fu, L., Niu, B., Zhu, Z., Wu, S., and Li, W. (2012). CD-HIT: accelerated for clustering the next-generation sequencing data. *Bioinformatics*, 28(23), 3150–3152. https://doi.org/10.1093/bioinformatics/bts565.

Girgis H. Z. (2015). Red: an intelligent, rapid, accurate tool for detecting repeats de-novo on the genomic scale. *BMC bioinformatics*, 16, 227. https://doi.org/10.1186/s12859-015-0654-5.

Gurevich, A., Saveliev, V., Vyahhi, N., and Tesler, G. (2013). QUAST: quality assessment tool for genome assemblies. *Bioinformatics*, 29(8), 1072–1075. https://doi.org/10.1093/bioinformatics/btt086.

Haas BJ, Delcher AL, Wortman JR and Salzberg SL. (2004) DAGchainer: a tool for mining segmental genome duplications and synteny. *Bioinformatics*. 20(18):3643-3646. doi:10.1093/bioinformatics/bth397.

Hasing, T., Tang, H.B., Brym, M., Khazi, F., Huang, T.F., and Chambers, A.H. (2020). A phased *Vanilla planifolia* genome enables genetic improvement of flavour and production. *Nature Food* 1:811-819. 10.1038/s43016-020-00197-2.

Haug-Baltzell, A., Stephens, S. A., Davey, S., Scheidegger, C. E., and Lyons, E. (2017). SynMap2 and SynMap3D: web-based whole-genome synteny browsers. *Bioinformatics*, 33(14), 2197–2198. https://doi.org/10.1093/bioinformatics/btx144.

Hoede, C., Arnoux, S., Moisset, M., Chaumier, T., Inizan, O., Jamilloux, V., and Quesneville, H. (2014). PASTEC: an automatic transposable element classification tool. *PloS one*, 9(5), e91929. https://doi.org/10.1371/journal.pone.0091929.

Jiao, Y.N., Li, J.P., Tang, H.B., and Paterson, A.H. (2014). Integrated syntenic and phylogenomic analyses reveal an ancient genome duplication in monocots. *Plant Cell* **26**:2792-2802. 10.1105/tpc.114.127597.

Jones, P., Binns, D., Chang, H. Y., Fraser, M., Li, W., McAnulla, C., McWilliam, H., Maslen, J., Mitchell, A., Nuka, G., Pesseat, S., Quinn, A. F., Sangrador-Vegas, A., Scheremetjew, M., Yong, S. Y., Lopez, R., and Hunter, S. (2014). InterProScan 5: genome-scale protein function classification. *Bioinformatics,* 30(9), 1236–1240. https://doi.org/10.1093/bioinformatics/btu031.

Jung, S., Cheng, C. H., Buble, K., Lee, T., Humann, J., Yu, J., Crabb, J., Hough, H. and Main, D. (2021) Tripal MegaSearch: a tool for interactive and customizable query and download of big data. *Database*. doi: 10.1093/database/baab023.

Kanehisa, M., Sato, Y., and Morishima, K. (2016). BlastKOALA and GhostKOALA: KEGG tools for functional characterization of genome and metagenome sequences. *Journal of molecular biology*, *428*(4), 726–731. https://doi.org/10.1016/j.jmb.2015.11.006.

Karp, P. D., Paley, S., and Romero, P. (2002). The Pathway Tools software. *Bioinformatics*, 18, S225–S232. https://doi.org/10.1093/bioinformatics/18.suppl_1.s225.

Kim, D., Paggi, J. M., Park, C., Bennett, C., and Salzberg, S. L. (2019). Graph-based genome alignment and genotyping with HISAT2 and HISAT-genotype. *Nature biotechnology*, 37(8), 907–915. https://doi.org/10.1038/s41587-019-0201-4.

Kolmogorov, M., Yuan, J., Lin, Y. and Pevzner, P.A. (2019) Assembly of long, error-prone reads using repeat graphs. *Nature Biotechnology*, 37:540.

Kumar, S., Stecher, G., Suleski, M. and Hedges, SB. (2017) TimeTree: A Resource for Timelines, Timetrees, and Divergence Times. *Mol Biol Evol* doi:10.1093/molbev/msx116.

Lamesch, P., Berardini, TZ., Li, D., Swarbreck, D., Wilks, C., Sasidharan, R., Muller, R., Dreher, K., Alexander, DL., Garcia-Hernandez, M., Karthikeyan, AS., Lee, CH., Nelson, WD., Ploetz, L., Singh, S., Wensel, A. and Huala, E. (2012) The Arabidopsis Information Resource (TAIR): improved gene annotation and new tools. *Nucleic acids research*. 40 Database issue D1202-10.

Li, H. (2018). Minimap2: pairwise alignment for nucleotide sequences. *Bioinformatics*, 34(18), 3094-3100.

Lyons, E. and Freeling, M. (2008) How to usefully compare homologous plant genes and chromosomes as DNA sequences. *The Plant Journal* 53 (4), 661-673.

Martin, J., and Hesemann, C. U. (1988). Cytogenetic investigations in wheat, rye and triticale. I. Evaluation of improved Giemsa C-and fluorochrome banding techniques in rye chromosomes. *Heredity*, 61(3), 459-467.

Mendes, F. K., Vanderpool, D., Fulton, B., and Hahn, M. W. (2020). CAFE 5 models variation in evolutionary rates among gene families. *Bioinformatics,* btaa1022. Advance online publication. https://doi.org/10.1093/bioinformatics/btaa1022.

Perez-Silva, A., Odoux, E., Brat, P., Ribeyre, F., Rodriguez-Jimenes, G., Robles-Olvera, V., Garcia-Alvarado, M.A., and Gunata, Z. (2006). GC-MS and GC-olfactometry analysis of aroma compounds in a representative organic aroma extract from cured vanilla (*Vanilla planifolia* G. Jackson) beans. *Food chemistry,* 99:728-735. 10.1016/j.foodchem.2005.08.050.

Pertea, M., Pertea, G. M., Antonescu, C. M., Chang, T. C., Mendell, J. T., and Salzberg, S. L. (2015). StringTie enables improved reconstruction of a transcriptome from RNA-seq reads. *Nature biotechnology*, 33(3), 290–295. https://doi.org/10.1038/nbt.3122.

Price, A. L., Jones, N. C., and Pevzner, P. A. (2005). *De novo* identification of repeat families in large genomes. *Bioinformatics*, 21, i351–i358. https://doi.org/10.1093/bioinformatics/bti1018.

Quinlan, A. R., and Hall, I. M. (2010). BEDTools: a flexible suite of utilities for comparing genomic features. *Bioinformatics*, 26(6), 841–842. https://doi.org/10.1093/bioinformatics/btq033.

Sallet, E., Gouzy, J., and Schiex, T. (2019). EuGene: An automated integrative gene finder for Eukaryotes and Prokaryotes. *Methods in molecular biology* (Clifton, N.J.), 1962, 97–120. https://doi.org/10.1007/978-1-4939-9173-0_6.

Sandler, G., Bartkowska, M., Agrawal, A.F., and Wright, S.I. (2020). Estimation of the SNP mutation rate in two vegetatively propagating species of duckweed. *G3-Genes Genomes Genetics* 10:4191-4200. 10.1534/g3.120.401704.

Schweizer, D. (1976). Reverse fluorescent chromosome banding with chromomycin and DAPI. *Chromosoma*, 58(4), 307-324.

Shumate, A., and Salzberg, S. L. (2021). Liftoff: accurate mapping of gene annotations, *Bioinformatics*, 37, 1639–1643, https://doi.org/10.1093/bioinformatics/btaa1016.

Siljak-Yakovlev, S., Cerbah, M., Coulaud, J., Stoian, V., Brown, S. C., Zoldos, V., Jelenic, S., and Papes, D. (2002). Nuclear DNA content, base composition, heterochromatin and rDNA in *Picea omorika* and *Picea abies*. *Theoretical and Applied Genetics*, 104(2), 505-512.

Solano-De la Cruz, M.T., Adame-García, J., Gregorio-Jorge, J., Jiménez-Jacinto, V., Vega-Alvarado, L., Iglesias-Andreu, L. G., Escobar-Hernández, E. E., and Luna-Rodríguez, M. (2019) Functional categorization of *de novo* transcriptome assembly of *Vanilla planifolia* Jacks. potentially points to a translational regulation during early stages of infection by *Fusarium oxysporum f. sp. vanillae*. *BMC Genomics*, 20(1):826. PMID: 31703622.

Tang, H., Bowers, J. E., Wang, X., and Paterson, A. H. (2010). Angiosperm genome comparisons reveal early polyploidy in the monocot lineage. *Proceedings of the National Academy of Sciences of the United States of America*, *107*(1), 472–477. https://doi.org/10.1073/pnas.0908007107.

Tarailo-Graovac, M., and Chen, N. (2009). Using RepeatMasker to identify repetitive elements in genomic sequences. *Current protocols in bioinformatics*, https://doi.org/10.1002/0471250953.bi0410s25.

Walker, B.J., Abeel, T., Shea, T., Priest, M., Abouelliel, A., Sakthikumar, S., Cuomo, C.A., Zeng, Q., Wortman, J., 1 Young, S.K. and Earl, A.M. (2014) Pilon: an integrated tool for comprehensive microbial variant detection and genome assembly improvement. *PLoS One*, 9:e112963. doi: 10.1371/journal.pone.0112963.

Wang, Y., Tang, H., Debarry, J.D., Tan, X., Li, J., Wang, X., Lee, T.H., Jin, H., Marler, B., Guo, H., Kissinger, J.C. and Paterson, A.H. (2012) MCScanX: a toolkit for detection and evolutionary analysis of gene synteny and collinearity. *Nucleic Acids Research*, 40(7):e49. doi: 10.1093/nar/gkr1293.

Weisenfeld, N. I., Kumar, V., Shah, P., Church, D. M., and Jaffe, D. B. (2017). Direct determination of diploid genome sequences. *Genome research*, *27*(5), 757-767.

Wicker, T., Sabot, F., Hua-Van, A., Bennetzen, J. L., Capy, P., Chalhoub, B., Flavell, A., Leroy, P., Morgante, M., Panaud, O., Paux, E., SanMiguel, P., and Schulman, A. H. (2007). A unified classification system for eukaryotic transposable elements. *Nature reviews. Genetics*, 8(12), 973–982. https://doi.org/10.1038/nrg2165.

Yang, Z. (2007) PAML 4: phylogenetic analysis by maximum likelihood. *Molecular Biology and Evolution*, 24(8):1586-1591. doi:10.1093/molbev/msm088.

Supplemental figures

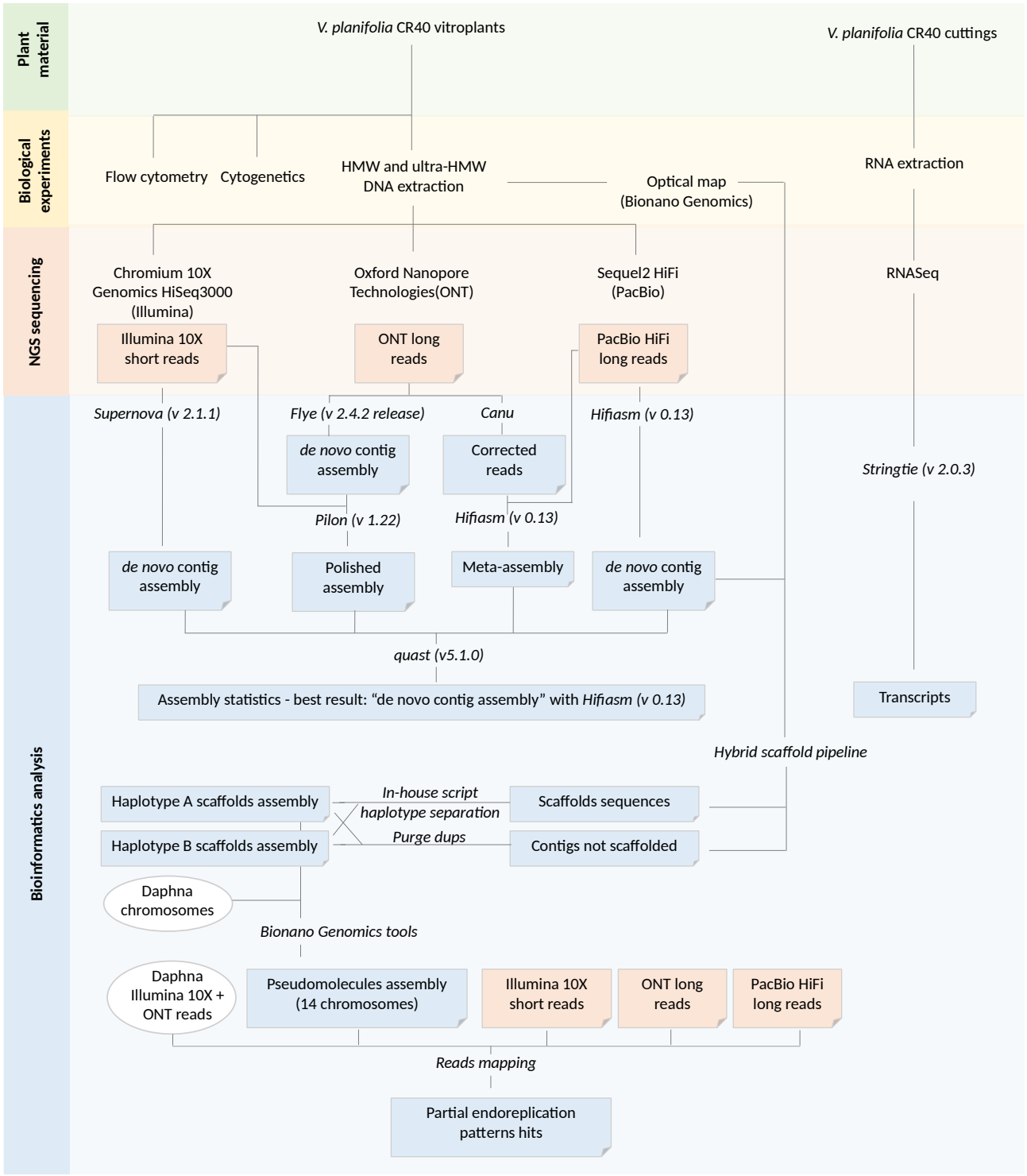

Supplemental Figure 1 Schematic representation of CR0040 genome sequencing strategy. Data represented with white circles were retrieved from *V. planifolia* Daphna genome (Hasing et al, 2020).

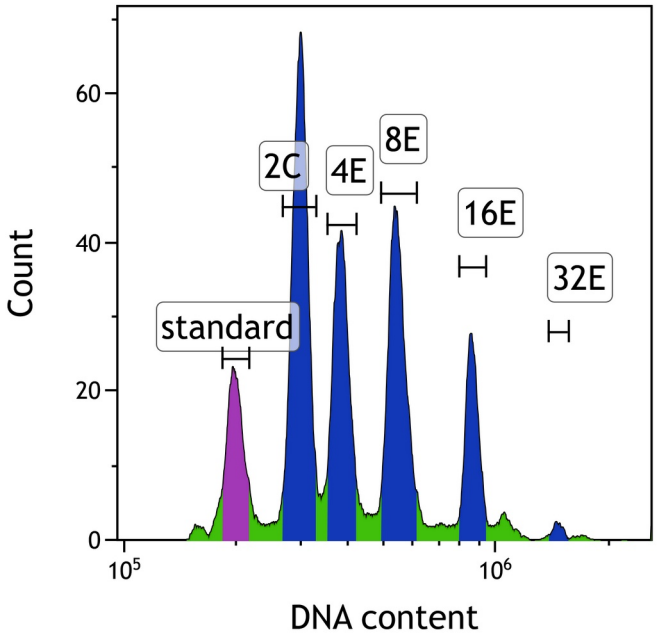

Supplemental Figure 2 Example of DNA content histogram of nodal tissue from *Vanilla planifolia* CR0040.

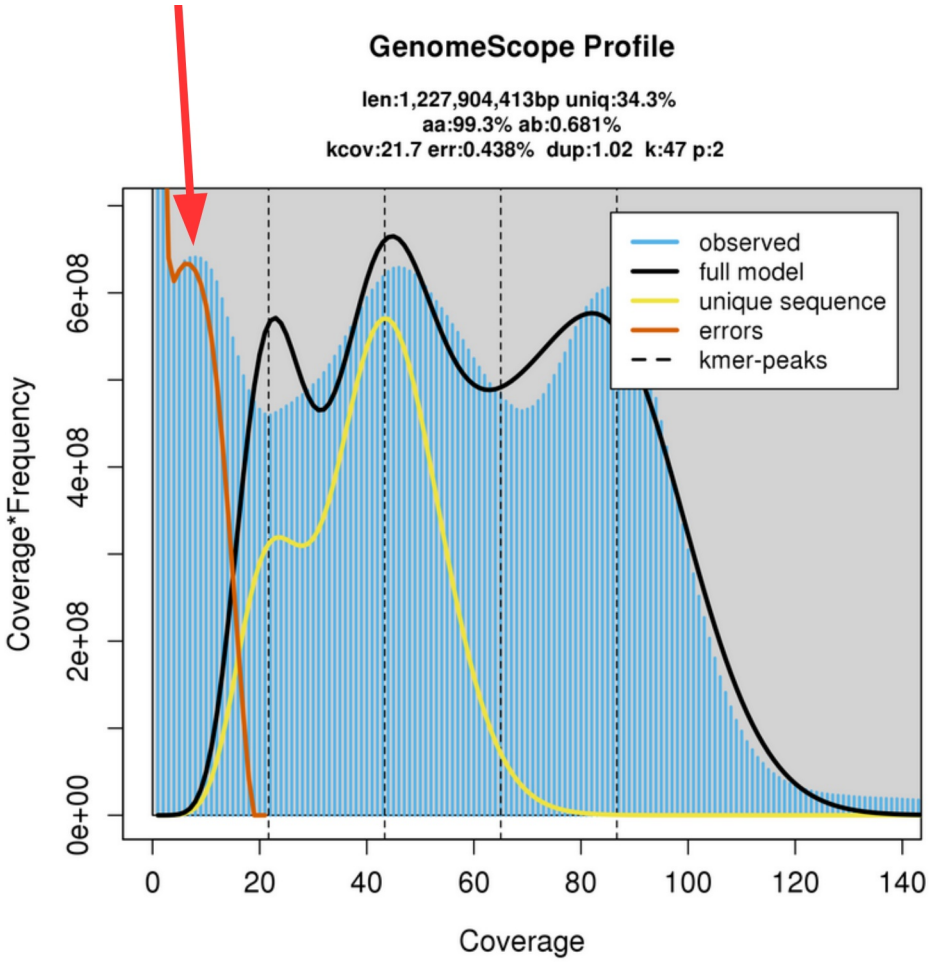

Supplemental Figure 3 GenomeScope2 k-mer profile of the CR0040 genome assembly

The red arrow shows k-mers from the non-endoreplicated part of the CR0040 genome whose distribution is centered at 10X. The two k-mers distributions centered at 42X and 84X, represent the classical diploid distribution with the heterozygous and homozygous k-mer content.

3

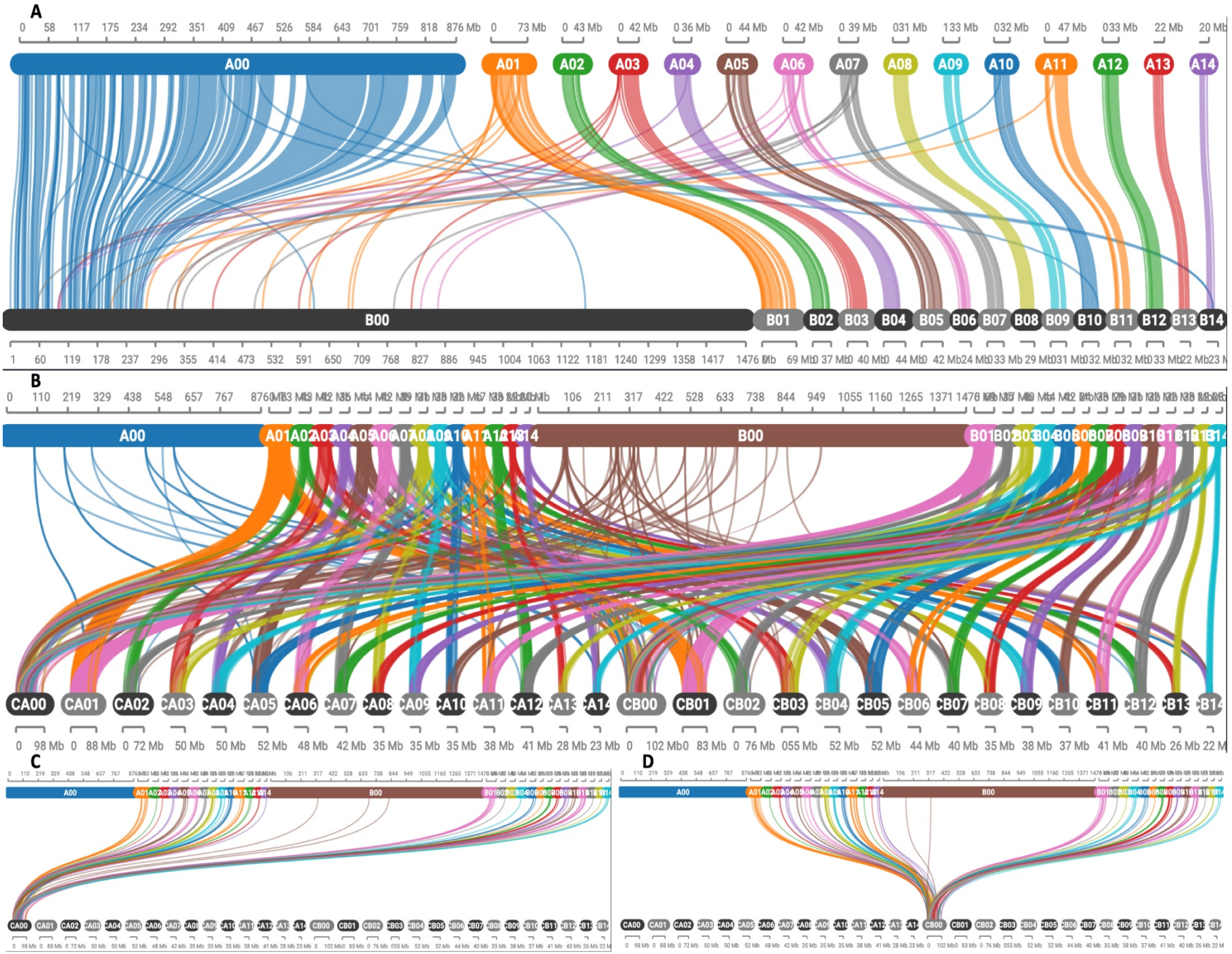
A
A00
A01
A02
A03
A04
A05
A06
A07
A08
A09
A10
A11
A12
A13
A14
B00
B01
B02
B03
B04
B05
B06
B07
B08
B09
B10
B11
B12
B13
B14
B
A00
B00
CA00
CA01
CA02
CA03
CA04
CA05
CA06
CA07
CA08
CA09
CA10
CA11
CA12
CA13
CA14
CB00
CB01
CB02
CB03
CB04
CB05
CB06
CB07
CB08
CB09
CB10
CB11
CB12
CB13
CB14
C
D

4

Supplemental Figure 4 Synteny view of the two *V. planifolia* genomes.

A. Comparison of MCScanX allelic blocks of both CR0040 haplotypes A and B. B) Comparison of MCScanX allelic blocks of both CR0040 haplotypes and of both Daphna haplotypes. C) Same as B) but it only shows syntenic relationships between the unknown random pseudomolecule of Daphna haplotype A (A0) and the CR0040 pseudomolecules in order to pinpoint improvement of CR0040 scaffolding. D) same as C) but with Daphna B0. Screenshots were done from https://vanilla-genome-hub.cirad.fr/synvisio.

5

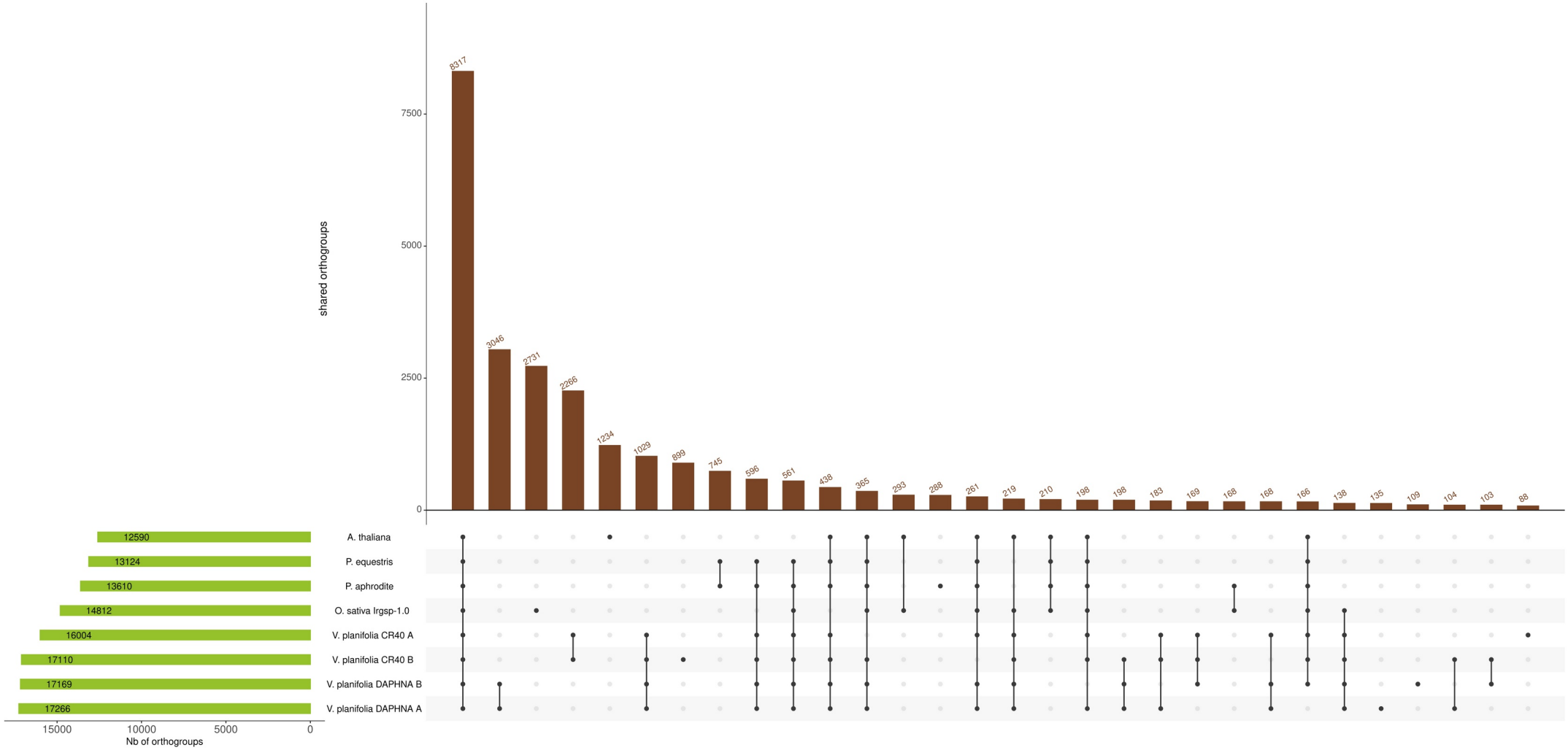

Supplemental Figure 5 UpSet plot of the inferred orthogroups.

The number of orthogroups identified with OrthoFinder for each species and *V. planifolia* haplotype is displayed inside horizontal green bars. Numbers above vertical brown bars represent numbers of orthogroups shared by a given intersection of species/haplotypes illustrated downside each vertical bar. For clarity reasons, only the 30 most frequent intersections were displayed on the plot (Nb, numbers).

6

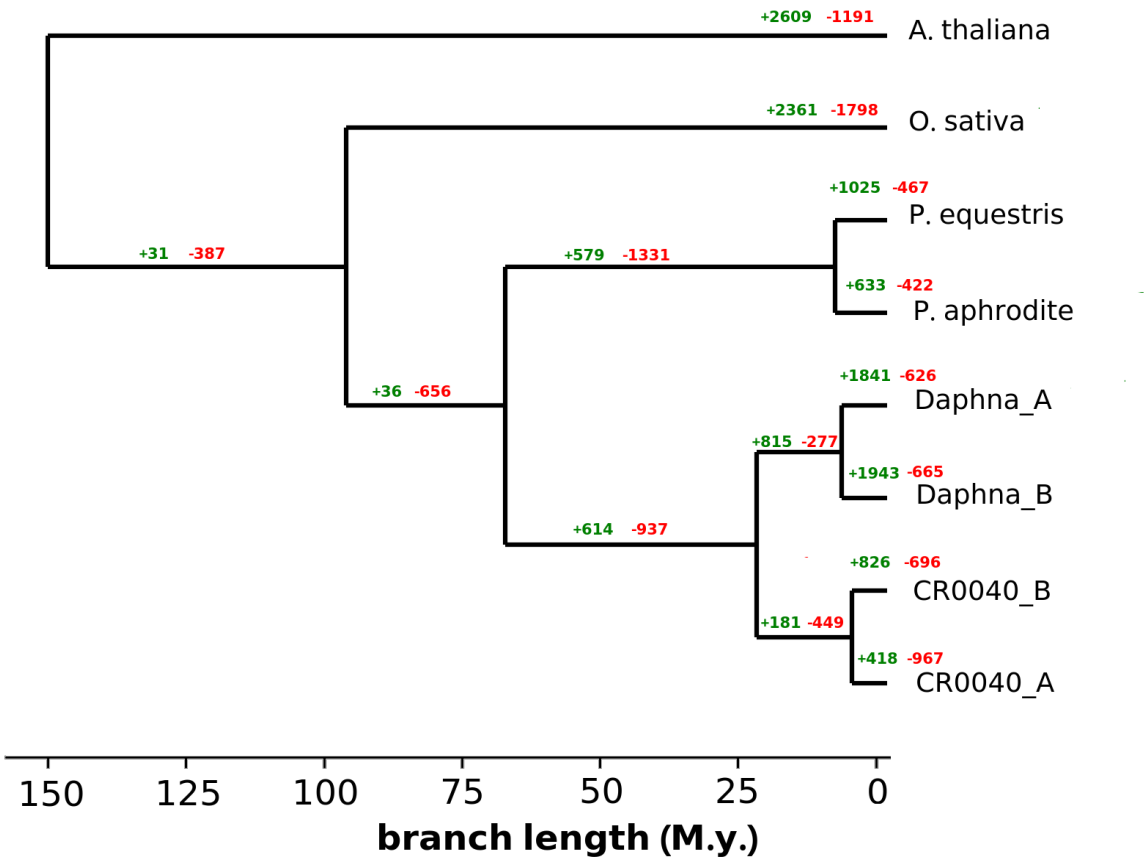

Supplemental Figure 6 Expansion and reduction of gene families in six proteomes. Orthogroups from OrthoFinder on six proteomes (CR0040_A, CR0040_A, Daphna_A, *Phalaenopsis equestris, P. aphrodite, Arabidopsis thaliana, Oryza sativa*) were analyzed with CAFE. The values represent the number of genes gained/lost.

7

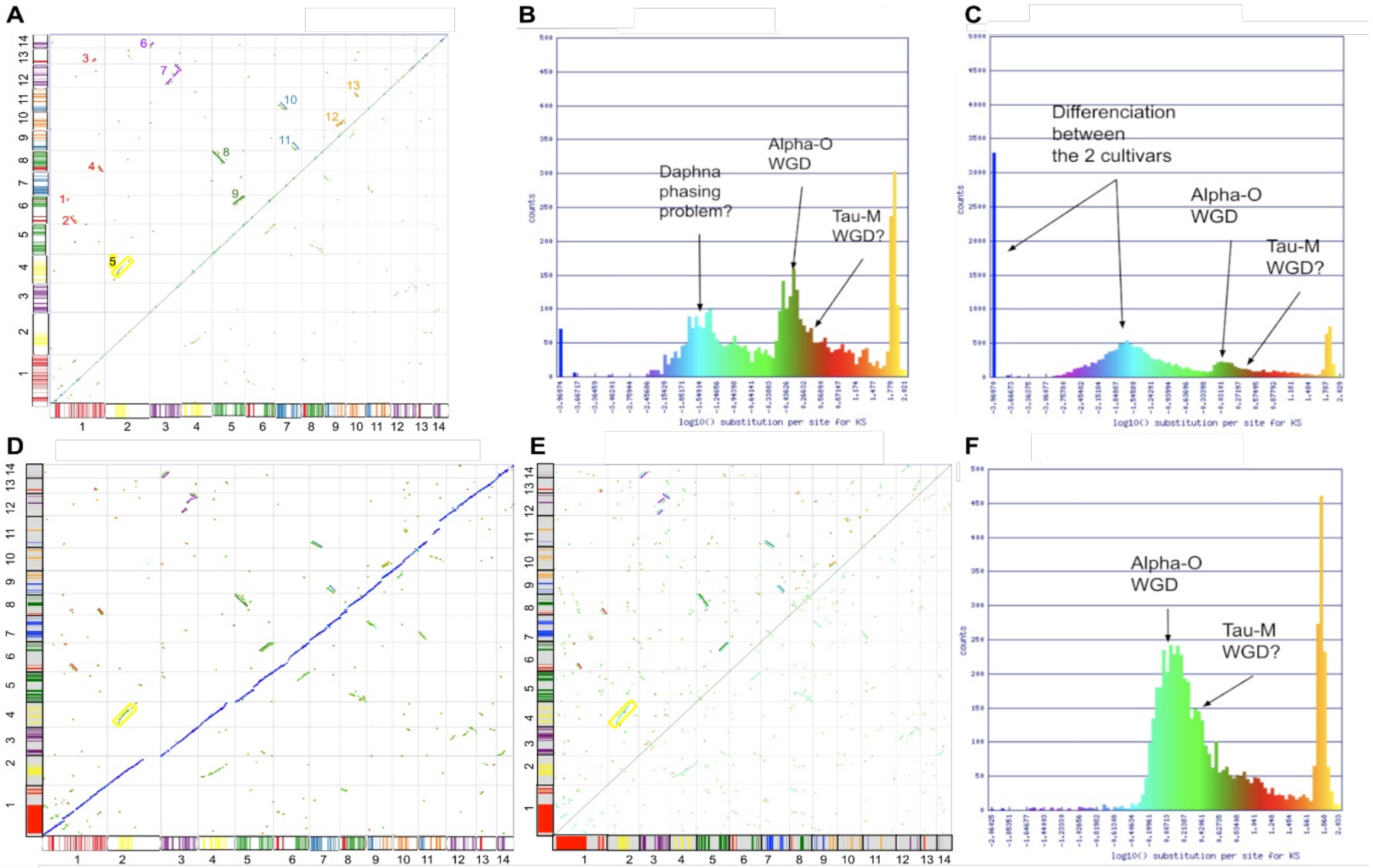
A
B
Daphna
phasing
problem?
Alpha-O
WGD
Tau-M
WGD?
counts
log10() substitution per site for KS
C
Differenciation
between
the 2 cultivars
Alpha-O
WGD
Tau-M
WGD?
counts
log10() substitution per site for KS
D
E
F
Alpha-O
WGD
Tau-M
WGD?
counts
log10() substitution per site for KS

8

Supplemental Figure 7 Synmap pairwise genome synteny analyses between CR0040 and Daphna cultivars and between themselves.

Haplotype A syntenic comparisons of Daphna CDS against themselves (A, B, see details in https://genomevolution.org/r/1jei9), between CR0040 and Daphna cultivars (C, D, see details in https://genomevolution.org/r/1jeid) and of CR0040 against itself (E, F, see details in https://genomevolution.org/r/1j9ym) were visualized with dotplots (A, D, E) and histograms of Ks values (B, C, F). Daphna karyotype painted according six pairs of duplicated regions illustrating the pan-orchid α^{o} WGD of Figure 4 (Hasing et al., 2020) has been cut out and positioned below the corresponding chromosomes of the dotplots (A, D). 13 paralog blocks were then projected onto the diagonals. Furthermore, using reciprocal best hits, the Daphna karyotype could be transferred to CR0040 (D, E).

9

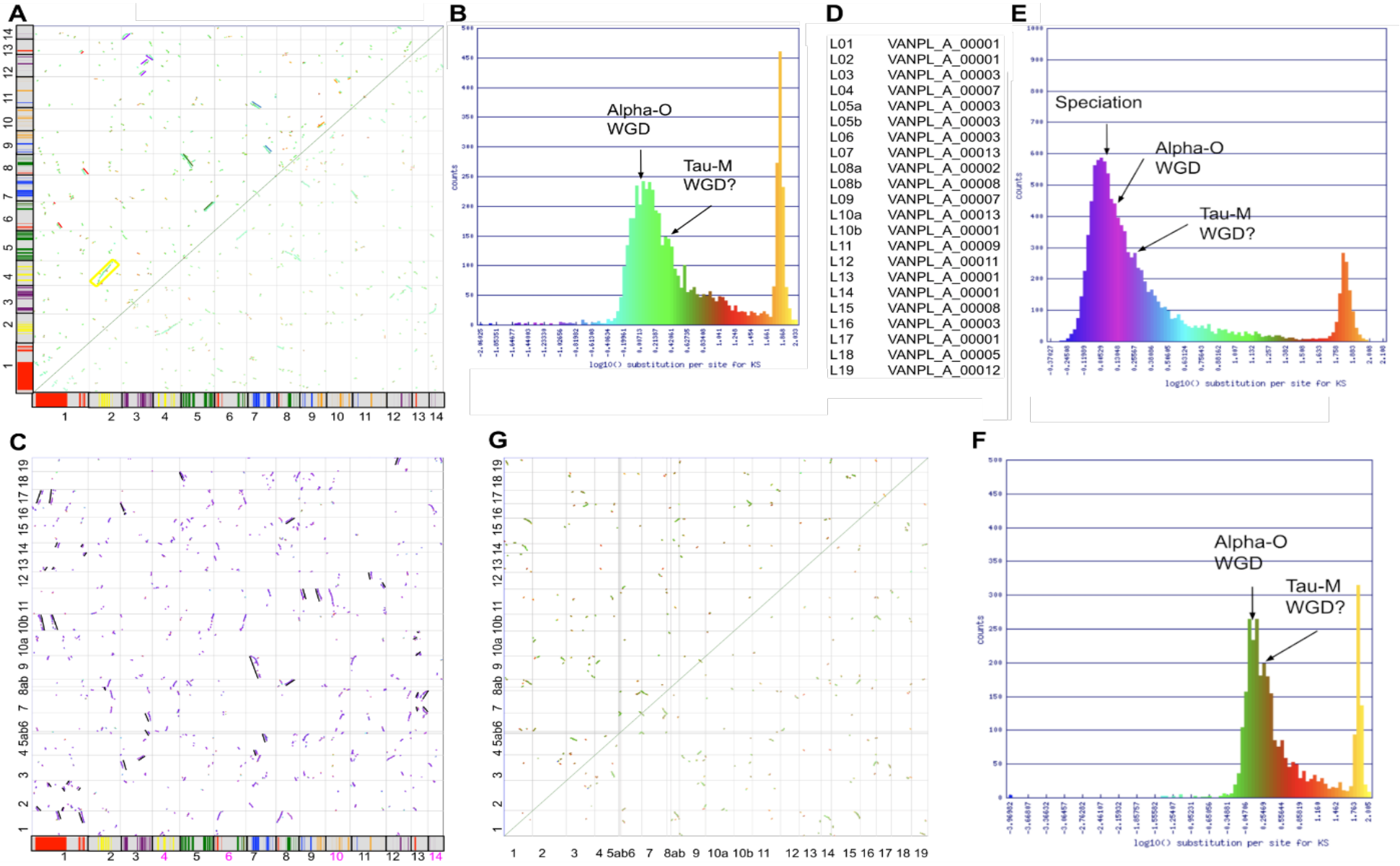
A
B
Alpha-O
WGD
Tau-M
WGD?
log10() substitution per site for KS
counts
D
L01 VANPL_A_00001
L02 VANPL_A_00001
L03 VANPL_A_00003
L04 VANPL_A_00007
L05a VANPL_A_00003
L05b VANPL_A_00003
L06 VANPL_A_00003
L07 VANPL_A_00013
L08a VANPL_A_00002
L08b VANPL_A_00008
L09 VANPL_A_00007
L10a VANPL_A_00013
L10b VANPL_A_00001
L11 VANPL_A_00009
L12 VANPL_A_00011
L13 VANPL_A_00001
L14 VANPL_A_00001
L15 VANPL_A_00008
L16 VANPL_A_00003
L17 VANPL_A_00001
L18 VANPL_A_00005
L19 VANPL_A_00012
E
Speciation
Alpha-O
WGD
Tau-M
WGD?
log10() substitution per site for KS
counts
C
G
F
Alpha-O
WGD
Tau-M
WGD?
log10() substitution per site for KS
counts

10

Supplemental Figure 8 Synmap pairwise genome synteny analyses between CR0040 *V. planifolia* and *P. aphrodite* and between themselves. Haplotype A syntenic comparisons of CR0040 CDS against themselves (A, B, see details in https://genomevolution.org/r/1j9ym), between CR0040 and *P. aphrodite* genome (C, D, E, see details in https://genomevolution.org/r/1jekr) and *P. aphrodite* genome itself (G, F, see details in https://genomevolution.org/r/1jekt) were visualized with dotplots (A, C, G), histograms of Ks values (B, E, F) and correspondence between the chromosomes of the two species was indicated according to Syntenic Path Assembly (D; SPA option; https://genomevolution.org/r/1jjmm). The CR0040 karyotype comes from the transfer of that of Daphna (Hasing et al., 2020) using reciprocal best hits. It has been cut out and positioned below the corresponding chromosomes of dotplots (A, C). Thus, six pairs of duplicated regions illustrating the pan-orchid α^o WGD allowed to project paralog blocks onto the diagonals (A). The orthologous blocks between CR0040 and *P. aphrodite* were highlighted with black lines (C) according to SPA results (D).

11

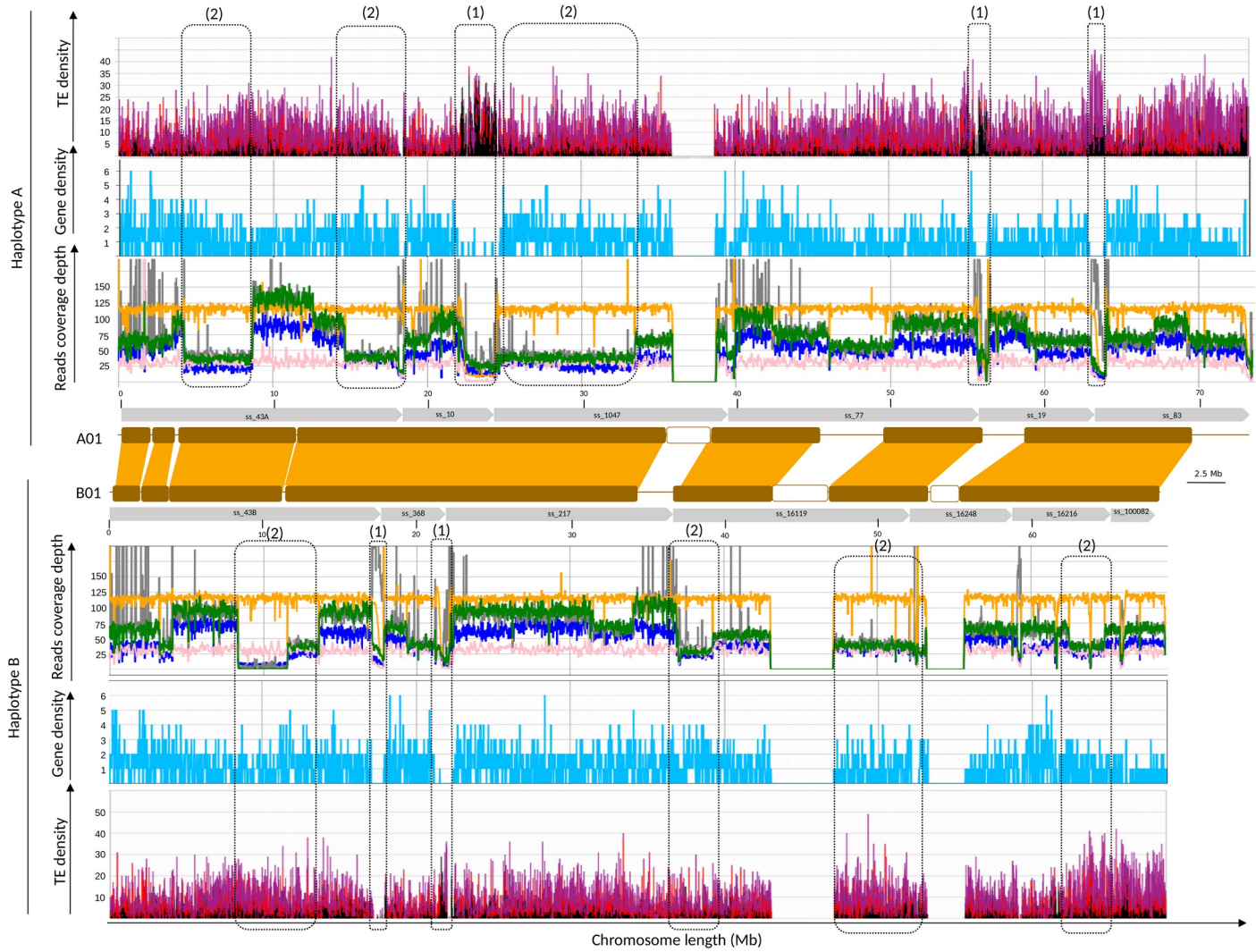

Supplemental Figure 9 Sequencing depth along the CR0040 chromosomes obtained by mapping Daphna Illumina (yellow) and ONT (pink) reads, CR0040 PacBio Hifi (blue), Nanopore (green) and Illumina (grey) reads on the CR0040 assembly. Synteny between homologous chromosomes are represented by central boxes. Gaps (N stretches) explaining sudden drops in sequencing depth are shown with white blocks. (1) Pattern 1 corresponds to low level of sequencing depth for all data. (2) Pattern 2 corresponds to inverted level of sequencing depth for CR0040 between haplotypes A and B, and constant level of sequencing depth for both Daphna haplotypes. Gene and retrotransposons distributions along the chromosomes are represented by a blue line chart and a stacked histogram (copia: red, gypsy: purple, other retrotransposons: black) respectively.

12

Supplemental Figure 9 continued

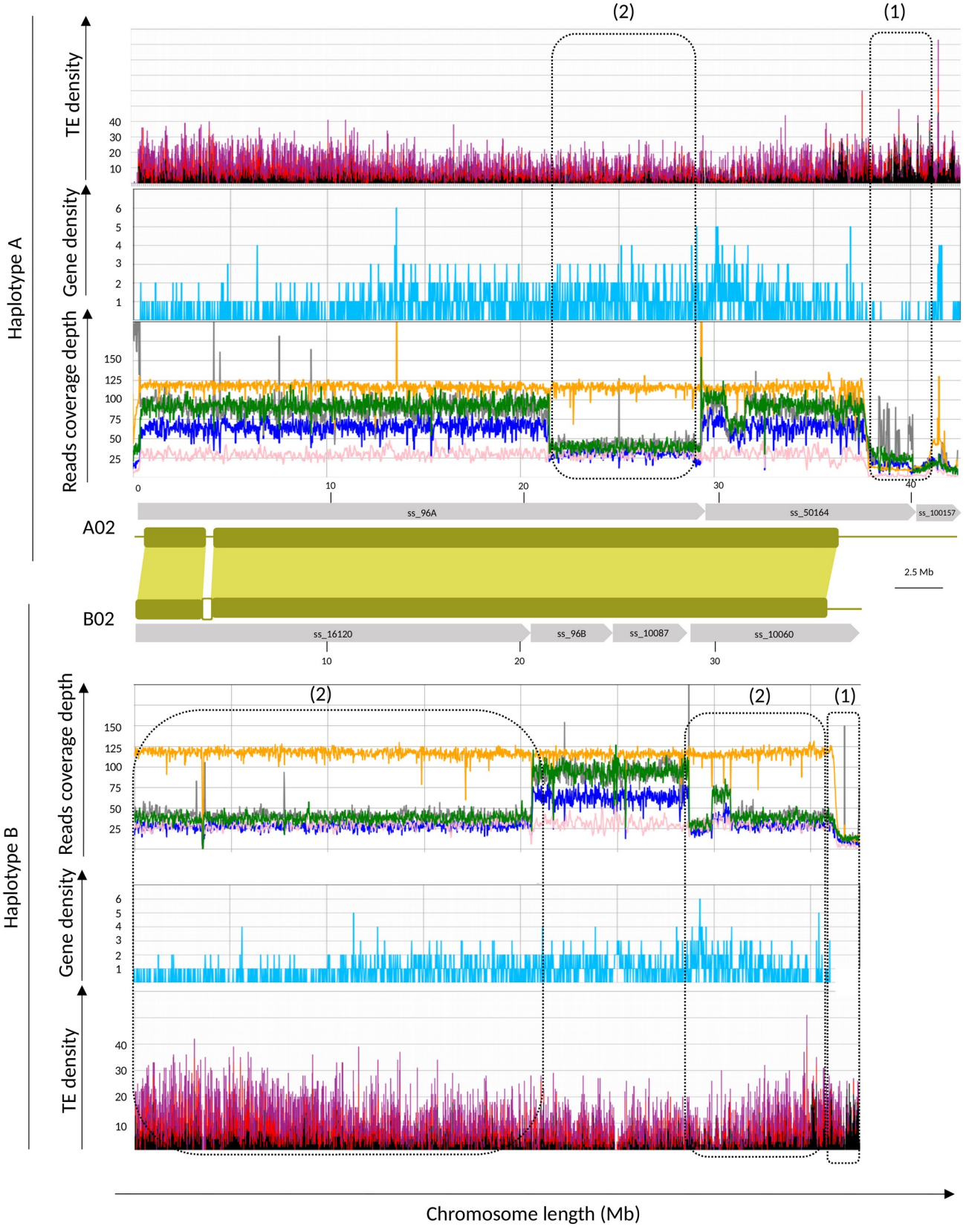

13

Supplemental Figure 9 continued

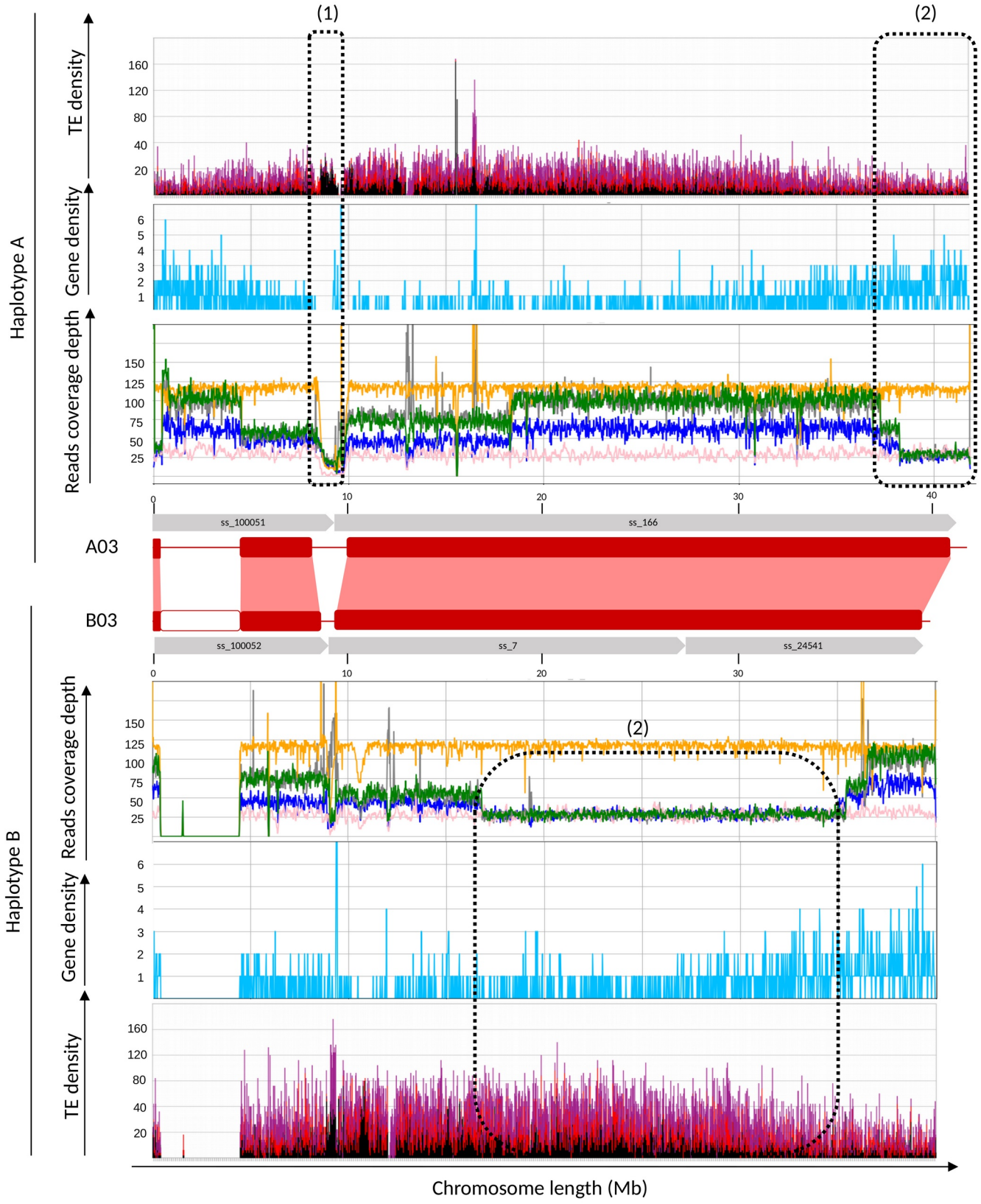

14

57 Supplemental Figure 9 continued

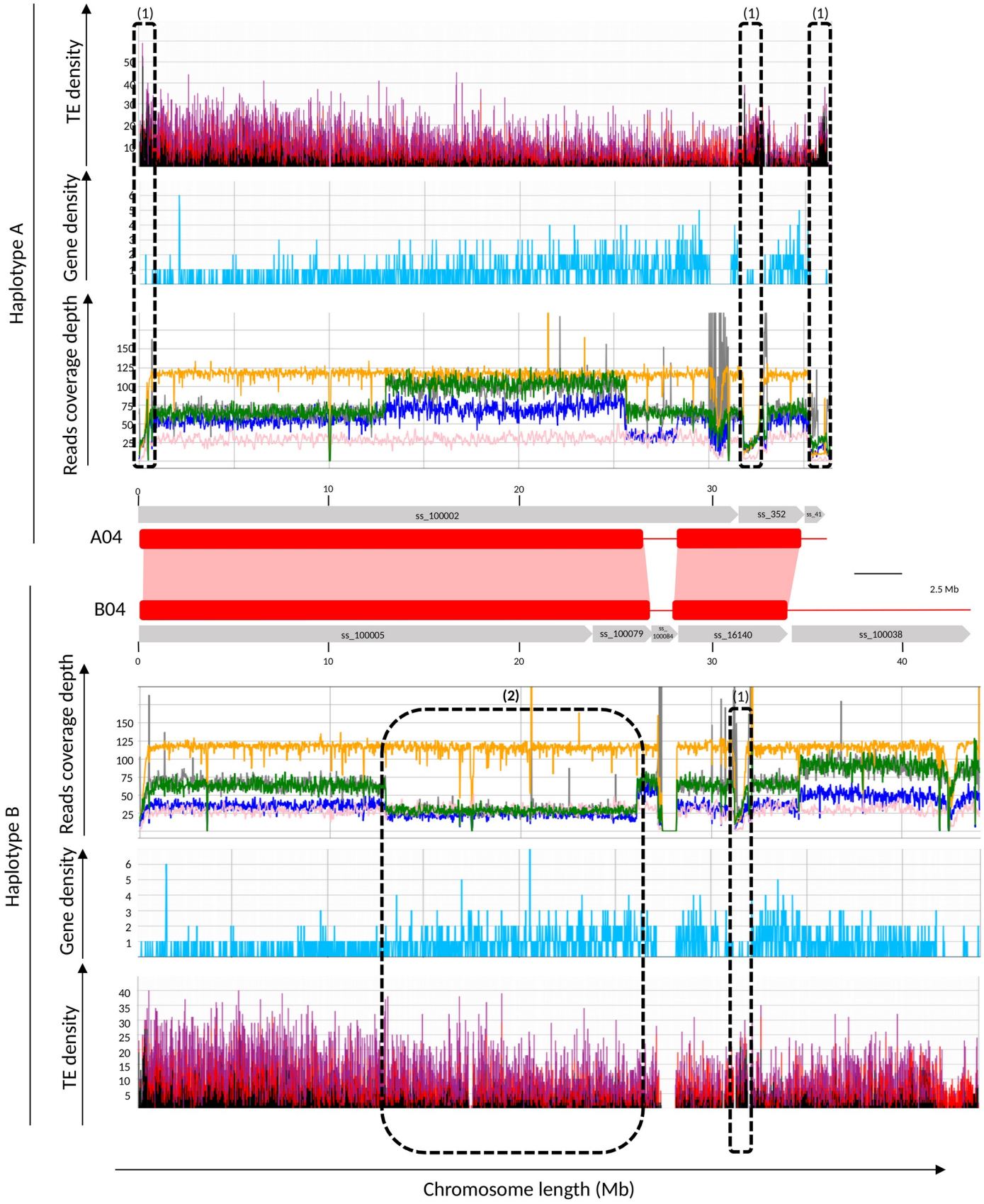

15

Supplemental Figure 9 continued

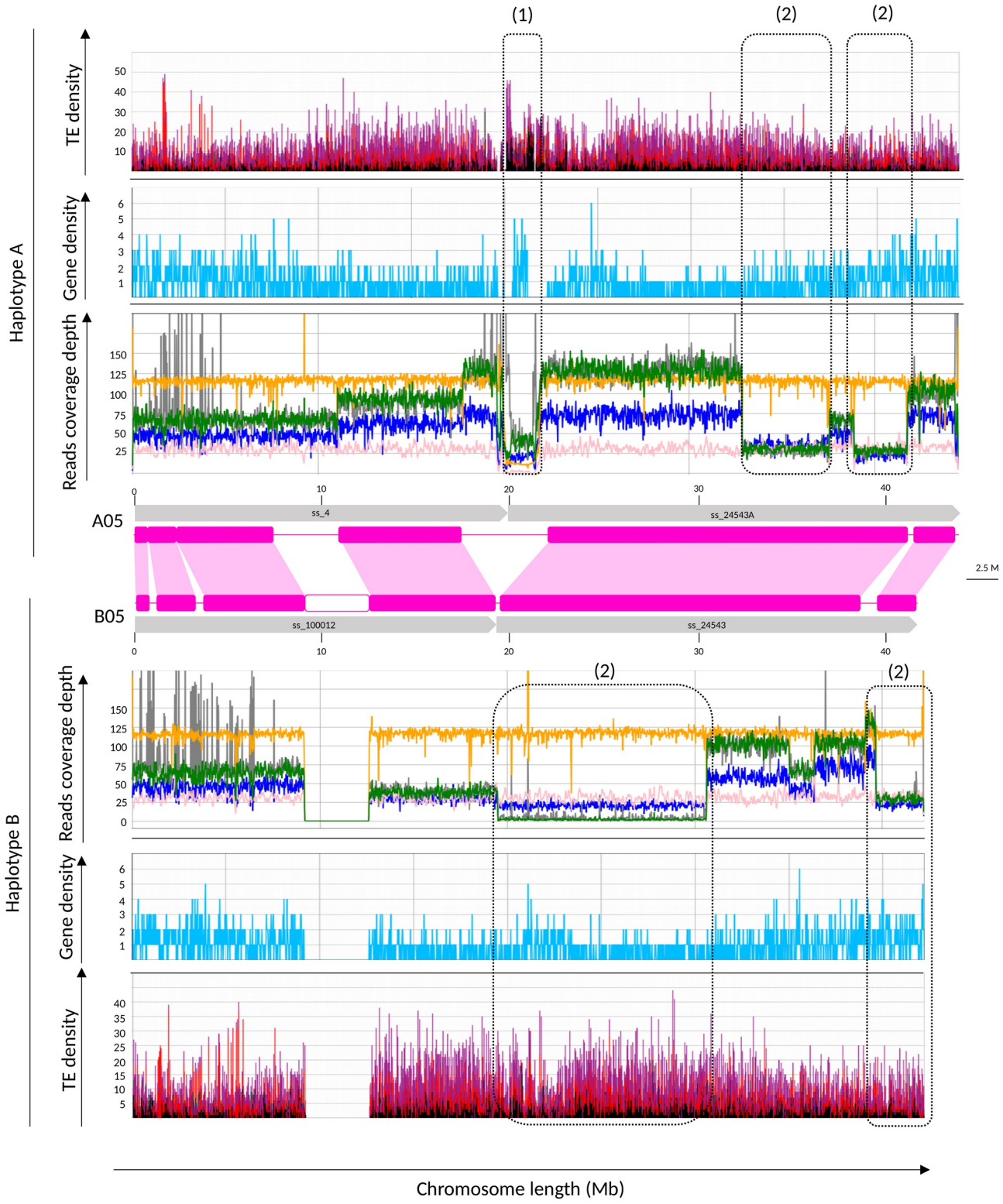

16

59 Supplemental Figure 9 continued

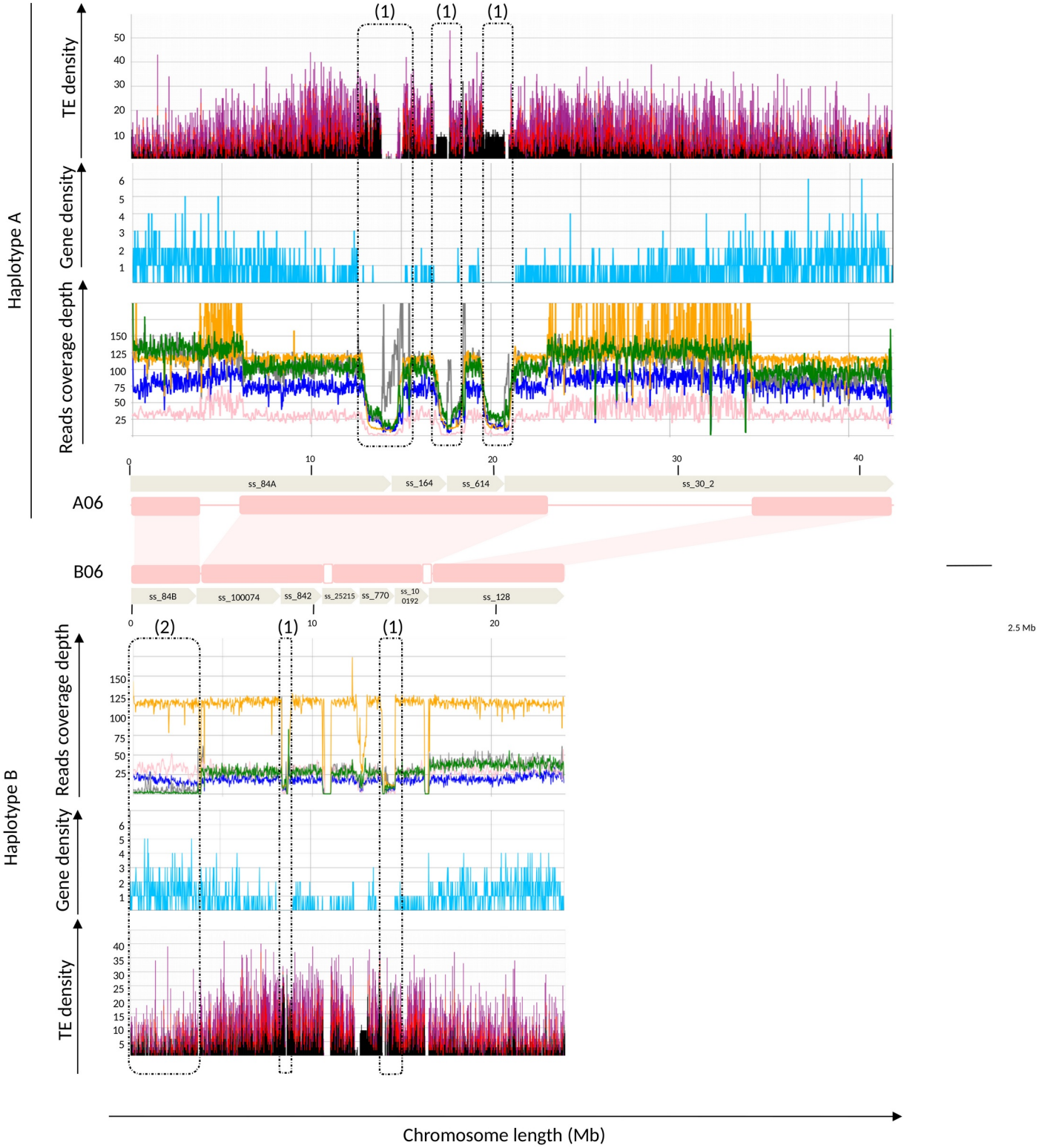

17

60 Supplemental Figure 9 continued

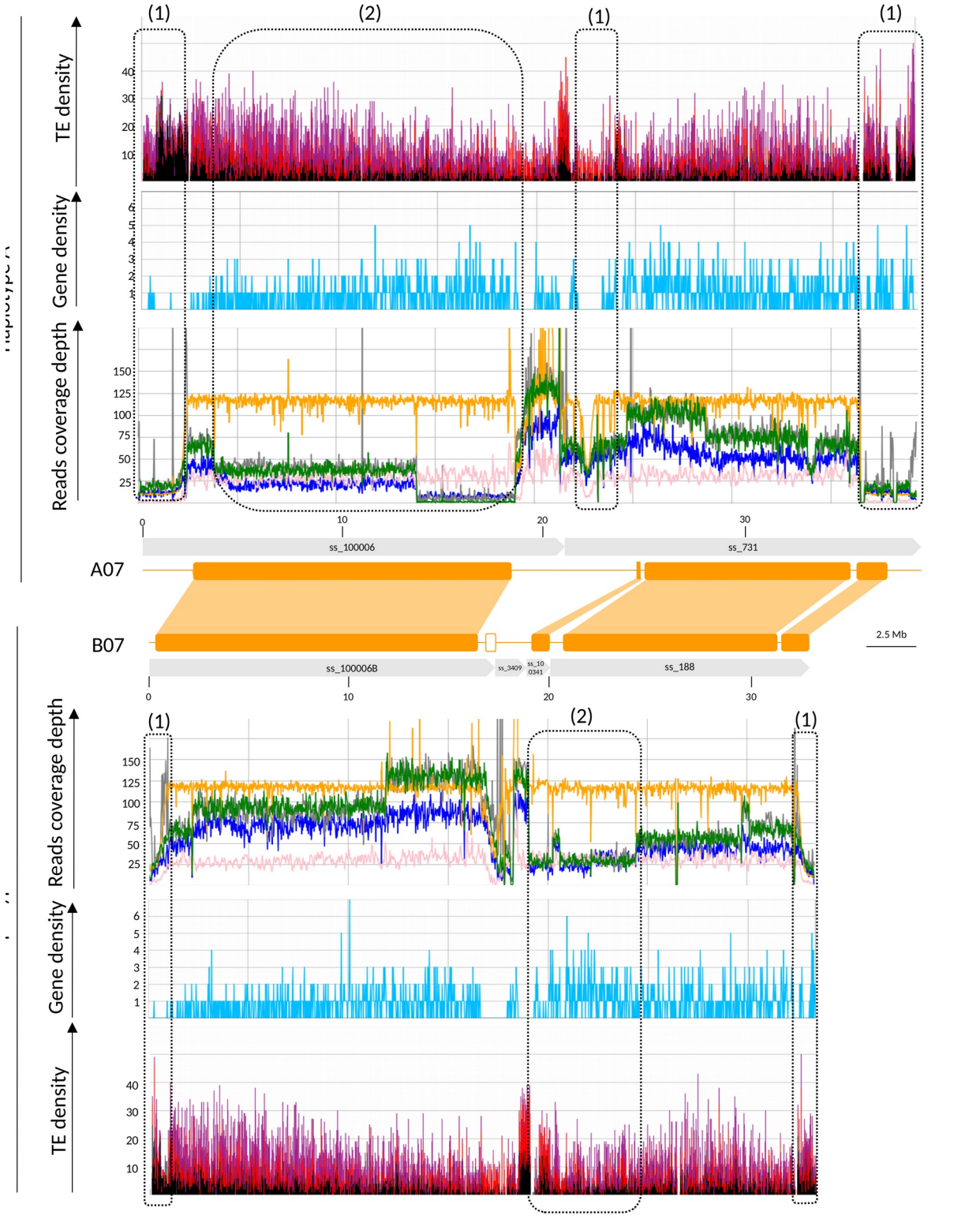

18

61 Supplemental Figure 9 continued

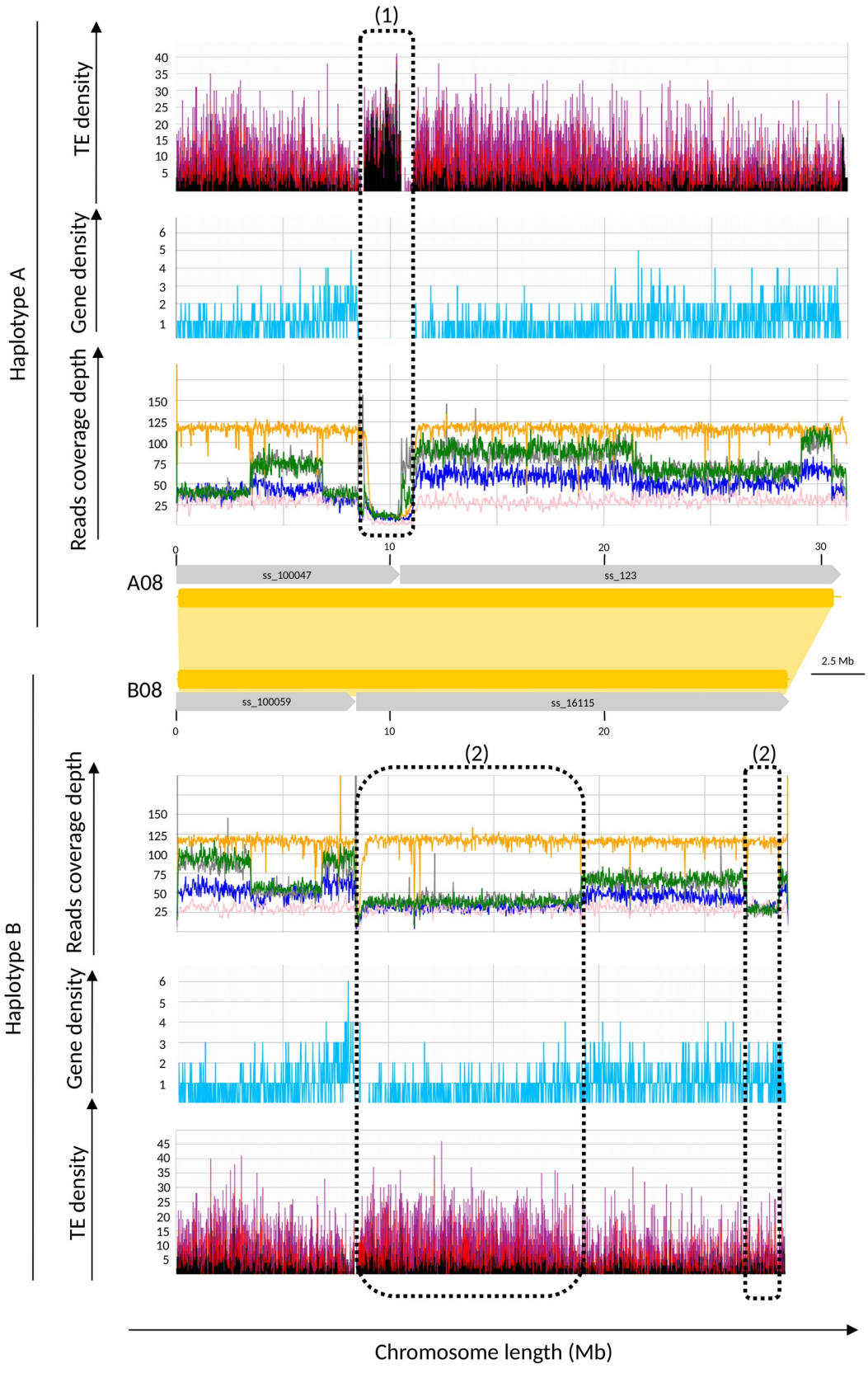

62 Supplemental Figure 9 continued

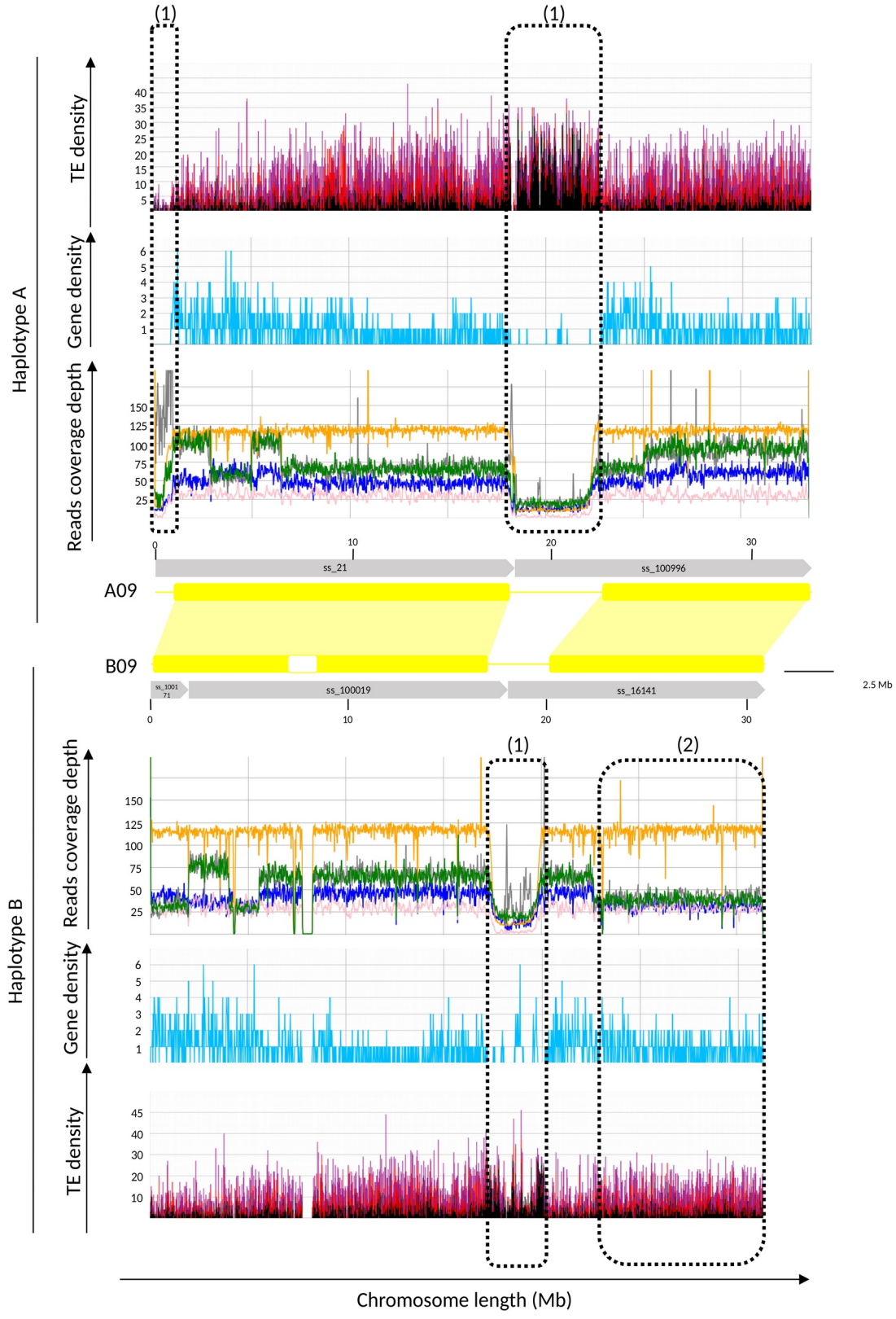

20

63 Supplemental Figure 9 continued

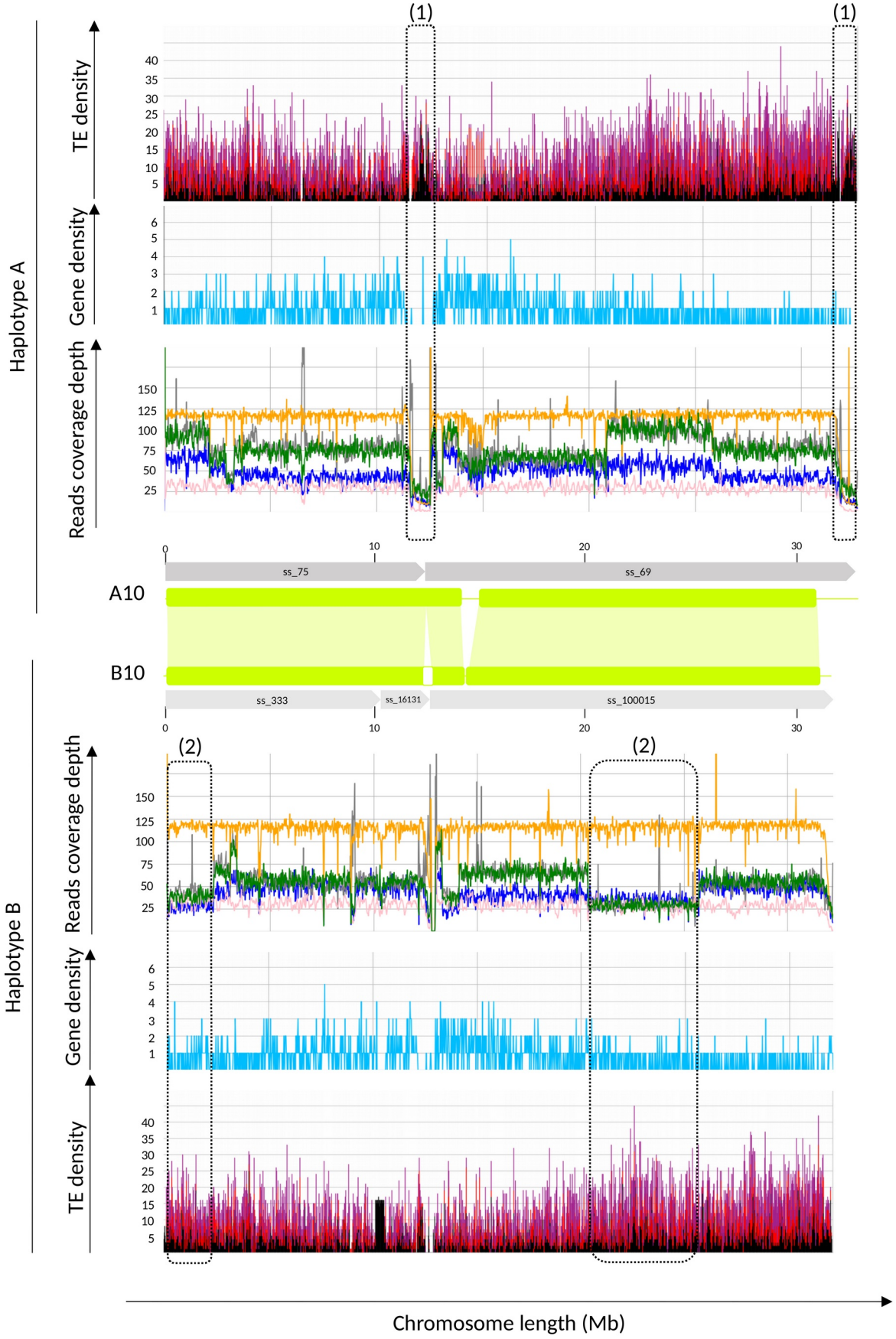

21

64 Supplemental Figure 9 continued

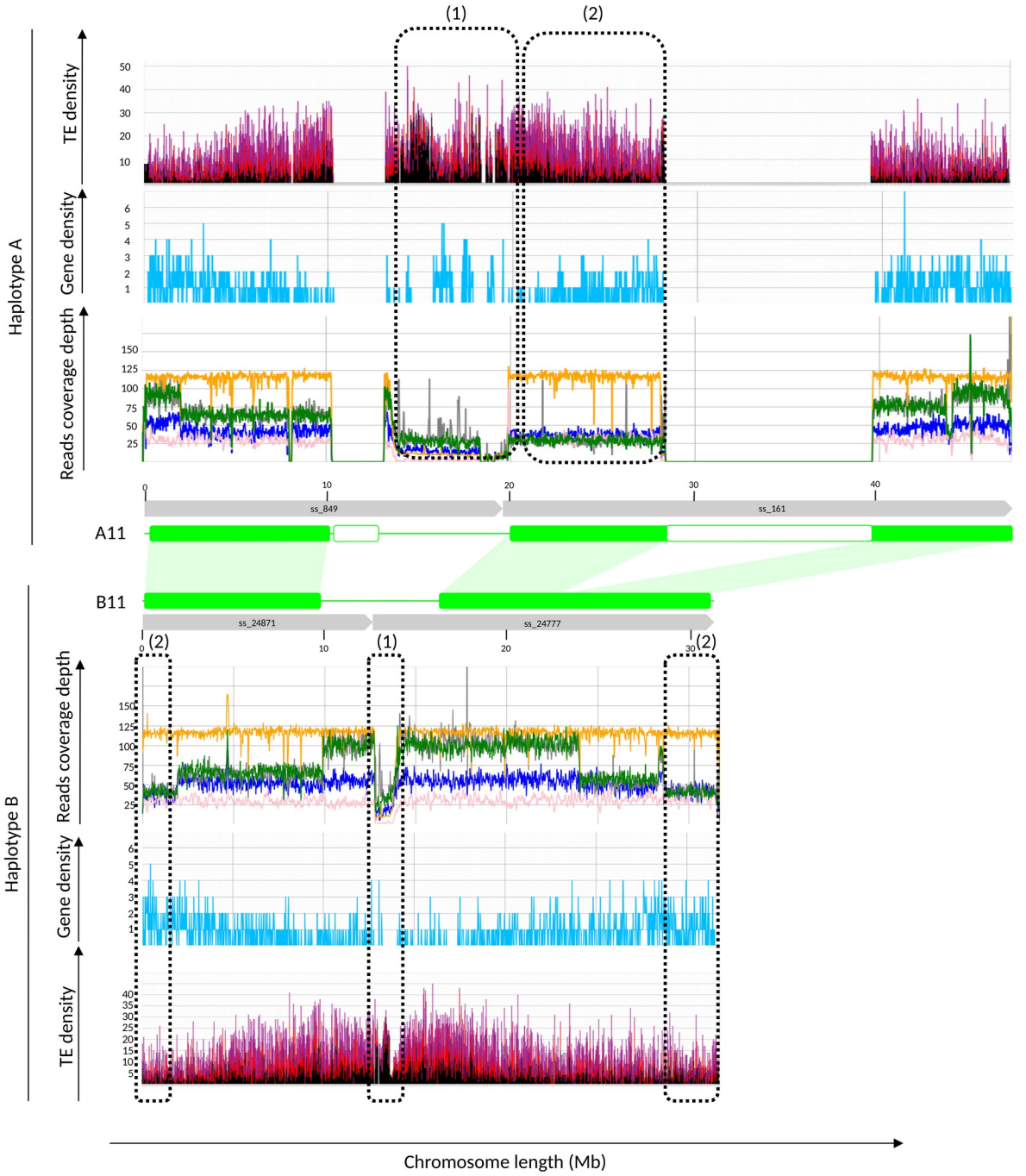

22

65 Supplemental Figure 9 continued

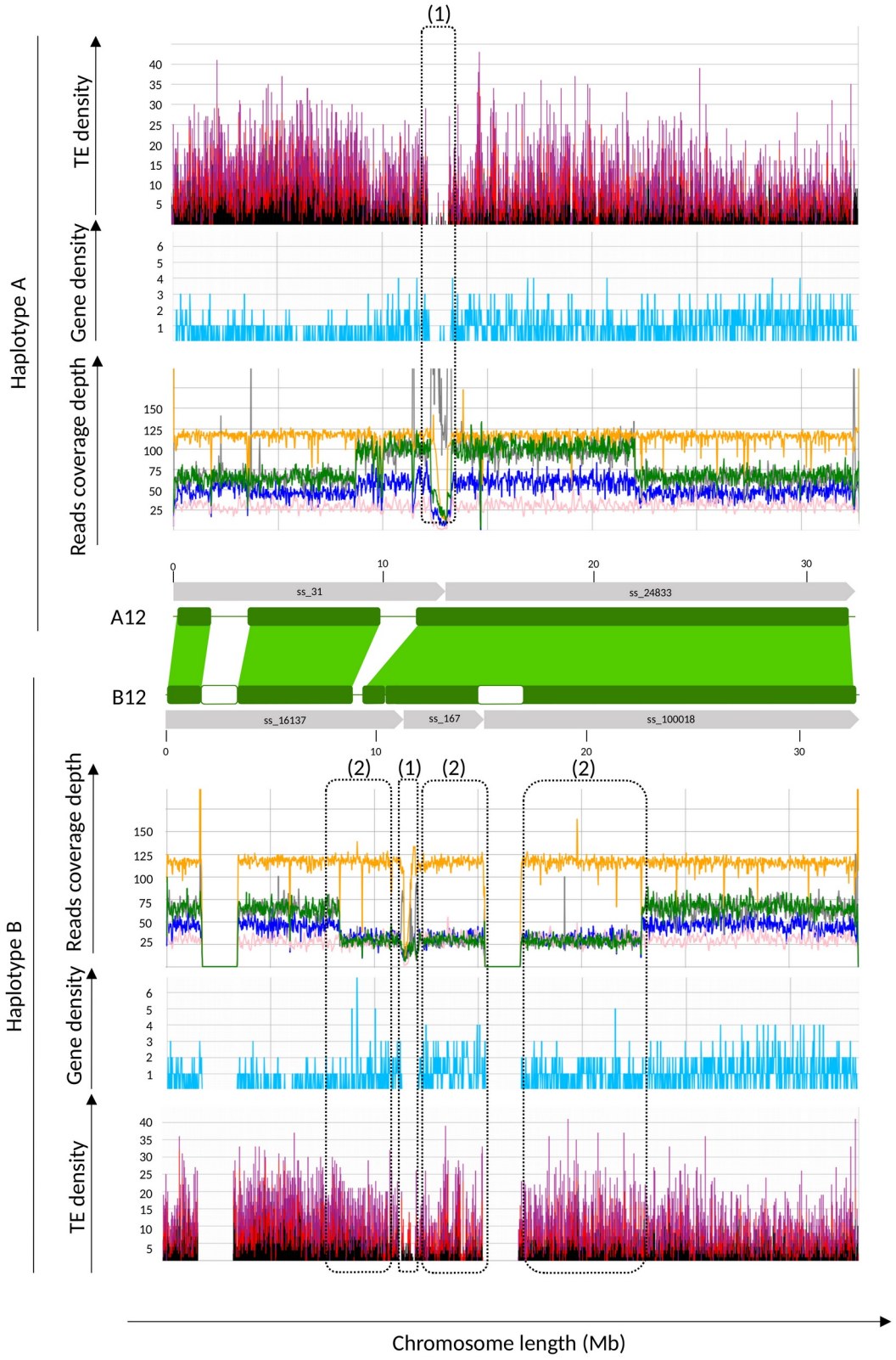

23

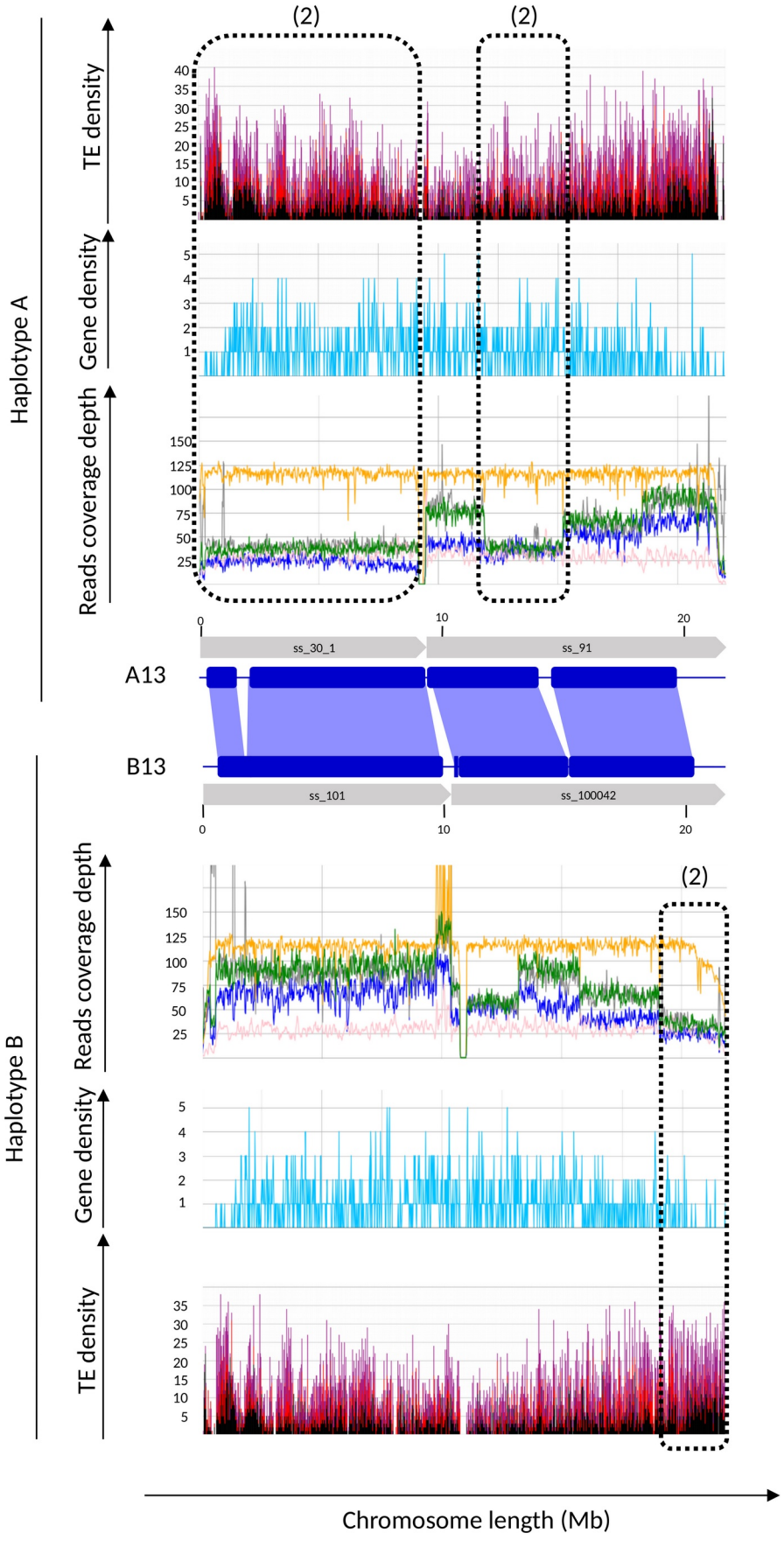
Haplotype A
TE density
Gene density
Reads coverage depth
(2)
(2)
ss_30_1
ss_91
A13
B13
ss_101
ss_100042
Haplotype B
Reads coverage depth
Gene density
TE density
(2)
Chromosome length (Mb)

24

67 Supplemental Figure 9 continued

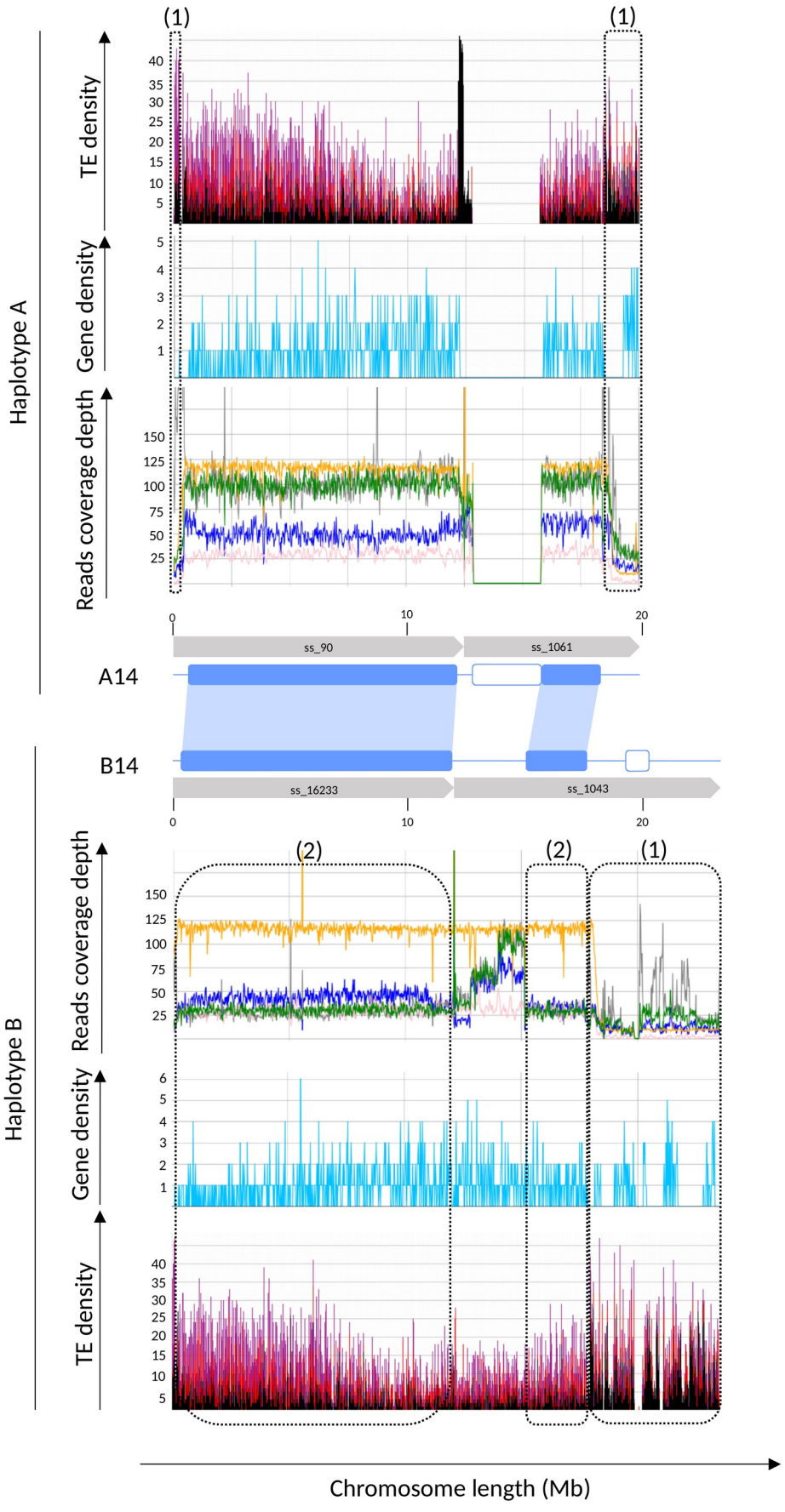

25

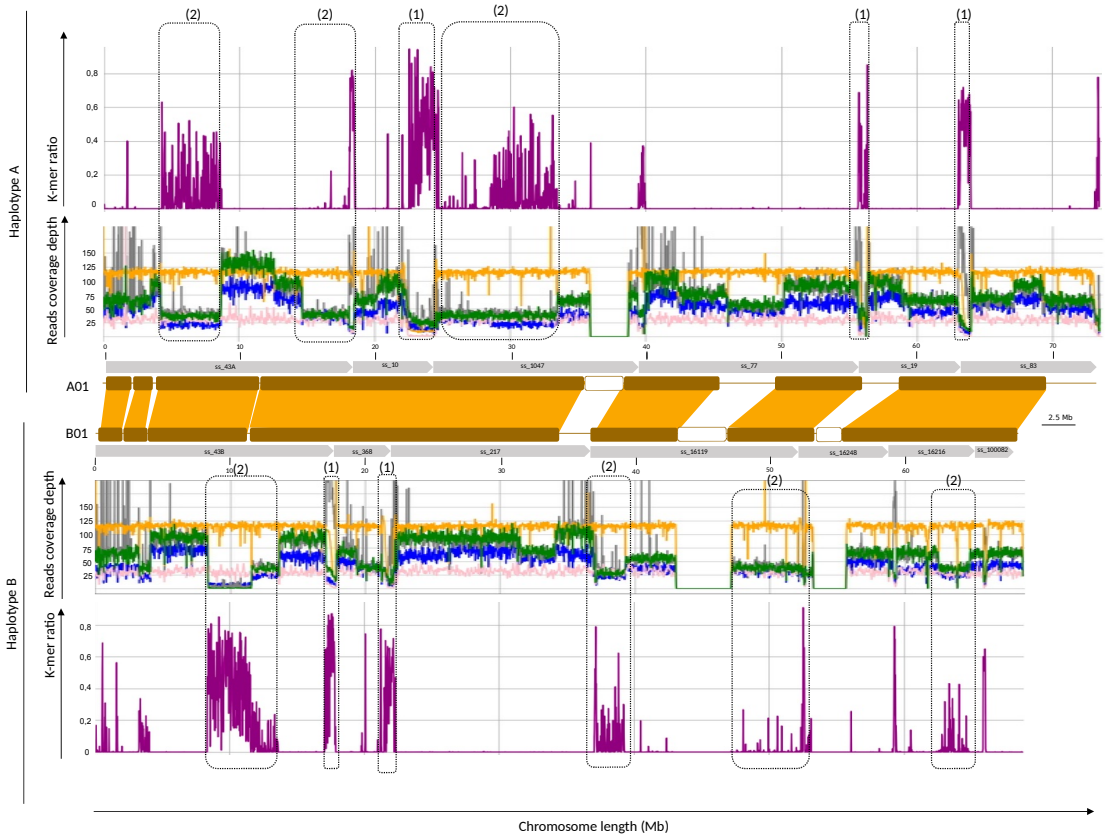

68 Supplemental Figure 10 Sequencing reads coverage depth and 5X-15X depth k-mers density
69 distribution along the 14 pairs of chromosomes

70 Obtained by mapping Daphna Illumina reads (yellow), CR0040 PacBio Hifi (blue), Nanopore
71 reads (green) and optical mapping data (red) on the CR0040 assembly. The ratio of k-mers
72 (47-mers) of depth between 5X and 15X are represented along each pair of chromosomes
73 (genomic windows of 20Kb). For other details see the legend of Supplemental Figure 9.

26

74 Supplemental Figure 10 continued

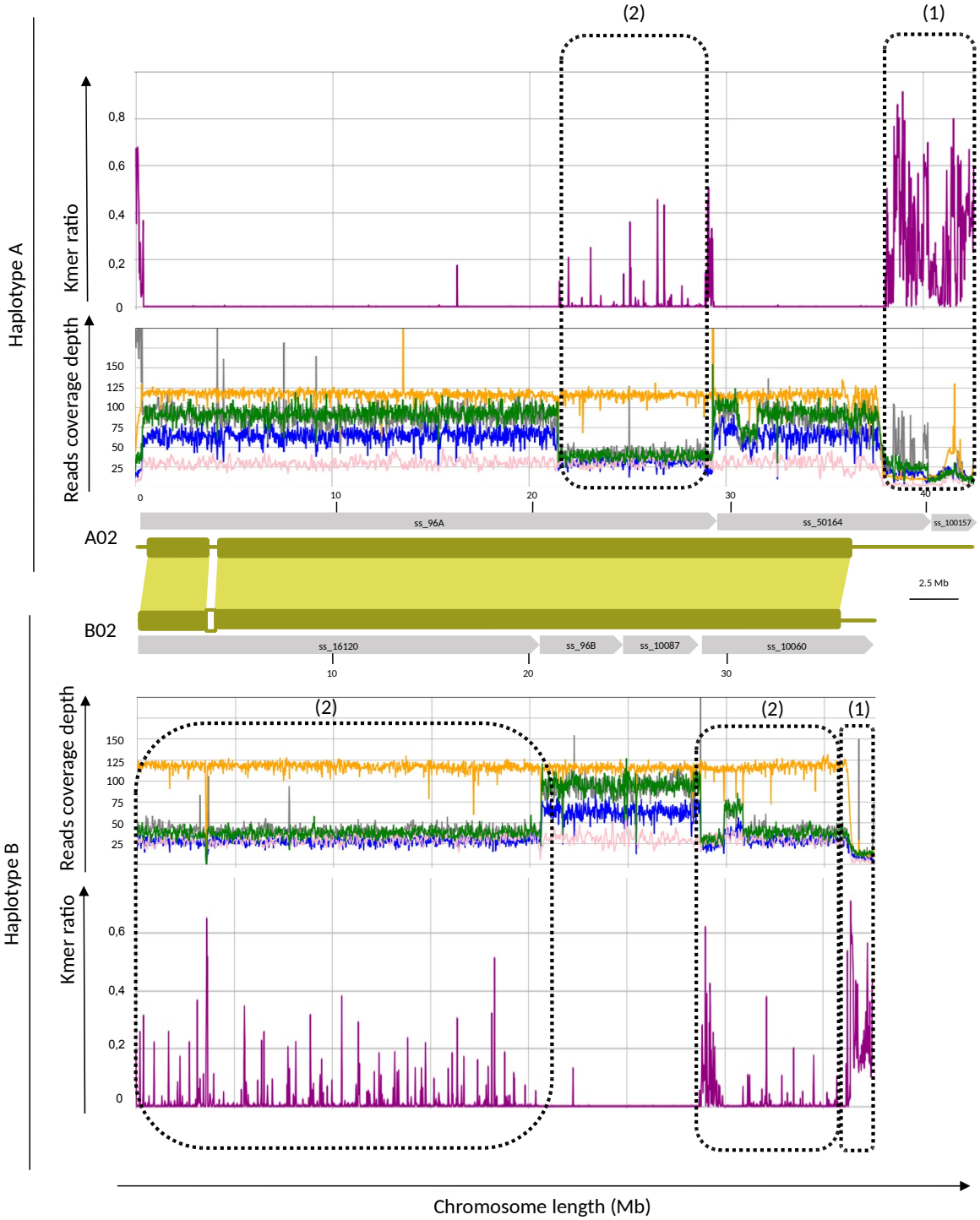

27

75 Supplemental Figure 10 continued

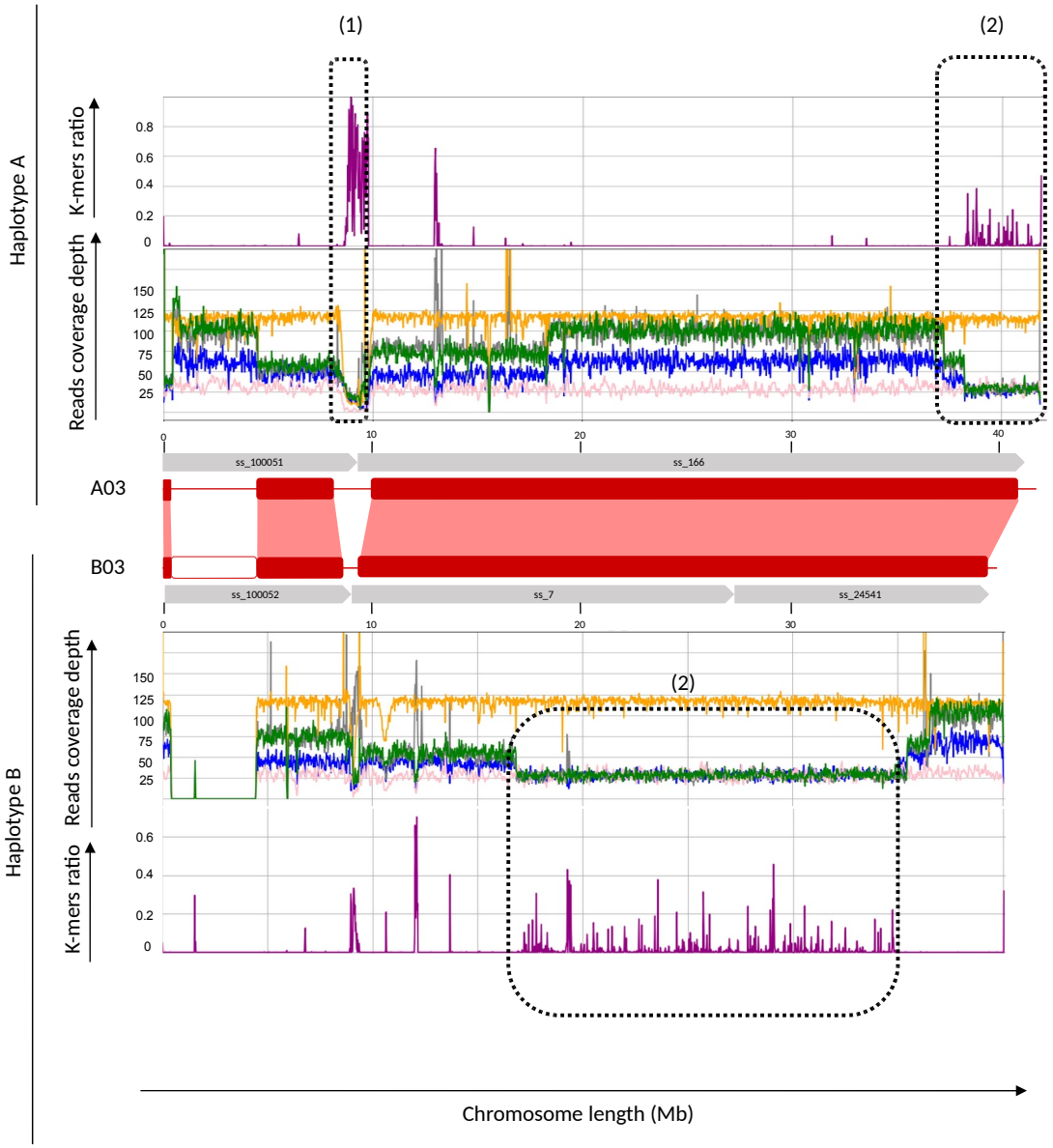

28

76 Supplemental Figure 10 continued

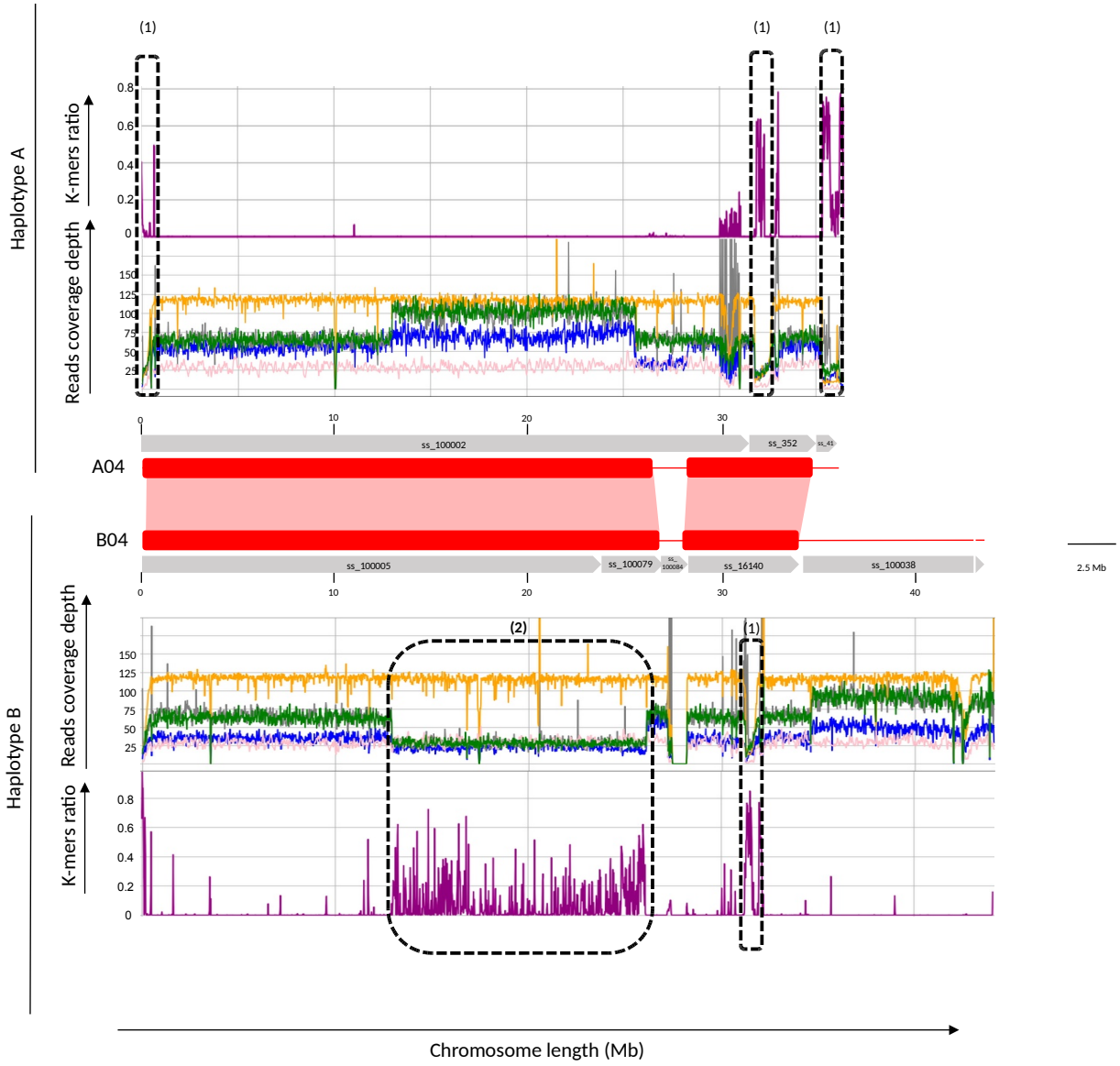

29

77 Supplemental Figure 10 continued

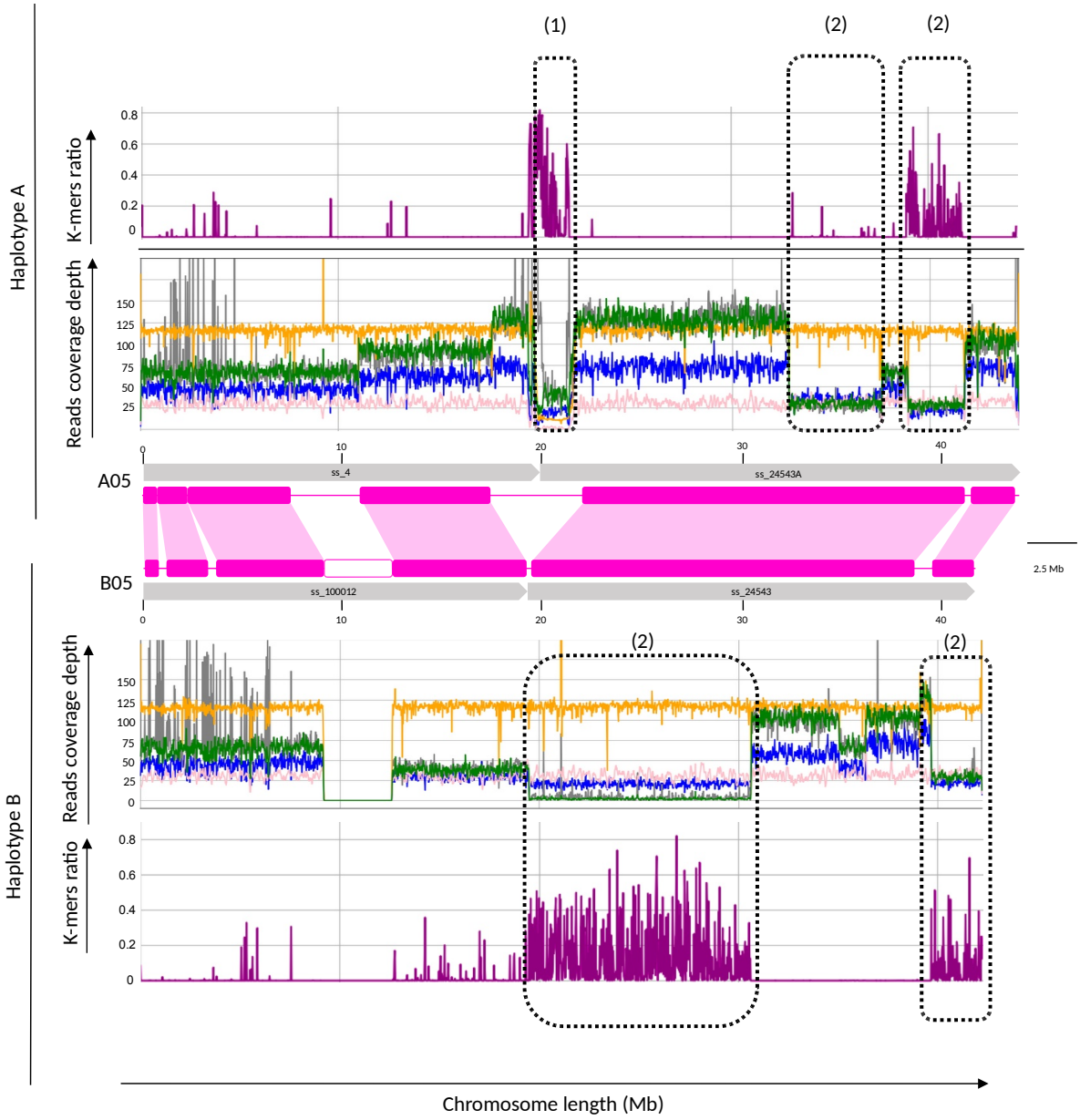

30

78 Supplemental Figure 10 continued

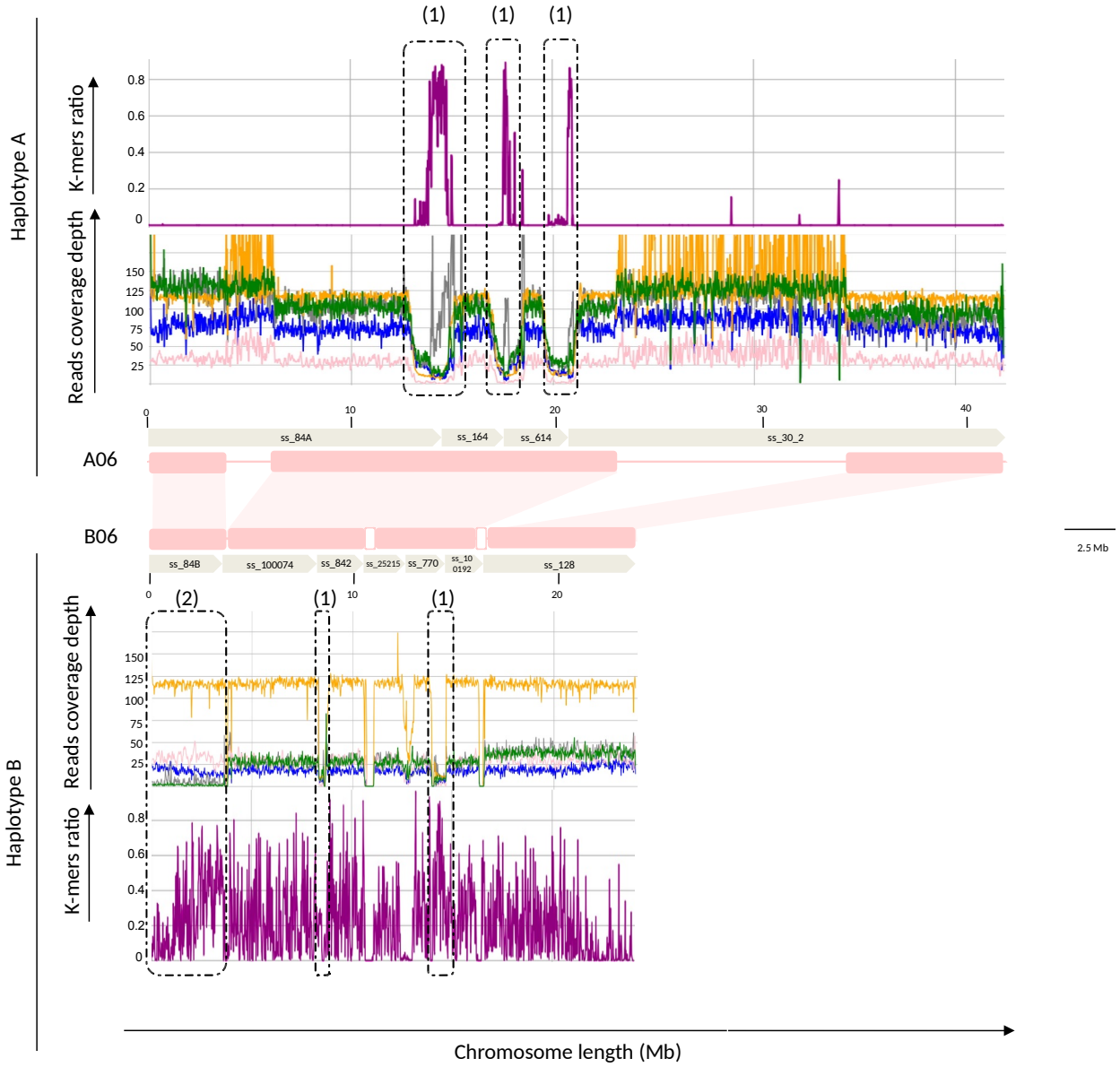

31

79 Supplemental Figure 10 continued

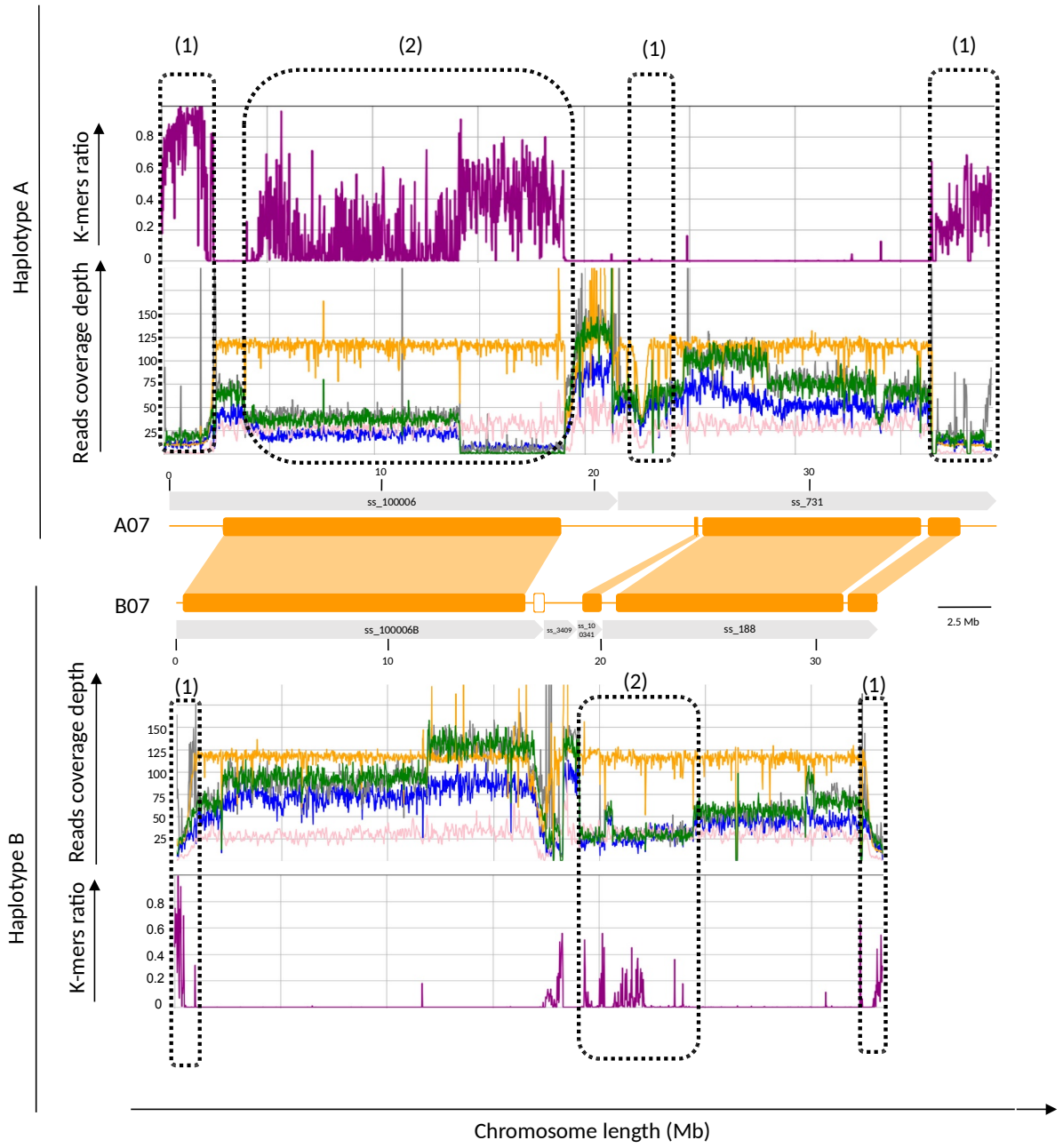

32

80 Supplemental Figure 10 continued

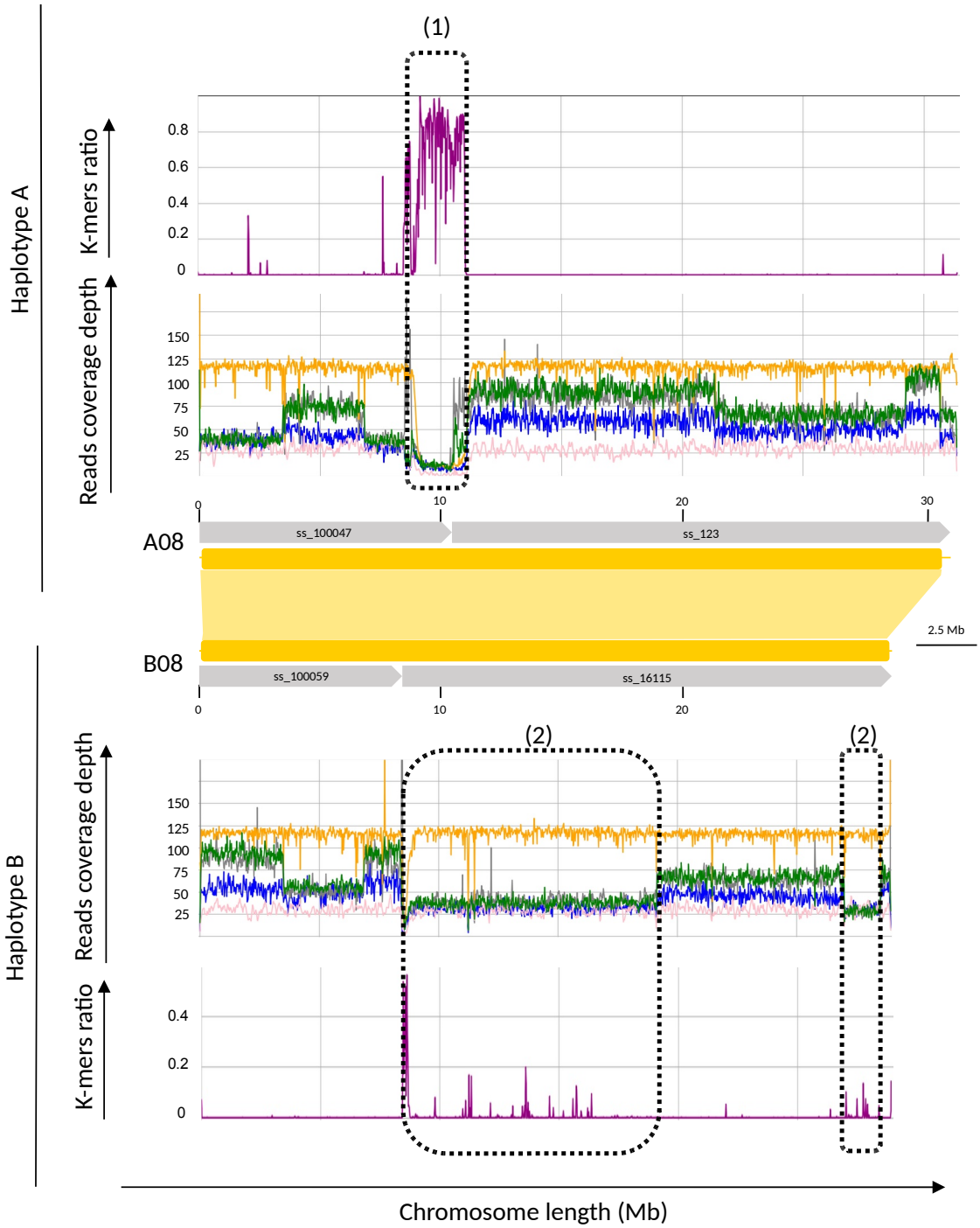

33

81 Supplemental Figure 10 continued

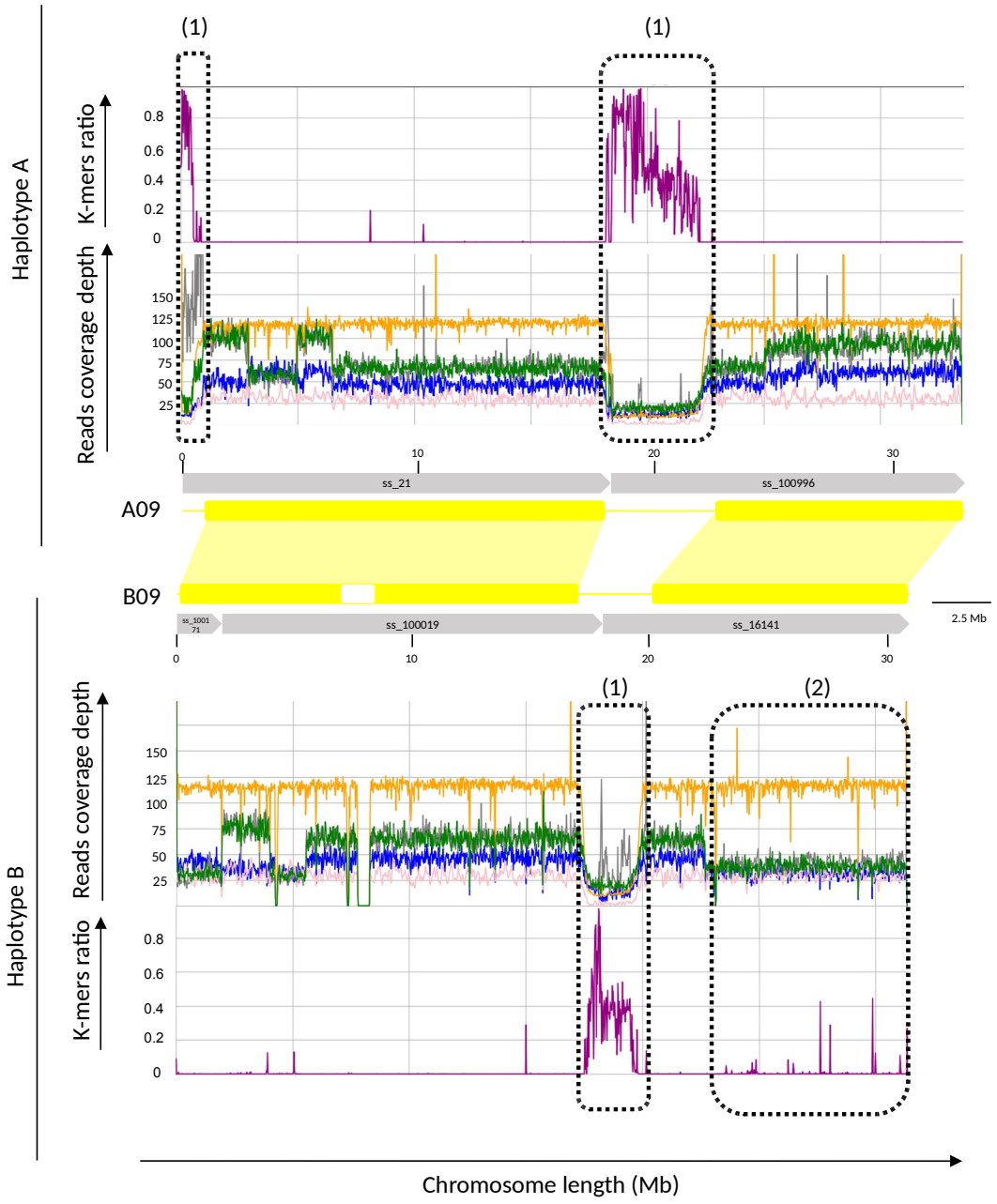

34

82 Supplemental Figure 10 continued

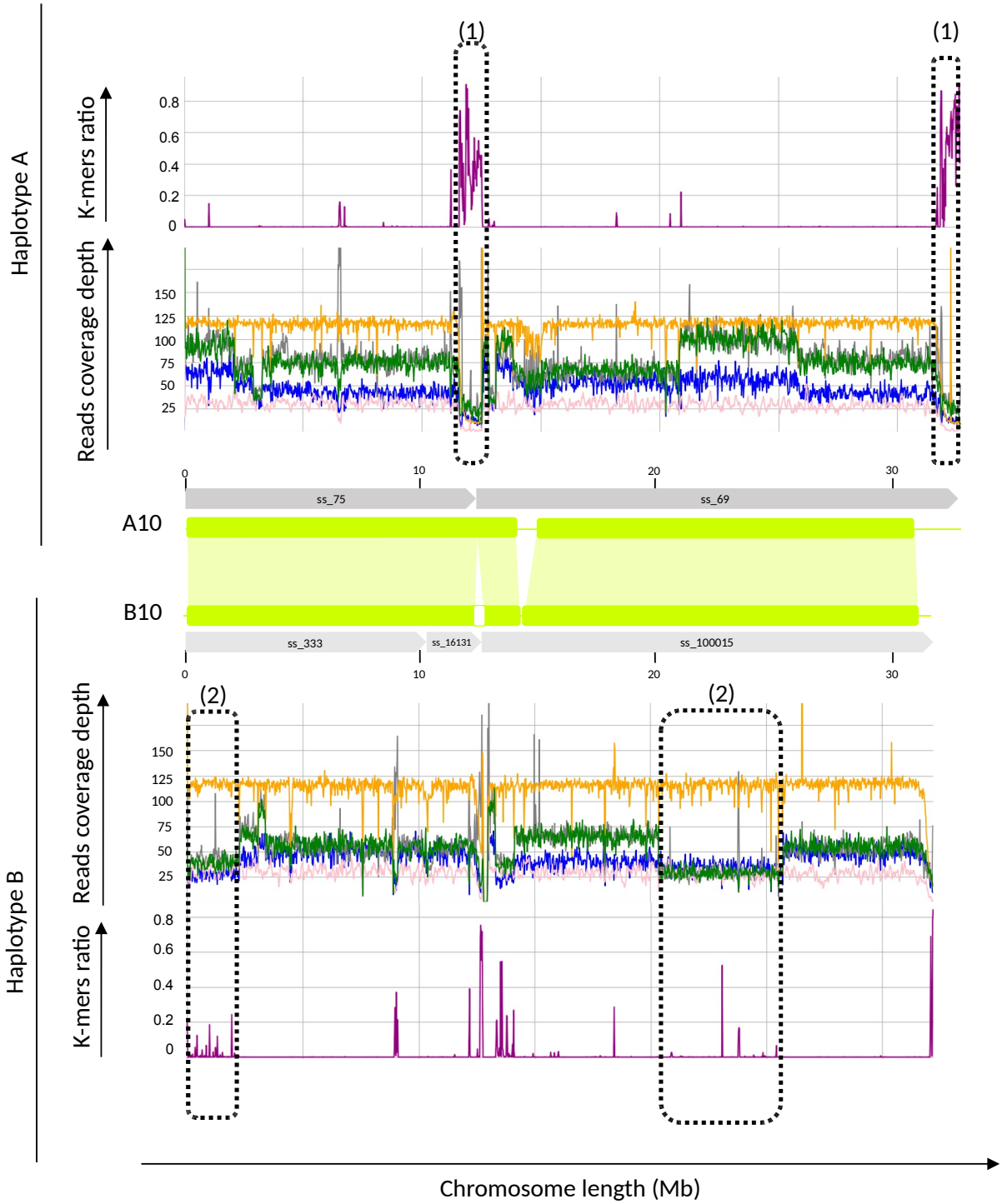

35

83 Supplemental Figure 10 continued

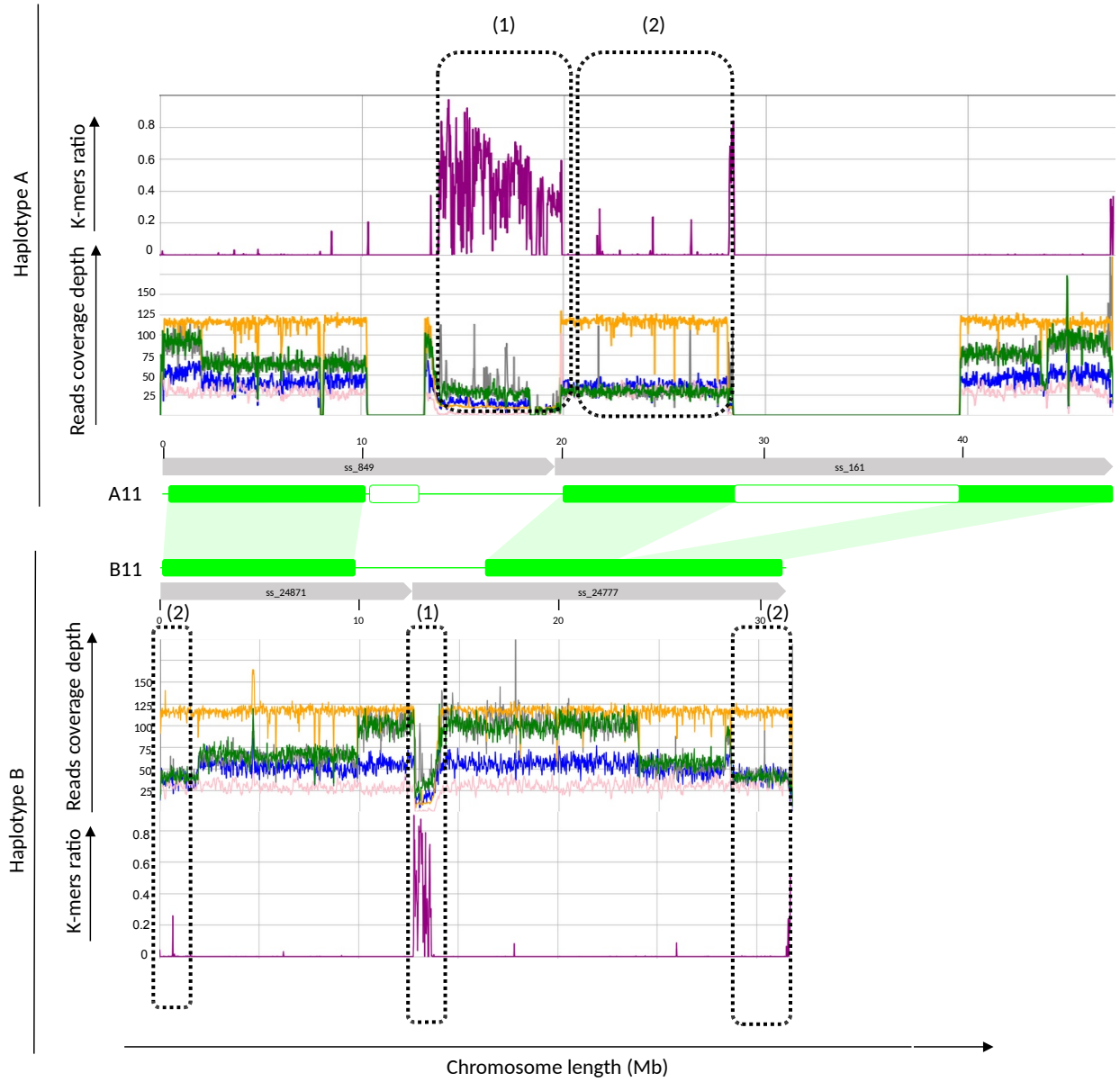

36

84 Supplemental Figure 10 continued

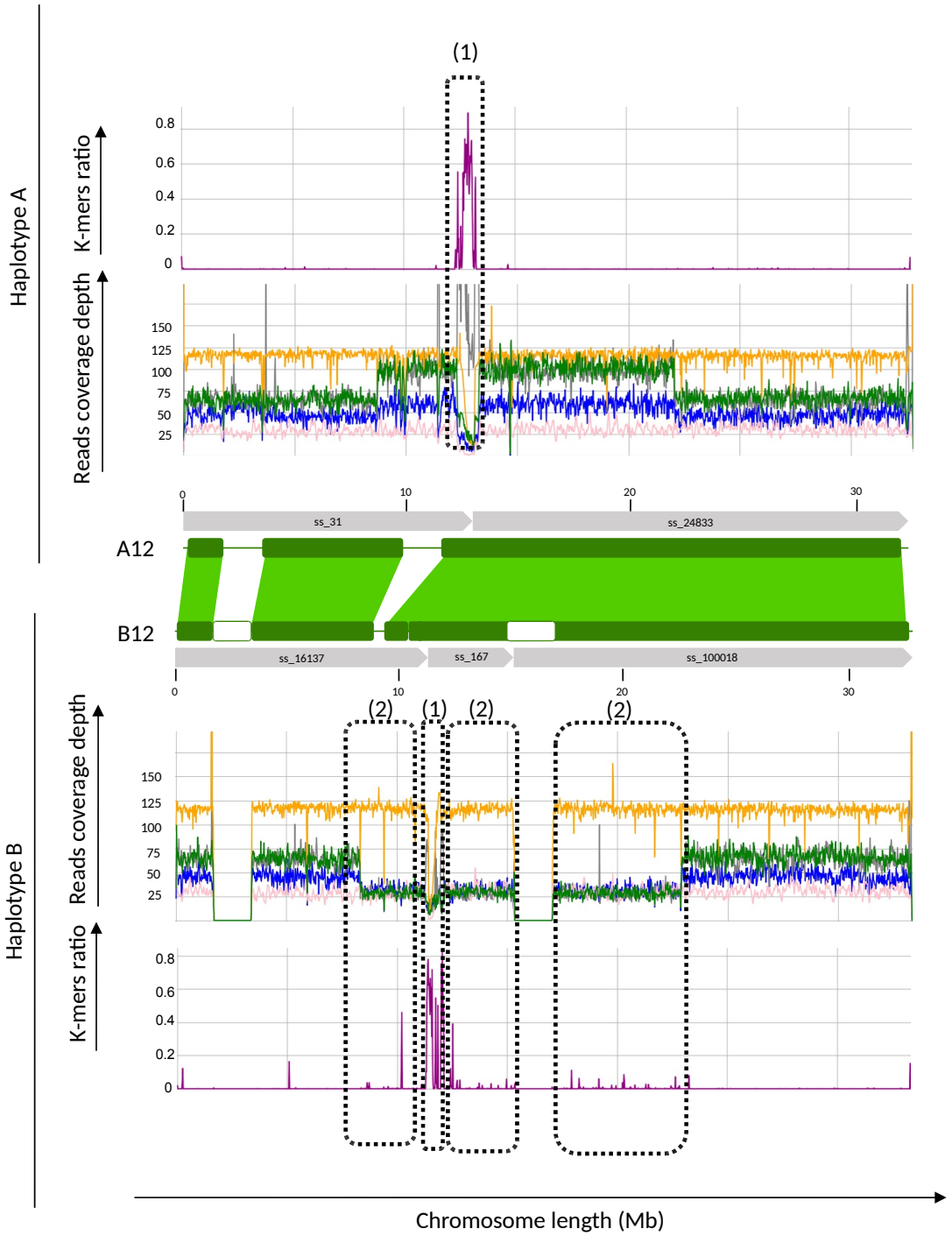

37

85 Supplemental Figure 10 continued

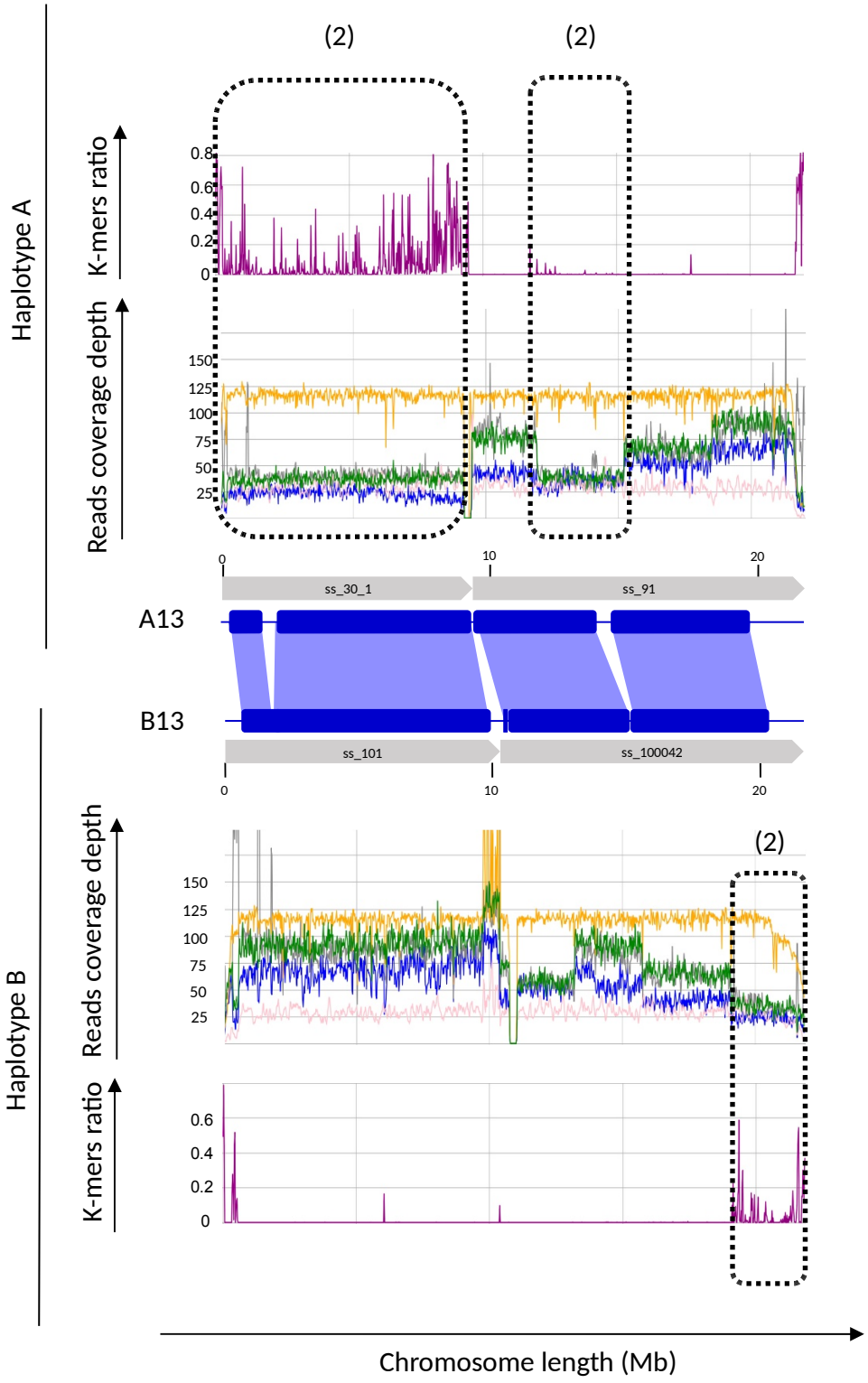

38

86 Supplemental Figure 10 continued

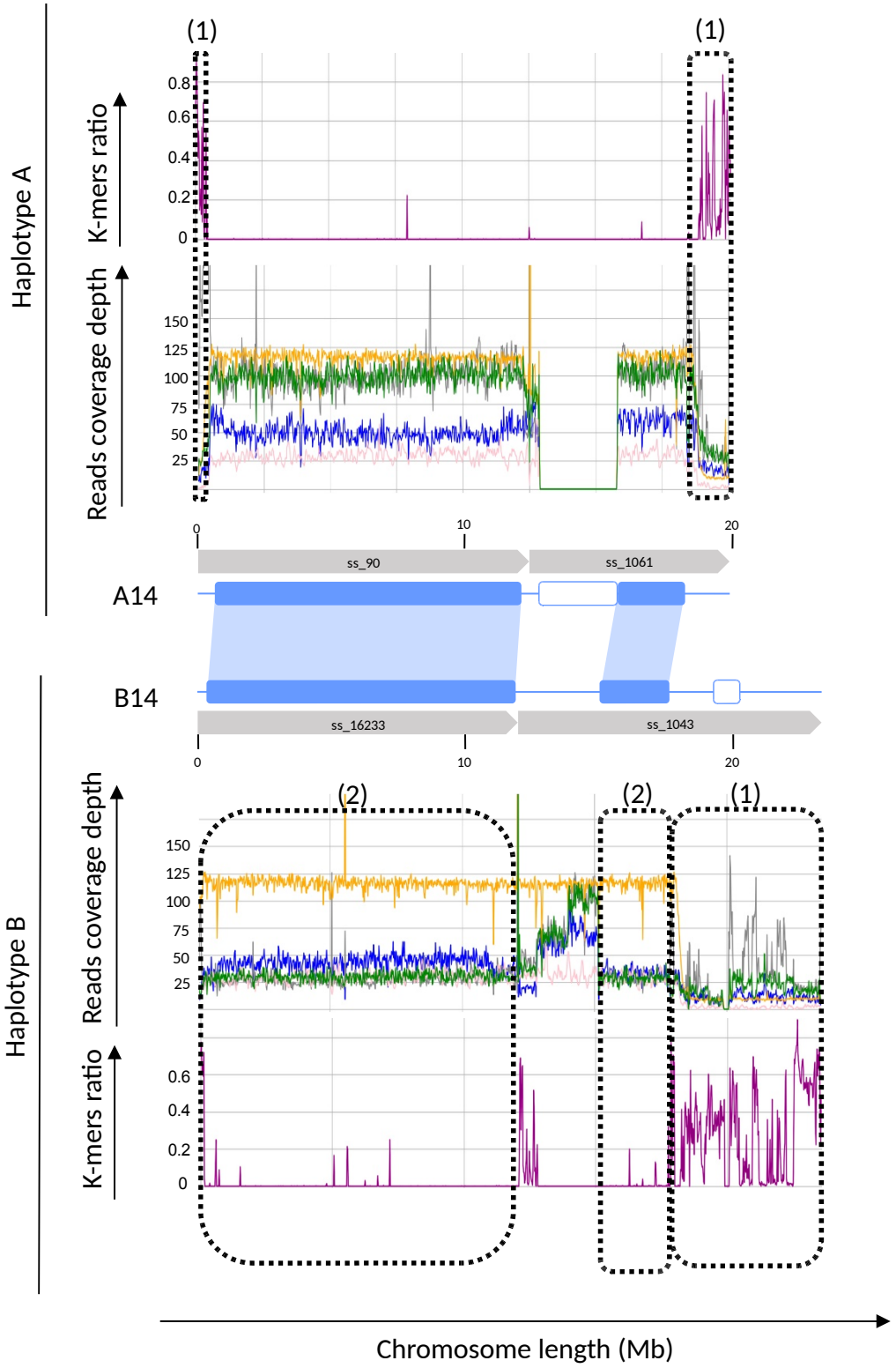

39

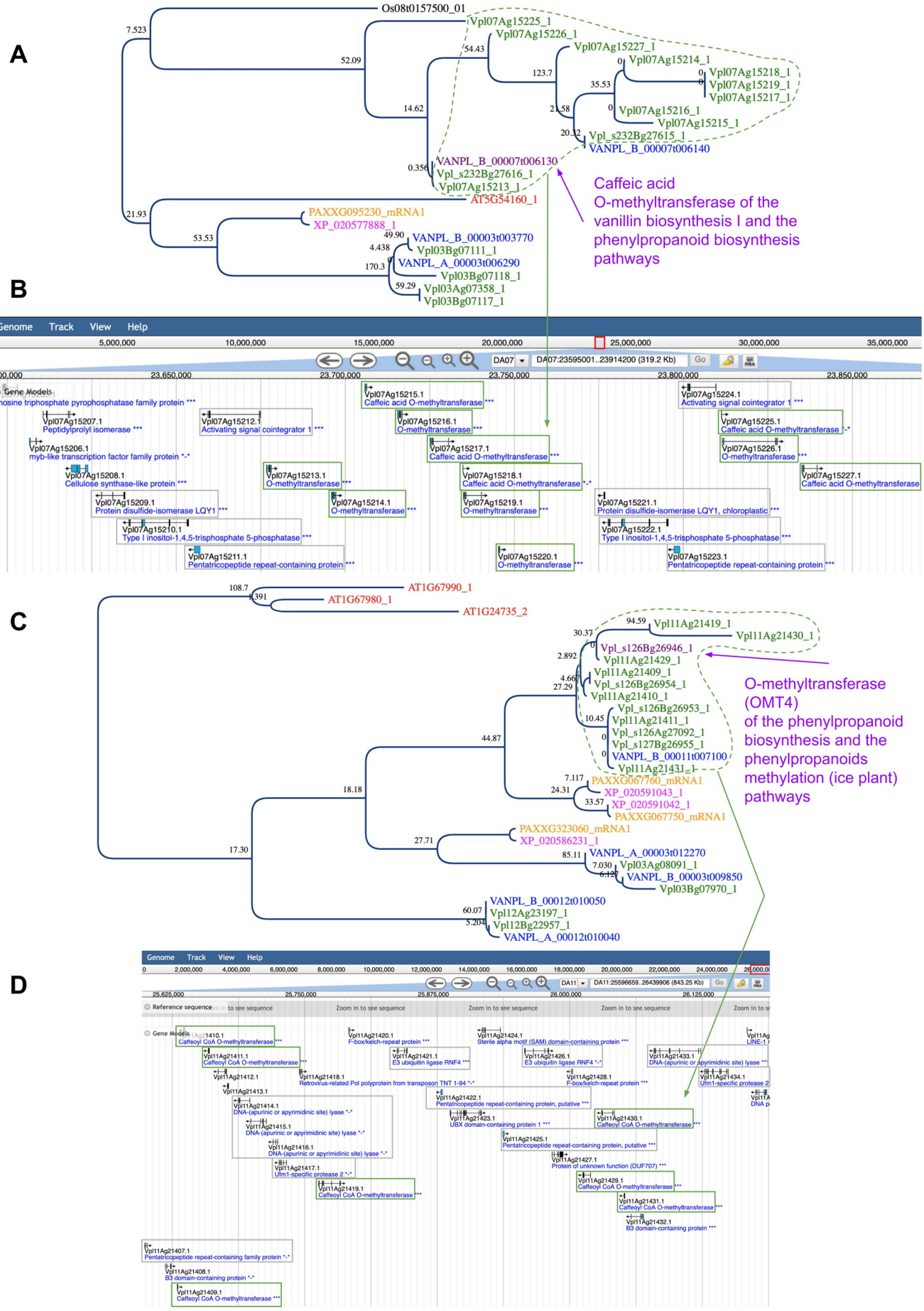
A
Os08t0157500_01
Vpl07Ag15225_1
Vpl07Ag15226_1
Vpl07Ag15227_1
Vpl07Ag15214_1
Vpl07Ag15218_1
Vpl07Ag15219_1
Vpl07Ag15217_1
Vpl07Ag15216_1
Vpl07Ag15215_1
Vpl_s232Bg27615_1
VANPL_B_00007t006140
VANPL_B_00007t006130
Vpl_s232Bg27616_1
Vpl07Ag15213_1
AT5G54160_1
PAXXG095230_mRNA1
XP_020577888_1
VANPL_B_00003t003770
Vpl03Bg07111_1
VANPL_A_00003t006290
Vpl03Bg07118_1
Vpl03Ag07358_1
Vpl03Bg07117_1
Caffeic acid O-methyltransferase of the vanillin biosynthesis I and the phenylpropanoid biosynthesis pathways
B
Genome
Track
View
Help
C
AT1G67990_1
AT1G67980_1
AT1G24735_2
Vpl11Ag21419_1
Vpl11Ag21430_1
Vpl_s126Bg26946_1
Vpl11Ag21429_1
Vpl11Ag21409_1
Vpl_s126Bg26954_1
Vpl11Ag21410_1
Vpl_s126Bg26953_1
Vpl11Ag21411_1
Vpl_s126Ag27092_1
Vpl_s127Bg26955_1
VANPL_B_00011t007100
Vpl11Ag21431_1
PAXXG067760_mRNA1
XP_020591043_1
XP_020591042_1
PAXXG067750_mRNA1
PAXXG323060_mRNA1
XP_020586231_1
VANPL_A_00003t012270
Vpl03Ag08091_1
VANPL_B_00003t009850
Vpl03Bg07970_1
VANPL_B_00012t010050
Vpl12Ag23197_1
Vpl12Bg22957_1
VANPL_A_00012t010040
O-methyltransferase (OMT4) of the phenylpropanoid biosynthesis and the phenylpropanoids methylation (ice plant) pathways
D
Genome
Track
View
Help

40

Supplemental Figure 11 Caffeic acid O-methyltransferase cluster comparison between CR0040 and Daphna. Phylogenetic trees and genomic positions of clusters of genes encoding for Caffeic acid O-methyltransferase (A, B; OG0000841; e.g. VANPL_B_00007t006130) and for O-methyltransferase (C, D; OG0000449; e.g. VANPL_B_00011t00710 Vpl_s126Bg26946.1). JBrowse screenshots were done from https://vanilla-genome-hub.cirad.fr/content/v-planifolia-daphna, DA07:23595079..23914278 (319.2 Kb) and DA11:25632407..26200506 (568.1 Kb).

41

Supplemental tables

Supplemental Table 1 Nuclear classes in flow cytometry samples from *Vanilla planifolia* CR0040 nodal tissues

Nuclear populations	2C	4E	8E	16E	32E
Proportion Frequency (%, mean (sd) of 13 independent measures)	17.31 (10.08)	18.52 (7.21)	33.95 (11.41)	21.5 (7.84)	8.72 (12.73)
Mean (sd) of previous interpeak ratio* (Brown et al., 2017)		1.28 (0.01)	1.44 (0.02)	1.62 (0.03)	1.75 (0.02)
Mean (sd) of interpeak ratio*		1.30 (0.03)	1.42 (0.03)	1.61 (0.02)	1.73 (0.08)

* Interpeak Ratio is the fluorescence intensity (I, arbitrary units) of peak n to peak (n — 1).

sd, standard deviation.

Supplemental Table 2 Main statistics of sequencing data production

Technology	Instrument	Sample type	Number of sequences	Raw data (Gb)	N50 (Kb)
Illumina	HiSeq3000	DNA 10X genomics	1,363,939,362	205	0.15
ONT	GridION	DNA	2,855,136	16	13
ONT	PromethION	DNA	18,044,495	131	18
Pacific BioSciences	Sequel II	DNA	15,306,231	1,178	15.2*
Illumina	NovaSeq6000	mRNA	857,606,502	129	0.15

Gb, giga bases ; Kb, kilo bases.

*N50 for 69.75 Gb of HiFi reads

2

Supplemental Table 3 Main metrics of CR0040 genome assemblies

	10X	ONT	PacBio HiFi	Meta-assembly
Input data	200 Gb	150 Gb	69 Gb	
Estimated coverage	100X	75X	35X	
Cumulative size (Gb)	1.68	1.9	3.4	3.3
Contig number	254,400	21,443	24,534	180,957
N50 (kb)	25	115	924	133
Max size (Mb)	9.6	23.4	31	28.7

Gb, giga bases ; Kb, kilo bases ; Mb, mega bases.

11 Supplemental Table 4 Main metrics for the best genome assembly

	All contigs	Hybrid scaffolds	Contigs not scaffolded	Haplotype A	Haplotype B
Cumulative size (Gb)	3.4	1.9	1.5	1.5	1.9
Numbers	24,534	874	23,037	3,874	17,655
N50 (Mb)	0.92	6.2	0.09	3	0,4
Max Size (Mb)	31	32	10	73	69
N's (Mb)	0	79	0	37	40

12 Gb, giga bases ; Mb, mega bases.

13 Supplemental Table 5 Genic completeness for CR0040 genome

	Haplotype A	Haplotype B	Haplotypes A+B
Genes in Viridiplantae database	425	425	425
Complete single-copy	379 (89.2%)	367 (86.4%)	17 (4%)
Complete duplicated	17 (4.0%)	17 (4%)	395 (92.9%)
Fragment	1 (0.2%)	27 (6.4%)	1 (0.2%)
Missing	28 (6.6%)	14 (3.3%)	12 (2.9%)
Genes in Embryophyta database	1,614	1,614	1,614
Complete single-copy	1,436 (89%)	1,410 (87.4%)	182 (11.3%)
Complete duplicated	53 (3.3%)	86 (5.3%)	1,367 (84.7%)
Fragment	13 (0.8%)	20 (1.2%)	13 (0.8%)
Missing	112 (6.9%)	98 (6.1%)	52 (3.2%)
Genes in Liliopsida database	3,236	3,236	3,236
Complete single-copy	2,639 (81.6%)	2,589 (80%)	402 (12.4%)
Complete duplicated	111 (3.4%)	174 (5.4%)	2,475 (76.5%)
Fragment	223 (6.9%)	249 (7.7%)	230 (7.1%)
Missing	263 (8.1%)	224 (6.9%)	129 (4%)

14 Supplemental Table 6 Main characteristics of RNA samples

BioSample accession	Tissue	Nanodrop concentration (ng/μL)	RNA Integrity Number
SAMN20691786	Fruit	32.02	8.7
SAMN20691787	Leaf	119.00	8.1
SAMN20691788	Flower	121.50	8.7
SAMN20691789	Stem	47.55	8.8
SAMN20691790	Soil root	179.40	9.1
SAMN20691791	Aerial root	98.32	8.0
SAMN20691792	Bud	326.80	9.1
SAMN20691793	Flower bud	112.70	9.4
SAMN20691794	Ovary	91.66	9.0
SAMN20691795	Mix	57.28	8.5

Supplemental Table 7 Main statistics of RNA-seq experiment

	Number of reads	Alignment rate (%)	Number of transcripts	Mean transcript size (bases)
Bud	47,018,576	93.84	90,813	2,049
Flower bud	49,472,733	92.87	86,515	1,971
Aerial roots	40,920,676	82.19	81,970	1,905
Leaves	40,129,580	93.55	79,462	1,959
Flowers	33,920,088	92.68	75,827	1,966
Fruits	32,941,273	89.28	72,767	1,903
Ovary	43,083,064	93.53	83,388	2,101
Soil root	43,969,059	90.39	85,318	2,063
Stem	43,692,744	92.60	85,396	1,932
Mixed tissues	53,655,458	90.12	92,217	1,989

16 Supplemental Table 8 Genic completeness for transcriptomes (BUSCO)

	Complete single-copy	Complete duplicated	Fragment	Missing
Bud	5 (1.2%)	409 (96.2%)	1 (0.2%)	10 (2.4%)
Flower bud	4 (0.9%)	410 (96.5%)	1 (0.2%)	10 (2.4%)
Aerial roots	14 (3.3%)	392 (92.2%)	5 (1.2%)	14 (3.3%)
Leaves	7 (1.6%)	404 (95.1%)	1 (0.2%)	13 (3.1%)
Flowers	29 (6.8%)	362 (85.2%)	15 (3.5%)	19 (4.5%)
Fruits	37 (8.7%)	348 (81.9%)	15 (3.5%)	25 (5.9%)
Ovary	11 (2.6%)	400 (94.1%)	3 (0.7%)	11 (2.6%)
Soil root	9 (2.1%)	402 (94.6%)	2 (0.5%)	12 (2.8%)
Stem	7 (1.6%)	405 (95.3%)	2 (0.5%)	11 (2.6%)
Mixed tissues	7 (1.6%)	407 (95.8%)	1 (0.2%)	10 (2.4%)
Merged transcriptomes	2 (0.5%)	412 (96.9%)	1 (0.2%)	10 (2.4%)

Supplemental Table 9 Summary statistics of protein coding genes per haplotype

	Haplotype A	Haplotype B
Number of protein coding genes	26,392	32,736
Number of exons	140,181	158,279
Mean gene length (bp)	7,865	6,692
Mean exon length (bp)	269	269
Mean number of exons per mRNA	5.3	4.8
Number of single exon gene	5,097	7,460
Mean coding sequence length (bp)	1,072	995
Mean protein length (aa)	356	331
Orthologs 1 to 1	15,844	15,844
Orthologs 1 to many	1,335	1,999
Orthologs many to 1	6,052	4,721
Orthologs many to many	847	704
Haplotype A specific orthologs	742	-
Haplotype B specific orthologs	-	4,724
Orthogroups unassigned genes	985	4,515

bp, base pairs ; aa, amino acid.

9

19 Supplemental Table 10 Genic completeness for CR0040 annotation with BUSCO

BUSCO 5.0.0	Haplotype A	Haplotype B	Haplotype A+B
	26392	32736	59128
Genes in Viridiplantae database	425	425	425
Complete single-copy	343 (80.7%)	337 (79.3%)	65 (15.3%)
Complete duplicated	18 (4.2%)	27 (6.4%)	331 (77.9%)
Fragment	26 (6.1%)	29 (6.8%)	13 (3.1%)
Missing	38 (9.0%)	32 (7.5%)	16 (3.7%)
Genes in Embryophyta database	1,614	1,614	1,614
Complete single-copy	1,292 (80.0%)	1,271 (78.7%)	231 (14.3%)
Complete duplicated	56 (3.5%)	95 (5.9%)	1,245 (77.1%)
Fragment	88 (5.5%)	79 (4.9%)	54 (3.3%)
Missing	178 (11%)	169 (10.5%)	84 (5.3%)
Genes in Liliopsida database	3,236	3,236	3,236
Complete single-copy	2,383 (73.6%)	2,354 (72.7%)	539 (16.7%)
Complete duplicated	106 (3.3%)	187 (5.8%)	2,270 (70.1%)
Fragment	313 (9.7%)	310 (9.6%)	222 (6.9%)
Missing	434 (13.4%)	385 (11.9%)	205 (6.3%)

Supplemental Table 11 RepeatMasker summary report

	Haplotype A (nb)	Haplotype B (nb)	Haplotype A (Mb)	Haplotype B (Mb)	Haplotype A (%bp)	Haplotype B (%bp)	Haplotype A+B (%bp)
Total interspersed repeats	914,993	1,270,877	659.98	930.76	46.6	47.3	47.0
Total retroelements	690,136	992,412	577.09	827.14	40.7	42.0	41.5
Total LTR	378,082	563,026	229.77	344.86	16.2	17.5	17.0
LTR/Copia	134,148	173,060	89.02	118.81	6.3	6.0	6.1
LTR/Gypsi	209,894	346,287	123.85	203.4	8.7	10.3	9.7
LINES	136,139	170,984	168.91	236.34	11.9	12.0	12.0
Unclassified retroelements	170,906	252,117	177.45	244.74	12.5	12.4	12.5
SINE	5,009	6,285	0.96	1.2	0.1	0.1	0.1
DNA transposons	64,797	79,501	21.8	26.44	1.5	1.4	1.4
Unclassified repeats	159,752	198,616	61.03	77.12	4.3	3.9	4.1
Simple repeats	306,532	477,099	191.41	330.64	13.5	16.8	15.4
Low complexity regions	58,671	77,463	129.99	197.09	9.18	10.0	9.7

nb, number ; Mb, mega bases ; bp, base pairs.

Supplemental Table 12 Number and repartition of protein coding genes and repeats per chromosome and per haplotype of CR0040

	CR0040 Haplotype A					CR0040 Haplotype B				
Chr	w N	wo N	genes	cds wo N (%bp)	TEs wo N (%bp)	w N	wo N	genes	cds wo N (%bp)	TEs wo N (%bp)
1	73.50	70.63	3,532	6.12	30.16	68.78	62.17	3,293	6.55	27.95
2	42.59	42.57	1,426	4.14	39.09	37.53	37.47	1,375	4.73	35.03
3	41.87	41.79	1,341	3.95	43.63	40.03	35.97	1,095	3.72	43.54
4	36.44	36.24	1,179	4.05	40.06	44.10	43.14	1,429	4.12	40.53
5	44.52	44.52	1,907	5.36	31.34	42.22	38.80	1,777	5.66	30.64
6	42.39	42.39	1,346	3.98	36.93	24.06	23.18	933	5.08	35.12
7	39.34	38.93	1,455	4.50	40.82	33.37	33.15	1,307	4.85	38.37
8	31.38	31.38	1,229	4.89	35.05	28.94	28.93	1,225	5.26	33.21
9	33.51	33.50	1,336	4.79	37.56	31.37	30.67	1,354	5.21	36.04
10	32.65	32.65	1,240	4.58	35.05	32.20	32.01	1,184	4.62	34.77
11	47.22	32.47	1,228	4.48	40.81	31.72	31.72	1,179	4.63	37.93
12	32.78	32.76	1,276	4.89	34.45	33.34	29.92	1,279	5.27	33.50
13	22.01	21.81	1,007	5.48	36.55	21.85	21.59	981	5.57	36.18
14	20.09	17.17	695	4.85	36.22	23.58	23.33	977	4.75	39.58
1-14	540.27	518.80	20,197	4.77	36.61	493.10	472.06	19,388	5.03	35.56
0	876.47	860.02	6195	0.41	47.33	1,476.30	1,455.48	13,348	0.60	46.97
1-14-0	**1,416.74**	**1,378.82**	26,392	2.05	43.30	1,969.40	1,927.54	32,736	1.68	44.19

Pseudomolecules lengths with (w N) and without (wo N) the Ns (any base) nucleotide in Mbp.

The percentage of CDS/repeats is calculated as the percentage of bases covered by the CDS/repeats sequences per chromosome.

Supplemental Table 13 Number and repartition of protein coding genes per chromosome and per haplotype of Daphna

	Daphna Haplotype A			Daphna Haplotype B		
Chr	w N	wo N	genes	w N	wo N	genes
1	88.30	88.28	4,619	83.42	83.40	4,177
2	72.75	72.74	1,962	76.19	76.18	2,126
3	50.16	50.15	1,670	54.87	54.86	1,781
4	50.01	50.00	1,817	52.15	52.14	1,781
5	52.22	52.21	2,571	52.41	52.40	2,391
6	48.33	48.32	1,739	43.88	43.87	1,673
7	42.01	42.00	1,722	40.07	40.06	1,555
8	35.52	35.52	1,538	34.78	34.77	1,583
9	35.31	35.31	1,681	37.56	37.56	1,661
10	35.05	35.04	1,314	37.45	37.44	1,494
11	37.57	37.56	1,410	40.79	40.78	1,504
12	41.05	41.04	1,712	40.14	40.13	1,738
13	27.55	27.55	1,213	25.81	25.80	1,210
14	23.25	23.25	1,066	22.80	22.80	1,093
1-14	639.09	638.96	26,034	642.33	642.19	25,767
0	97.73	97.66	3133	101.93	101.87	3413
1-14-0	736.82	736.62	29,167	744.26	744.06	29,180

Pseudomolecules lengths with (w N) and without (wo N) the Ns (any base) nucleotide in Mbp.

Supplemental Table 14 Conserved and specific gene groups

	Gene number	Genes in orthogroups	Number of conserved orthogroups	Number of specific orthogroups	Number of specific singleton genes
CR0040 Haplotype A	26,392	25,779	15,916	88	613
CR0040 Haplotype B	32,736	29,689	16,211	899	3,047
Daphna Haplotype A	29,167	26,506	17,131	135	2,661
Daphna Haplotype B	29,180	26,478	17,060	109	2,702
Phalaenopsis equestris	20,081	19,662	13,045	79	419
Phalaenopsis aphrodite	28,903	27,946	13,322	288	957
Oryza sativa	43,770	32,466	12,081	2,731	11,304

14

Supplemental Table 15 Sequencing depth of CR0040 genome per technology

	Haplotype A			Haplotype B		
	PacBio HiFi	ONT	Illumina	PacBio HiFi	ONT	Illumina
Chr0	10.97	19.08	50.55	9.62	15.74	45.26
Chr1	45.53	64.55	73.13	38.93	55.94	62.44
Chr2	51.98	73.30	75.01	34.81	49.41	51.10
Chr3	51.47	81.00	83.68	33.91	43.69	45.16
Chr4	56.02	74.51	76.93	32.98	55.89	58.90
Chr5	53.17	82.57	87.21	34.24	43.53	50.84
Chr6	71.49	103.11	102.67	17.30	24.86	26.50
Chr7	50.15	34.58	55.71	54.54	74.65	76.21
Chr8	47.15	68.15	68.65	56.91	41.25	62.25
Chr9	46.44	69.27	74.45	37.00	49.75	53.92
Chr10	46.74	74.06	80.02	41.63	51.10	53.22
Chr11	24.79	36.80	42.83	49.90	73.66	74.02
Chr12	50.19	77.09	87.36	35.28	44.44	44.44
Chr13	36.78	52.40	55.33	53.44	75.91	76.66
Chr14	40.99	78.69	86.60	35.22	32.76	37.31

32 Supplemental Table 16 Sequencing depth of CR0040 genome using Daphna data sequences

	Haplotype A		Haplotype B	
	ONT	Illumina	ONT	Illumina
Chr0	2.50	17.93	3.18	24.05
Chr1	28.40	106.18	27.12	101.70
Chr2	26.85	104.49	28.96	112.48
Chr3	28.71	114.75	25.02	105.23
Chr4	27.21	108.87	27.74	112.54
Chr5	29.20	110.89	28.37	107.20
Chr6	31.17	116.08	27.51	106.37
Chr7	26.00	100.27	28.48	110.39
Chr8	27.39	108.01	29.08	115.18
Chr9	26.45	102.54	26.89	104.81
Chr10	28.53	110.27	28.93	113.21
Chr11	17.10	66.85	29.10	111.80
Chr12	29.42	114.87	26.51	103.46
Chr13	29.32	112.36	28.49	111.60
Chr14	22.67	90.23	23.43	91.57

33 Supplemental Table 17 Cell cycle regulation genes found in CR0040 genome

		A. thaliana	CR0040 haplotype A	CR0040 haplotype B	*P. aphrodite*
CDKs	CDKA	At3g48750	VANPL_A_00001t012310	VANPL_B_00001t011840	PAXXG231470
			VANPL_A_00014t005470	VANPL_B_00014t007380	
	CDKB	At3g54180	VANPL_A_00007t008490	VANPL_B_00007t007640	PAXXG089720
		At2g38620	VANPL_A_00009t001400	VANPL_B_00009t001350	PAXXG113920
		At1g76540			
		At1g20930			
CYCs					
	CYCA	At1g80370	VANPL_A_00008t011460	VANPL_B_00004t012020	PAXXG008040
		At1g15570	VANPL_A_00005t000960	VANPL_00313t000620	PAXXG183010
		At5g25380		VANPL_B_00008t011460	PAXXG054020
		At5g11300		VANPL_B_00005t001350	
		At5g43080			
		At1g47210			
		At1g47220			
		At1g47230			
	CYCB	AT4G34160			
		At4g37490	VANPL_A_00001t011770	VANPL_B_00001t011320	PAXXG000750
		At5g06150	VANPL_A_00001t024950	VANPL_B_00001t019080	PAXXG156550
		At3g11520	VANPL_00050t000750	VANPL_B_00001t011320	PAXXG228890

		At2g26760	VANPL_A_00001t019600	VANPL_B_00005t000920	PAXXG028470
		At1g34460	VANPL_A_00001t011770		PAXXG000750
		At4g35620	VANPL_A_00001t024950		PAXXG156550
		At2g17620	VANPL_00050t000750		PAXXG219870
		At1g16330	VANPL_A_00005t000640		
			VANPL_A_00005t000650		
			VANPL_A_00005t000650		
	CYCD3-1	At4g34160			
FZR (CCS52A)		At4g22910	VANPL_A_00010t004300	VANPL_B_00010t004420	PAXXG076980
		At4g11920	VANPL_A_00001t012550	VANPL_B_00001t012090	PAXXG084080
		At5g13840		VANPL_13258t000030	PAXXG082520
WEE1		At1g02970	VANPL_A_00011t010580	VANPL_B_00011t010080	PATC144561
KRP		At2g23430	VANPL_A_00008t003440	VANPL_B_00006t003720	PAXXG048550
		At3g50630	VANPL_A_00004t006200	VANPL_B_00008t003330	PAXXG111330
		At5g48820	VANPL_A_00002t006250	VANPL_B_00004t006400	PAXXG290150
		At2g32710	VANPL_A_00001t031310	VANPL_B_00002t006550	PAXXG115580
		At3g24810		VANPL_B_00001t028840	
		At3g19150		VANPL_B_00001t020090	
		At1g49620		VANPL_00053t001550	
ILP1		At5g08550	VANPL_A_00012t005730	VANPL_B_00012t005680	PAXXG094170
ADF		At3g46010	VANPL_A_00010t001900	VANPL_B_00009t008980	PAXXG101780
		At3g46000	VANPL_A_00011t003650	VANPL_B_00010t001860	PAXXG066610
		At5g59880	VANPL_A_00009t008690	VANPL_B_00002t003560	PAXXG194280

At5g59890	VANPL_A_00001t019380	VANPL_B_00009t002390	PAXXG119700
At2g16700	VANPL_A_00002t003620	VANPL_B_00001t012150	PAXXG241790
At2g31200	VANPL_A_00014t004200	VANPL_B_00011t003680	PAXXG043520
At4g25590	VANPL_A_00005t008770	VANPL_B_00001t018850	PAXXG173900
At4g00680	VANPL_A_00003t000430	VANPL_B_00014t004330	PAXXG146670
At4g34970	VANPL_A_00009t002490	VANPL_00170t000390	PAXXG125360
At1g01750	VANPL_A_00006t002570	VANPL_01089t000240	PAXXG160710
At3g45990			PAXXG009590
At5g52360			PAXXG386760
			PAXXG302270

CDKs : Cyclin-Dependent Kinases ; CYCs : Cyclins ; FZR : Fizzy-Related protein ; WEE1 : WEE1 like protein kinase ; KRP : cyclin-dependent kinase inhibitor ; ILP : Transcriptional repressor ILP1 ; ADF : Actin-Depolymerizing Factor ;